Modeling the Panchromatic Spectral Energy Distributions of Galaxies

Charlie Conroy

Department of Astronomy and Astrophysics, University of California, Santa Cruz, California 95064; email: conroy@ucsc.edu

Annu. Rev. Astron. Astrophys. 2013. 51:393–455

The *Annual Review of Astronomy and Astrophysics* is online at astro.annualreviews.org

This article's doi:
10.1146/annurev-astro-082812-141017

Keywords

stars, abundances, dust, stellar populations, galaxies: stellar content, galaxy evolution

Abstract

The spectral energy distributions (SEDs) of galaxies are shaped by nearly every physical property of the system, including the star-formation history, metal content, abundance pattern, dust mass, grain size distribution, star-dust geometry, and interstellar radiation field. The principal goal of stellar population synthesis (SPS) is to extract these variables from observed SEDs. In this review I provide an overview of the SPS technique and discuss what can be reliably measured from galaxy SEDs. Topics include stellar masses, star-formation rates and histories, metallicities and abundance patterns, dust properties, and the stellar initial mass function.

1. INTRODUCTION

Many of the fundamental properties of unresolved stellar populations are encoded in their spectral energy distributions (SEDs). These properties include the star-formation history (SFH), stellar metallicity and abundance pattern, stellar initial mass function (IMF), total mass in stars, and the physical state and quantity of dust and gas. Some of these properties are easier to measure than others, and each provides important clues regarding the formation and evolution of galaxies. It is precisely these quantities, measured from the SEDs of galaxies, that have provided the foundation for our modern understanding of galaxy formation and evolution.

Over the past several decades considerable effort has been devoted to extracting information from the SEDs of galaxies, exploiting information from the far-ultraviolet (FUV) to the far-infrared (FIR). Early attempts at understanding the visible and near-infrared (NIR) spectral windows approached the problem by combining mixtures of stars in ad hoc ways until a match was achieved with observations (e.g., Spinrad & Taylor 1971). More sophisticated versions of this technique were developed that incorporated physical constraints and automated fitting techniques (Faber 1972). At approximately the same time, synthesis models were being developed that relied on stellar evolution theory to constrain the range of possible stellar types at a given age and metallicity (e.g., Tinsley 1968; Searle, Sargent & Bagnuolo 1973; Tinsley & Gunn 1976; Bruzual 1983). The substantial progress made in stellar evolution theory in the 1980s and 1990s paved the way for the latter approach to become the de facto standard in modeling the SEDs of galaxies (e.g., Charlot & Bruzual 1991; Bruzual & Charlot 1993; Bressan, Chiosi & Fagotto 1994; Worthey 1994; Fioc & Rocca-Volmerange 1997; Leitherer et al. 1999; Vazdekis 1999). This modeling technique, which will be described in detail in the next section, is sometimes referred to as evolutionary population synthesis (e.g., Maraston 1998), although the term stellar population synthesis (SPS) has garnered wider use. The latter term will be used throughout this review.

The UV and IR spectral windows are rather more difficult to probe owing to the obscuring effects of the atmosphere. Nonetheless, numerous balloon and space-based observatories have opened up the UV and IR to detailed investigations. In these spectral regions dust plays a major role; it absorbs and scatters much of the UV light emitted by stars and reradiates that energy in the IR. In young stellar populations the UV is dominated by hot massive stars, whereas in old stellar populations the UV can be influenced by hot evolved stellar types such as post–asymptotic giant branch (AGB) and extreme horizontal branch (HB) stars (for details, see the review by O'Connell 1999).

The development of models for the IR SEDs of galaxies (e.g., Draine & Lee 1984; Zubko, Dwek & Arendt 2004) has proceeded in parallel with the development of models for UV, optical, and NIR SEDs, and it is only recently that models have been developed to simultaneously and self-consistently predict the FUV through FIR SEDs (e.g., Silva et al. 1998; Devriendt, Guiderdoni & Sadat 1999; da Cunha, Charlot & Elbaz 2008; Groves et al. 2008; Noll et al. 2009a).

Several broad questions will serve to focus this review:

- What have we learned about the physical properties of galaxies from their observed SEDs?
- How reliable are the quantities thus derived?
- What can be learned, in principle, from the SEDs of galaxies?

The first question is relatively straightforward to address, whereas the second and third are necessarily more complicated. Attention will be given to cases where answers to these questions are presently unknown but knowable (the "unknown unknowns," in Rumsfeld's sense, are of course the most interesting but the most difficult to discuss).

There are surprisingly few thorough reviews of SPS and its application to modeling SEDs. The foundational review by Tinsley (1980) is highly recommended to anyone seeking a broad yet

Spectral energy distribution (SED): light emitted over all or a portion of the FUV-FIR spectral domain, including broadband data and/or moderate-resolution spectra

SFH: star-formation history

IMF: initial mass function

FUV: far-ultraviolet

FIR: far-infrared

NIR: near-infrared

SPS: stellar population synthesis

AGB: asymptotic giant branch

HB: horizontal branch

intuitive understanding of stellar populations and galaxy formation. The reviews by Faber (1977) and Frogel (1988) are more narrowly focused on old stellar populations, but they are informative because many of the issues raised therein are still relevant today. Recently, Walcher et al. (2011) presented an excellent review of many aspects related to the modeling of galaxy SEDs.

SFR: star-formation rate

CSP: composite stellar population

SSP: simple stellar population

The topic of modeling galaxy SEDs is vast, and it would be impossible to provide a thorough review of the entire field. Hard decisions therefore had to be made. With regard to wavelength, energies higher than the FUV (roughly the Lyman limit) and lower than the submillimeter (approximately 1 mm) are not discussed. Nebular emission lines will also be neglected, except in a few cases. The measurement of and uncertainty induced by photometric redshifts are not discussed and active galactic nuclei (AGN) will be ignored. The technique of fitting models to data was reviewed recently by Walcher et al. (2011) and so is not discussed here. A whole review could (and should) be written on the evaluation and comparison of existing SPS models. This is not undertaken here, except in cases where different models, when applied to data, produce starkly different results. The reader is referred to Conroy & Gunn (2010) for a recent comparison of several popular models. Finally, it is worth emphasizing what this review is not: It is not a summary of science results derived with SPS models. There is an extensive literature devoted to applying SPS models to data in order to derive insights into the formation and evolution of galaxies. Results of this nature, though fascinating in their own right, will not feature prominently in this review. Readers are referred to Renzini (2006) and Blanton & Moustakas (2009) for recent reviews along these lines.

This review is organized as follows. An overview of SPS model construction and application is provided in Section 2. We then turn to the topics of mass-to-light ratios and stellar masses (Section 3), star-formation rates (SFRs), histories, and stellar ages (Section 4), stellar metallicities and abundance patterns (Section 5), dust (Section 6), and the IMF (Section 7). Several concluding remarks are provided in Section 8.

2. OVERVIEW OF STELLAR POPULATION SYNTHESIS

The construction of models for simple and composite stellar populations (CSPs) is conceptually straightforward. There are, however, certain constraints that make the creation of such models rather difficult in practice (incomplete isochrone tables, incomplete empirical stellar libraries, poorly calibrated physics, etc.). In this section the ingredients necessary for constructing model SEDs will be discussed. Areas of particularly large uncertainties will be highlighted, but it is not the goal of this review to provide an exhaustive intercomparison of various possible model choices. An overview of the entire process of constructing CSPs is given in **Figure 1**.

2.1. The Simple Stellar Population

The starting point of any SPS model is the simple stellar population (SSP), which describes the evolution in time of the SED of a single, coeval stellar population at a single metallicity and abundance pattern. An SSP therefore requires three basic inputs: stellar evolution theory in the form of isochrones, stellar spectral libraries, and an IMF, each of which may in principle be a function of metallicity and/or elemental abundance pattern. These components are typically combined in the following way:

$$f_{\rm SSP}(t,\,Z) = \int_{m_{\rm lo}}^{m_{\rm up}(t)} f_{\rm star}[T_{\rm eff}(M),\log g(M)|t,\,Z]\,\Phi(M)\,{\rm d}M\,, \qquad (1)$$

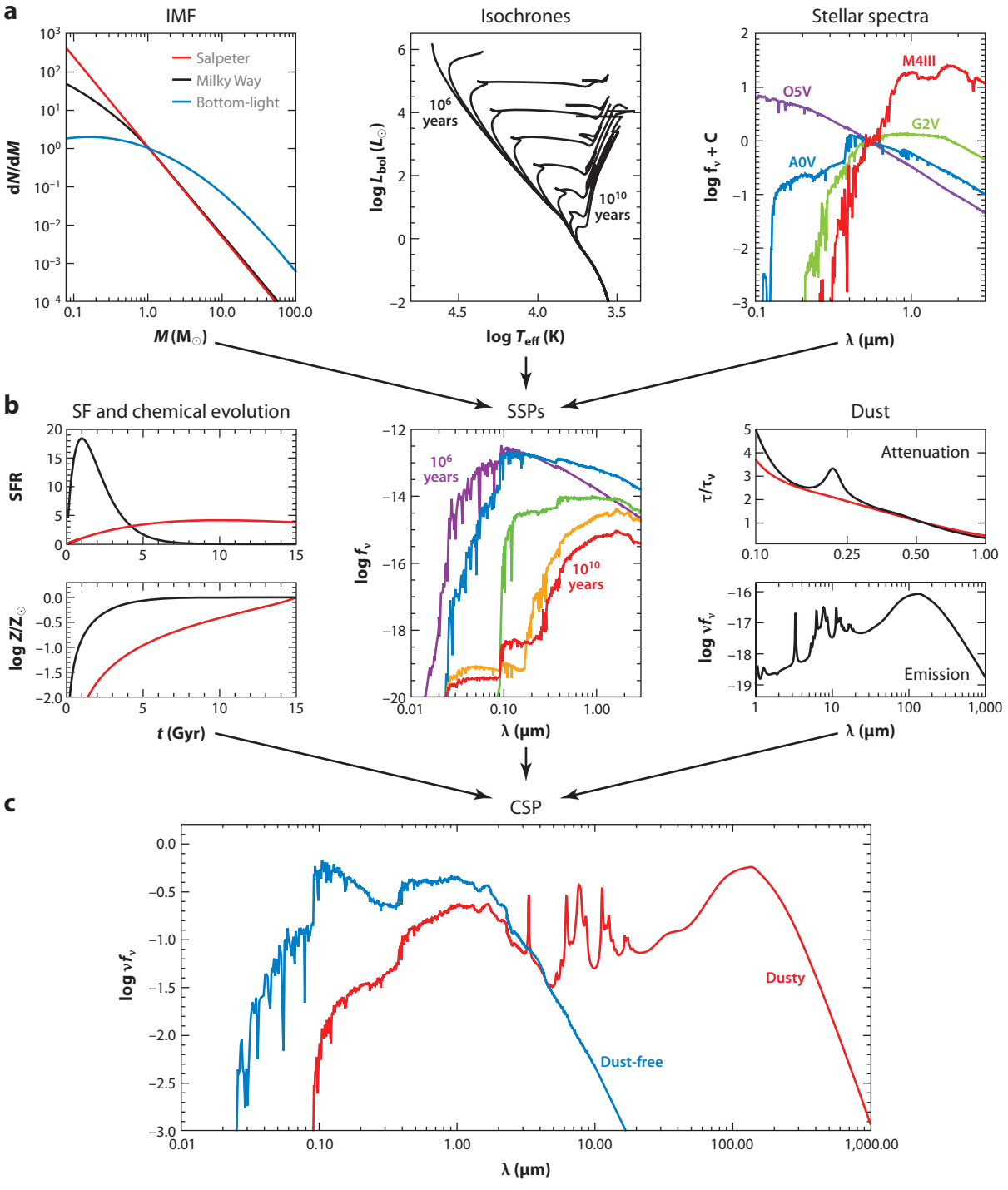

where M is the initial (zero-age main sequence) stellar mass, $\Phi(M)$ is the IMF, $f_{\rm star}$ is a stellar spectrum, and $f_{\rm SSP}$ is the resulting time and metallicity-dependent SSP spectrum. The lower limit of integration, $m_{\rm lo}$, is typically taken to be the hydrogen burning limit (either 0.08 or 0.1 $M_\odot$, depending on the SPS code), and the upper limit is dictated by stellar evolution. The isochrones determine the relation between $T_{\rm eff}$, $\log g$, and M for a given t and Z. This approach to constructing SSPs is common but not universal. Alternatives include the fuel consumption theorem (Renzini & Buzzoni 1986, Maraston 1998) or the use of empirical spectra of star clusters as templates for SSPs (Bica & Alloin 1986).

Nearly all SPS models provide SSPs as a black box (e.g., Leitherer et al. 1999, Bruzual & Charlot 2003, Maraston 2005, Vazdekis et al. 2010). The user therefore has little working knowledge of how SSPs are built and where major issues lie. The following discussion is therefore largely pedagogical and geared toward users of SPS models rather than model builders.

2.1.1. Stellar evolution and isochrones. An isochrone specifies the location in the Hertzsprung-Russell (HR) diagram of stars with a common age and metallicity. Isochrones are constructed from stellar evolution calculations for stars from the hydrogen burning limit ($\approx$0.1 $M_\odot$) to the maximum stellar mass ($\approx$100 $M_\odot$). The construction of isochrones is straightforward for stellar evolution tracks that are infinitely well sampled in mass and time. In practice, evolutionary tracks are discretely sampled, and this can lead to issues in isochrone construction for fast evolutionary phases. Modern sets of isochrones have been constructed specifically to ensure that the models are relatively immune to these effects (Charlot & Bruzual 1991).

A number of widely used isochrone tables exist in the literature. The most popular models span a wide range of age (masses) and chemical composition and cover most relevant evolutionary phases. Models in this category include the Padova (Bertelli et al. 1994, Girardi et al. 2000, Marigo et al. 2008) and the BaSTI models (Pietrinferni et al. 2004, Cordier et al. 2007). The Geneva models (Schaller et al. 1992, Meynet & Maeder 2000) are tailored to follow high-mass stars through advanced evolutionary phases, including the Wolf-Rayet (WR) phase, but they do not model low-mass stars. Other models have focused on the main sequence, RGB, and HB evolution of low-mass stars ($M < 3\,M_\odot$), including the Y^2 (Yi et al. 2001; Yi, Kim & Demarque 2003), Dartmouth (Dotter et al. 2008), and Victoria-Regina models (Vandenberg & Bell 1985, VandenBerg, Bergbusch & Dowler 2006). Finally, there are isochrones tailored to very-low-mass stars and brown dwarfs. The Lyon models are the most widely used in this regime (Chabrier & Baraffe 1997, Baraffe et al. 1998). It is noteworthy that none of the isochrones listed here cover the post-AGB evolutionary phase. Remarkably, the post-AGB isochrones computed by Schoenberner (1983), Vassiliadis & Wood (1994), and Bloecker (1995) are still widely used in modern SPS codes.

Implementing isochrones in an SPS model is challenging because no single set spans the necessary range of ages, metallicities, and evolutionary phases. It is common to use the Padova isochrones for the bulk of the age and metallicity range and to supplement with the Geneva models at young ages. Little attention is normally paid to the lowest-mass portion of the isochrones, because low-mass stars contribute only ~1% of the light of an old stellar population. An exception

Figure 1

Overview of the stellar population synthesis technique. (*a*) Ingredients necessary for constructing simple stellar populations (SSPs): an initial mass function (IMF), isochrones for a range of ages and metallicities, and stellar spectra spanning a range of $T_{\rm eff}$, $L_{\rm bol}$, and metallicity. (*b*) Ingredients necessary for constructing composite stellar populations (CSPs): star-formation (SF) histories and chemical evolution, SSPs, and a model for dust attenuation and emission. (*c*) Final CSPs both before and after a dust model is applied.

in this regard is the model of Conroy & van Dokkum (2012a), who paid special care to the modeling of low-mass stars for SPS. The splicing together of various isochrone sets can be difficult. For example, different codes make different assumptions regarding convection, rotation, etc., and so the age at which certain stars evolve off the main sequence varies between codes.

Modules for Experiments in Stellar Astrophysics (MESA) is a new, highly modular, and sophisticated stellar evolution code that includes the latest stellar interior ingredients, including opacity tables, equations of state, nuclear reaction networks, and surface boundary conditions (Paxton et al. 2011). There is great hope that MESA will be employed to produce high-quality isochrones over the full age and metallicity range and for all evolutionary phases.

In addition to the practical difficulty of implementing present isochrone libraries, stellar evolution calculations contain a number of uncertainties relevant to SPS. For example, all of the stellar models mentioned above are based on one-dimensional codes. As such, they require approximations to inherently three-dimensional processes such as convection, rotation, mass-loss, close binary interactions, and thermal pulses during AGB evolution. These processes lead to major uncertainties in the isochrones that impact the resulting SPS model predictions (e.g., Charlot 1996; Charlot, Worthey & Bressan 1996; Yi 2003; Lee et al. 2007; Conroy, Gunn & White 2009).

The cores of stars more massive than $M \sim 1.1\,M_\odot$ are convective, as are the envelopes of evolved giants and low-mass stars. Classically, the boundary between convective and radiative regions is specified by the Schwarzschild criterion. However, this criterion is effectively a requirement that the acceleration of a convective fluid element be zero. The fluid element will likely have a nonzero velocity as it crosses this boundary, and so some amount of overshooting is expected. This will result in a larger convective region than would be expected from the Schwarzschild criterion alone. With regard to the convective core, a wide body of observational evidence favors the existence of a moderate amount of overshooting in the mass range $1.1 < M/M_\odot < 7$ (Stothers 1991; Nordstroem, Andersen & Andersen 1997; VandenBerg & Stetson 2004; Keller & Wood 2006). The amount of core overshooting required to fit the data results in an ∼25% increase in the main sequence lifetime compared with models that do not include overshooting. Nearly all SPS models adopt isochrones with a modest amount of overshooting in the convective core, as supported by observations. The exception to this is the SPS model of Maraston (1998, 2005), which uses isochrones without core convective overshooting. The treatment of core overshooting has a noticeable effect on the color evolution of SSPs in the age range of ∼0.1–1 Gyr, by as much as ≈0.1 mag (Yi 2003, Conroy & Gunn 2010), and can therefore be an important source of systematic uncertainty when modeling SEDs.

As discussed in Cassisi (2004), the amount of overshooting in the convective envelopes of evolved giants is less constrained. This is unfortunate because the treatment of envelope convection affects, among other observables, the ratio of red to blue helium burning giants (Renzini et al. 1992). These stars can contribute several tens of percent to the integrated light, depending on the SFH (Melbourne et al. 2012), and so uncertainty in the amount of envelope overshooting should affect the integrated light predictions at a significant level. Overshooting in the convective envelope also affects the location of the luminosity bump in the RGB luminosity function. This fact was used by Alongi et al. (1991) and more recently by Cassisi et al. (2011) to argue for a modest amount of overshooting in the convective envelope.

The importance of stellar rotation has been investigated by the Geneva group, among others, over the past two decades (see Maeder & Meynet 2000, 2012 for reviews). Perhaps most important, rotation increases the main sequence lifetimes (by ∼25%) due to rotation-induced mixing bringing fresh fuel to the convective core. Rotation also lowers the effective surface gravity, lowers the opacity in the radiative envelope, increases the luminosity, and changes the ratio of red to blue supergiants. The mixing to the surface of hydrogen burning products caused by rotation will

also affect the number and type of WR stars. Vázquez et al. (2007) and Levesque et al. (2012) investigated the impact of rotating massive star models on integrated light properties through a comparison with nonrotating models and found that the number of ionizing photons increased by as much as an order of magnitude and colors became bluer by as much as 0.1–1 mag, depending on wavelength and age. The signatures of WR stars as a function of time and metallicity in integrated spectra are also different between rotating and nonrotating models.

Most massive stars are in binary systems, and there is some evidence that massive star binaries preferentially have comparable masses (Kobulnicky & Fryer 2007, Sana & Evans 2011). The interaction of close binary stars via mass transfer and common envelope evolution will affect the evolution of such stars and bring about further changes to their observable properties. Eldridge, Izzard & Tout (2008) demonstrated that in many respects the effects of binary star models without rotation are similar to single star models with rotation. Eldridge & Stanway (2012) argued that SPS models that include binary star evolution produced a better fit to UV spectra of star-forming galaxies. Regardless of the details, it is clear that where massive stars matter in galaxy SEDs, the effects of both rotation and binary evolution will play an important role. In fact, binary star evolution may also create blue straggler stars and extreme HB stars, which would suggest that binary evolution can affect older stellar populations as well (Han et al. 2002, 2003; Zhang et al. 2005). No popular SPS model includes the effects of binary star evolution.

The potential importance of thermally pulsating (TP-)AGB stars in the context of SPS models was emphasized by Maraston et al. (2006) and has since become a controversial topic. This phase occurs for stars in the mass range $\approx 1 < M/\mathrm{M}_{\odot} < 8$ (depending on metallicity) and is difficult to model for several reasons, including the fact that nuclear burning occurs in alternate hydrogen-rich and helium-rich shells. When the helium shell burns, it does so explosively because of a thin shell instability (Schwarzschild & Harm 1968), which gives rise to thermal pulses. Mass-loss becomes catastrophic during this phase, thereby terminating the life of the star. Recently, the Padova group has developed a new suite of isochrones with updated TP-AGB models calibrated against observations in the Large Magellanic Cloud (LMC) (Marigo & Girardi 2007, Marigo et al. 2008). However, Conroy & Gunn (2010) found that the updated Padova models failed to reproduce the colors of intermediate-age Magellanic Cloud star clusters, by as much as 0.5 mag in some cases. These researchers provided recalibrated SPS models in which the weight given to TP-AGB stars was reduced in order to match the LMC data. More recently, Melbourne et al. (2012) analyzed resolved color-magnitude diagrams (CMDs) in nearby dwarf galaxies and concluded that these updated models produce twice as much luminosity in the TP-AGB phase as observed, roughly independent of the inferred mass fraction in young stars. In addition, Melbourne et al. (2012) found that the latest Padova model predictions for the luminosity contributed by red core helium burning stars is a factor of two lower than that observed in dwarf galaxies. This problem in the models may be related to the treatment of convection in the envelopes of evolved giants.

Mass-loss is another critical parameter in stellar evolution models. At $M \lesssim 8\,\mathrm{M}_{\odot}$, mass-loss determines when a star will end its life as a white dwarf, and how massive the white dwarf will be. At higher masses mass-loss can qualitatively alter the course of advanced evolutionary phases, especially at $M > 40\,\mathrm{M}_{\odot}$. In high-mass stars the mass-loss mechanism is thought to be via line-driven winds, whereas in lower-mass stars ($\lesssim 8\,\mathrm{M}_{\odot}$) it is believed to be due to pulsation-induced, dust-driven winds (Willson 2000). In any event, the mass-loss prescription is another free parameter in these models, and it is a critical one because it strongly affects the lifetimes of advanced (and luminous) evolutionary phases. For example, the lifetime of TP-AGB stars and the number of thermal pulses they undergo depend strongly on the mass-loss prescription (Ventura & Marigo 2010).

In summary, the computation of isochrones for use in SPS depends on many uncertain aspects of stellar evolution, including the treatment of convection, close binary evolution, rotation effects, and mass-loss, among many others. The importance of these uncertainties on derived SPS results will be highlighted throughout this review.

2.1.2. Stellar remnants. Stars eventually die, usually leaving behind stellar remnants in the form of white dwarfs, neutron stars, or black holes (theory predicts that a certain class of very massive, metal-poor stars undergoes pair-instability supernovae that leave behind no stellar remnant; Heger et al. 2003). The relation between the initial, zero-age main sequence stellar mass and the final remnant mass is not well constrained observationally, especially for massive stars. The initial–final mass relation for white dwarfs can be reasonably well constrained by measuring white dwarf masses in open clusters with known ages (e.g., Kalirai et al. 2008). The initial–final mass relation is predicted to be a function of metallicity (Marigo 2001, Heger et al. 2003), further complicating the situation.

In SPS models stellar remnants are usually included in the total stellar mass budget, and their contribution can be significant. For example, if a certain amount of mass is formed into stars instantly, then after 13 Gyr only 60% of the mass remains in stars or stellar remnants; the other 40% has returned to the ISM. Of the remaining stellar mass, 25% is locked in stellar remnants. Of the total remnant mass, 73% is comprised of white dwarfs, 7% is in neutron stars, and 20% is in black holes. These numbers were computed assuming solar metallicity and a Kroupa (2001) IMF, with the initial–final mass relations from Renzini & Ciotti (1993). The Maraston (2005) SPS model predicts similar numbers (largely because the same initial–final mass relation was used). The point is that stellar remnants can make an important contribution to the total stellar mass of a system.

2.1.3. Stellar spectral libraries. Stellar spectral libraries are required to convert the outputs of stellar evolution calculations—surface gravities, g, and effective temperatures, $T_{\rm eff}$—as a function of metallicity, Z, into observable SEDs. There is, however, no single spectral library, whether theoretical or empirical, that covers the entire range of parameter space necessary for constructing SPS models. Stitching together various libraries, often of widely varying quality, is therefore necessary. Some modelers take the approach of constructing spectral libraries entirely from theoretical calculations, whereas others use purely empirical libraries. The benefits and drawbacks of these two approaches will be discussed in this section.

2.1.3.1. Theoretical libraries. Theoretical libraries offer the great advantage of densely covering parameter space, including spectral resolution, and of producing spectra that are not subject to observational issues such as flux calibration and atmospheric absorption. The clear disadvantage is that the libraries are only as good as the input atomic and molecular parameters and the approximations made in the computation of the models, as discussed below.

There are a number of decisions that must be made when computing synthetic spectral libraries, including how to treat convection and the microturbulent velocity profile and whether or not to model departures from local thermodynamic equilibrium and plane-parallel geometries. Additional important limitations include the incomplete and often inaccurate atomic and molecular line lists. As emphasized by Kurucz (2011), models still fail to reproduce all the observed features in ultra-high-resolution spectra of the Sun owing to incomplete atomic line lists. The situation is even more serious for cooler stars because the molecular line lists can carry fairly large uncertainties, in particular TiO (Allard, Homeier & Freytag 2011). A related problem is that a significant fraction of the atomic and molecular lines are derived from theoretical calculations,

rather than being measured in the laboratory, and so they have uncertain strengths and central wavelengths. Unfortunately, these predicted lines can be important for determining the overall SED shape of stars and hence of galaxies. Worse still, the partition function for many molecules is poorly known, so even the total abundance of particular molecules is uncertain.

The quality and state of the art of the theoretical models varies considerably as a function of $T_{\rm eff}$. At the high-temperature end, i.e., WR and O-type main sequence stars, the state-of-the-art libraries are from Smith, Norris & Crowther (2002) and Lanz & Hubeny (2003), whereas for hotter compact objects (e.g., post-AGB stars) the most up-to-date models are from Rauch (2003). By far the widest range in parameter space is covered by the BaSeL atlas (Lejeune, Cuisinier & Buser 1997, 1998; Westera et al. 2002). This library is comprised of a variety of theoretical models from Kurucz (1995, unpublished), Fluks et al. (1994), Bessell et al. (1989, 1991), and Allard & Hauschildt (1995). The broadband SEDs of the stars in this library have been modified to agree with observed *UBVRIJHKL* color–temperature relations for individual stars. The BaSeL atlas is almost universally used in modern SPS codes, despite the fact that the input theoretical spectra are now almost 20 years old. At the very coolest temperatures, the MARCS and NEXTGEN/PHOENIX grids are the state-of-the-art because of their comprehensive molecular line lists and treatment of spherical effects on the atmospheres and spectra of cool giants. Finally, the Aringer et al. (2009) models fill out the low-temperature end by providing carbon star spectra over a range of parameter space.

There are several modern spectral libraries computed by Coelho et al. (2005), Martins et al. (2005), and Munari et al. (2005) that offer fairly wide coverage in parameter space and are at high spectral resolution. The Martins et al. (2005) library has even been incorporated into a fully theoretical high-resolution SPS model (González Delgado et al. 2005). However, these libraries appear to be geared toward high-resolution spectroscopic analyses because they do not include the predicted lines. They therefore cannot be used to model broadband SEDs, or any spectral region that contains a significant contribution from predicted lines. However, progress can be made by making corrections to these high-resolution libraries for the effect of predicted lines on the broadband SED, as is done in, e.g., Coelho et al. (2007).

2.1.3.2. How accurate are the theoretical libraries? Normally, observed stars are assigned physical parameters based on a comparison with models. However, if one wants to constrain the models with observed stellar data, then one requires an independent estimate of the physical properties of stars. This is a significant obstacle to assessing the accuracy of the models. One can obtain essentially model-independent estimates of $T_{\rm eff}$ via angular diameter measurements, but these are very difficult to obtain for giants, let alone main sequence stars (Perrin et al. 1998, Boyajian et al. 2012a). A more widely used technique is the infrared flux method, first proposed by Blackwell & Shallis (1977). The basic idea is that the flux of a star depends only weakly on $T_{\rm eff}$ in the IR; thus one can deduce angular diameters from fluxes alone with only a weak model dependence. This technique underpins nearly all existing color-$T_{\rm eff}$ relations (e.g., Alonso, Arribas & Martinez-Roger 1996; Ramírez & Meléndez 2005, Casagrande et al. 2010).

The latest generation of model spectra succeeds in reproducing the broadband colors for FGK dwarfs and warm giants (Bertone et al. 2004, Kučinskas et al. 2005, Martins & Coelho 2007, Boyajian et al. 2012b). Not surprisingly, the models continue to have difficulty fitting the SEDs of the coolest stars and the flux in the Wien tail of the flux distribution (typically $\lesssim$5,000 Å for types G and later). The latter difficulty arises because the Wien tail is extremely sensitive to $T_{\rm eff}$; thus even minor changes to the model assumptions lead to large changes in that spectral region. In addition, metal line blanketing becomes very strong in the blue/UV spectral range, and so the requirements on the line lists are demanding. Martins & Coelho (2007) explored the ability of three

modern synthetic libraries to reproduce a variety of spectral features of observed stars. Overall, the agreement was found to be satisfactory, although there were notable deficiencies. Some models were unable to reproduce the observed CH features in cool stars, whereas other models failed to match the observed Mg *b* and MgH features. The majority of the model shortcomings were restricted to stars with $T_{\rm eff} < 4{,}500$ K. Modern models also have difficulty reproducing the strength of the TiO bands in cool stars (Kučinskas et al. 2005; Allard, Homeier & Freytag 2011).

The situation regarding the H_2O band strengths in the NIR should serve as a cautionary tale: Models have for decades predicted water bands in cool stars that are stronger than observations. Part of the problem seems to have been the molecular line lists, which improved steadily over the years, culminating in the Barber et al. (2006) line list, which contains 500 million transitions. However, Allard, Homeier & Freytag (2011) demonstrated that the recent revision of the solar abundance scale by Asplund et al. (2009), which entails a factor of two reduction in the oxygen abundance, has a much larger effect on the predicted strength of the water bands. Their new models with updated solar abundances reproduce remarkably well the NIR colors of M dwarfs, which have strong water band features. Thus, not only the atomic and molecular parameters but also the abundance patterns can have a very significant effect on theoretical spectra.

2.1.3.3. Empirical libraries. The strengths and weaknesses of the theoretical libraries are the weaknesses and strengths of the empirical libraries. Empirical spectra of course do not suffer from issues with line lists, treatment of convection, etc., but they are plagued by standard observational constraints such as correction for atmospheric absorption, flux calibration, and limited wavelength coverage and spectral resolution. Worse, the empirical libraries are woefully incomplete in their coverage of parameter space. This is a long-standing issue that is difficult to address owing to the fact that empirical libraries are drawn from samples of stars in the Solar Neighborhood. For example, hot main sequence stars at low metallicity are very rare, as are stars in rapid phases of stellar evolution such as WR and TP-AGB stars.

One of the first comprehensive empirical stellar spectral libraries was constructed by Gunn & Stryker (1983). Later optical/NIR libraries included those of Pickles (1998) and Jones (1999), ELODIE (Prugniel & Soubiran 2001), STELIB (Le Borgne et al. 2003), Indo-US (Valdes et al. 2004), NGSL (Gregg et al. 2006, Heap & Lindler 2011), MILES (Sánchez-Blázquez et al. 2006), IRTF (Rayner, Cushing & Vacca 2009), and the X-shooter library (Chen et al. 2011). Other, specialized libraries include a UV atlas compiled from *International Ultraviolet Explorer* data (Fanelli et al. 1992), a TP-AGB library (Lançon & Wood 2000), and the *Spitzer Space Telescope* IR stellar library (Ardila et al. 2010). The Sloan Digital Sky Survey (SDSS) has obtained spectra of several hundred thousand stars and devoted considerable effort to measuring stellar parameters from the spectra (Lee et al. 2008). As yet, there is no official stellar spectral library based on the SDSS stars, but it would clearly provide a great leap forward in terms both of coverage in parameter space and of uniformity in spectral quality.

Figure 2 shows an example of the difficulties posed by empirical libraries for SPS model construction as well as the location in the HR diagram of all stars from the MILES spectral library, with stellar parameters determined by Cenarro et al. (2007). MILES is the empirical library today that provides the greatest coverage in terms of log *g*, $T_{\rm eff}$, and [Fe/H] with a total of 985 stars. The metal-rich and metal-poor stars are shown in **Figure 2*a,b***. Overplotted are isochrones from the Padova group for ages ranging from $10^{6.5}$ to 10^{10} year. Although the lower main sequence and RGB are well covered by the empirical library over a wide range in metallicity, hotter stars are rare, especially at lower metallicity. Because the HR diagram is covered so sparsely in this regime, constructing SPS models based on empirical libraries at young ages ($\lesssim$1 Gyr) is clearly challenging.

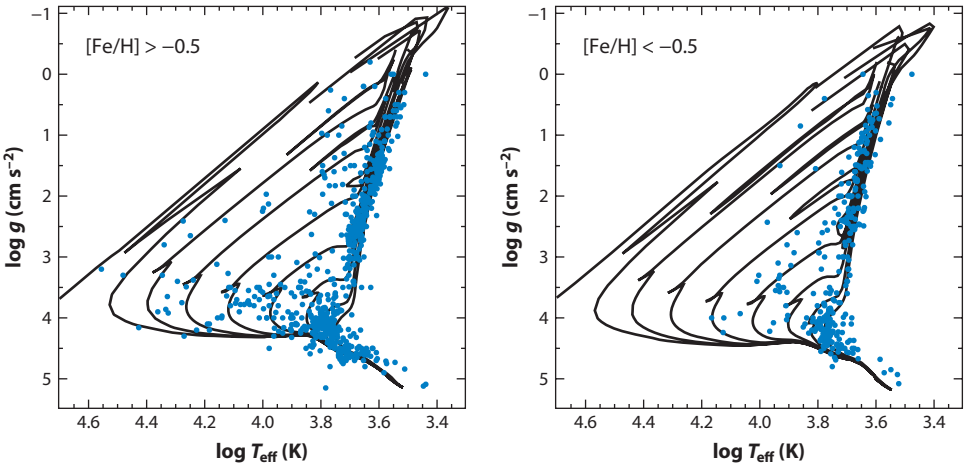

Figure 2

Physical properties of the MILES empirical spectral library, separated by [Fe/H] (*solid symbols*). Isochrones from the Padova group are overplotted for $t = 10^{6.5}$ to 10^{10} year. Typical errors on $T_{\rm eff}$ and log g are 60–100 K and 0.2 dex, respectively (Cenarro et al. 2007). Notice that the MILES library covers the lower main sequence and RGB both at high and low metallicity but only sparsely covers the upper main sequence and supergiants. This figure highlights the difficulty in constructing stellar population synthesis models based on empirical stellar libraries, especially at low metallicity.

A second, related problem with empirical libraries is irregular coverage in the HR diagram. Interpolation within the library, necessary for SPS model construction, can be difficult. Vazdekis et al. (2010) have developed a sophisticated algorithm to deal with this issue. These researchers assign quality numbers to the resulting SPS models based on the number of empirical spectra comprising each model. This is a profitable approach that should be standard in the field because it allows users to assess the reliability of various regions of parameter space.

A third problem associated with empirical libraries is the assignment of physical parameters to stars, including log g, $T_{\rm eff}$, and [Fe/H]. Of particular note is the $T_{\rm eff}$ determination, which carries an uncertainty of order 100 K (Alonso, Arribas & Martinez-Roger 1996; Ramírez & Meléndez 2005; Casagrande et al. 2010). Using theoretical models, Percival & Salaris (2009) explored the impact of uncertainties in $T_{\rm eff}$, log g, and [Fe/H] for individual stars on SPS models. They found that for models with old ages (>4 Gyr), the effect of changing the temperature scale by 100 K had significant effects [0.1–0.4 Å in equivalent width (EW) in the most extreme cases] on a variety of spectral absorption features, including the hydrogen Balmer lines and several commonly employed iron and magnesium lines used to interpret the stellar populations of early-type galaxies. The work of Percival & Salaris (2009) was mostly exploratory, and it would be desirable to consider the full propagation of these sorts of uncertainties into the derived properties of galaxies.

Yet another issue with empirical libraries is the abundance patterns of the stars. It is well known that low metallicity stars in the Galaxy tend to be α-enhanced, such that [Mg/Fe] $\approx$ 0.0 at [Fe/H] $\approx$ 0.0 and [Mg/Fe] $\approx$ 0.4 at [Fe/H] < -1.0 (Edvardsson et al. 1993). Thus, any model based on empirical stars at low metallicity must somehow correct for this [α/Fe] "bias" in the models (see, e.g., Thomas, Maraston & Bender 2003b; Schiavon 2007).

2.1.3.4. Variable abundance patterns. Moderate-resolution spectra (i.e., R $\sim$ 1,000–5,000) contain a wealth of information on the detailed abundance patterns of the stellar populations. In the

context of SPS models, abundance ratios have historically been estimated through the analysis of spectral indices. Ideally, an index is sensitive to a single feature (such as an atomic absorption line or a molecular band head). One usually defines a feature band pass and one or two pseudocontinua, and then an EW, or in some cases a magnitude, can be measured. The Lick/IDS system is the most popular index system, defining 21 indices in the wavelength range of 4,000–6,500 Å (Burstein et al. 1984, Worthey et al. 1994). Other index systems have been defined at other wavelengths (e.g., Fanelli et al. 1992; Alvarez et al. 2000; Cenarro et al. 2001; Serven, Worthey & Briley 2005). In practice, the use of indices is greatly complicated by the fact that there are rarely if ever clean regions of the spectrum from which one can estimate the continuum level. The strength of each index thus depends not only on the feature of interest but also on the features in the pseudocontinua.

Tripicco & Bell (1995) were the first to assess the sensitivity of the Lick/IDS indices to variation in the abundances of 10 elements with theoretical spectral models. Korn, Maraston & Thomas (2005) provided an update to these response functions with updated line lists and transition probabilities, and for a range in metallicity. Serven, Worthey & Briley (2005) considered variation in 23 elements, including several neutron-capture elements. These researchers defined new indices sensitive to a host of elements not considered in the earlier work. The Serven models were based on theoretical spectra of only two stars per abundance pattern, a turnoff star and a luminous giant, and the model effectively had a fixed age of ∼5 Gyr. Lee et al. (2009a) provided response functions for Lick indices by employing a larger number of synthetic spectra. Conroy & van Dokkum (2012a) produced theoretical stellar spectra with variation in 11 elements. These models contained theoretical spectra at 20 points along the isochrone, for ages from 3–13.5 Gyr. Rather than focusing on spectral indices, these models made predictions for the response of the full spectrum from 3,500 Å–2.4 μm to abundance variations. Sample response spectra from that work are shown in **Figure 3**. In this figure, the relative response of the spectrum to an increase in the abundance of a particular element is shown. The full spectrum is rich in diagnostic features beyond what any index system can capture.

To construct models with arbitrary abundance patterns, one would want to create synthetic spectra for each possible abundance pattern. When considering large numbers of elements, such an approach becomes computationally infeasible. Instead, the standard technique is to create arbitrary abundance patterns by treating the effect of each element on the spectrum as being independent of the other elements (e.g., Thomas, Maraston & Bender 2003b; Schiavon 2007; Lee et al. 2009a; Conroy & van Dokkum 2012a). This is a reasonable assumption for trace elements, but it is less realistic for elements such as C, N, O, Na, Ti, and Fe, which affect the opacity, free electron density, and/or molecular equilibrium. There has been surprisingly little work in the literature testing this assumption.

2.1.4. The initial mass function. The initial distribution of stellar masses along the main sequence, known as the stellar IMF, has been studied extensively for decades (e.g., Salpeter 1955, Scalo 1986, Scalo et al. 1998, Kroupa 2001, Chabrier 2003). As emphasized in a recent review by Bastian, Covey & Meyer (2010), there is no compelling evidence for variation in the IMF from direct probes, e.g., star counts. The canonical Salpeter IMF has the form $\mathrm{d}N/\mathrm{d}M \propto M^{-x}$ with $x = 2.35$. The IMF measured in the Solar Neighborhood deviates from the Salpeter form only at $M < 1\,\mathrm{M}_{\odot}$, where x becomes smaller (Kroupa 2001, Chabrier 2003).

From the perspective of SPS, the IMF (*a*) determines the overall normalization of the stellar mass-to-light ratio, M/L; (*b*) determines the rate of luminosity evolution for a passively evolving population; (*c*) affects the SED of CSPs; and (*d*) has a small effect on the shape of the SED of single stellar populations. The last point is due to the fact that the integrated light of a coeval population

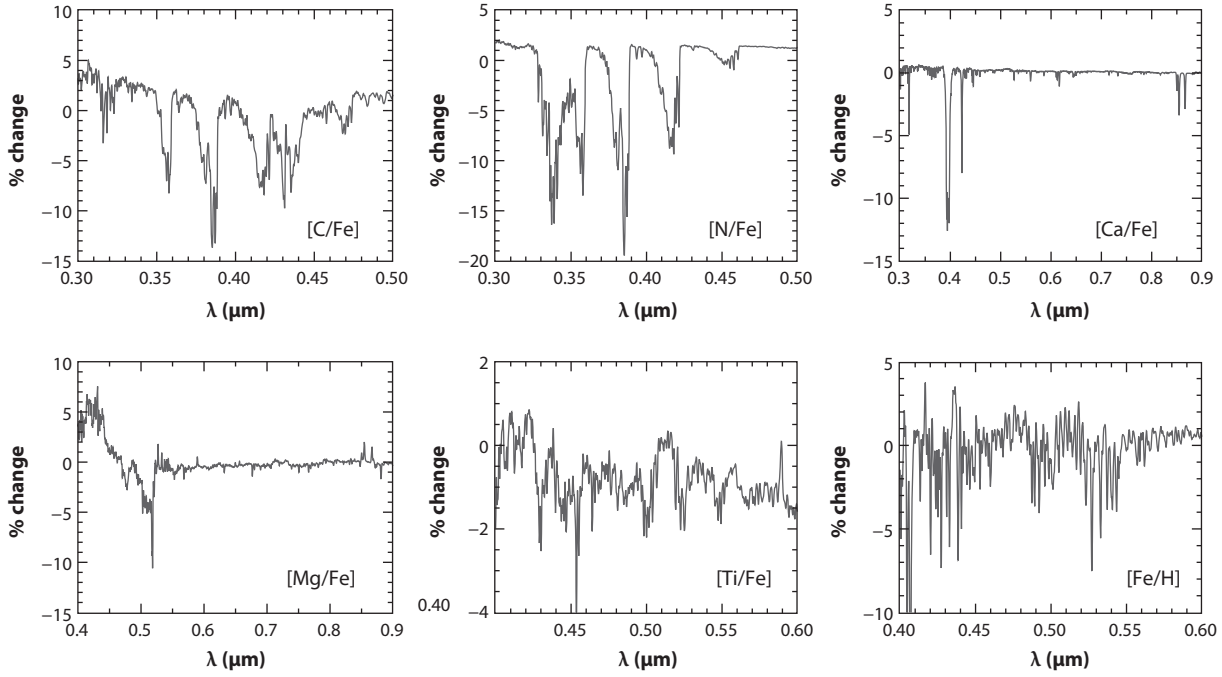

Figure 3

Variation in the spectrum of a 13-Gyr simple stellar population due to changes in individual elemental abundances. All abundance changes are +0.3 dex except for C and Ca, which have been varied by +0.15 dex. Spectra have been broadened to a velocity dispersion of 150 km s^{-1}. Notice the different *x*- and *y*-axis range in each plot. Prominent spectral features include the CH, CN, NH, C_2, CaI, CaII H and K, CaII triplet, MgH, and Mg *b* (MgI) features, along with numerous atomic Fe and Ti features. Computed from the models of Conroy & van Dokkum (2012a).

is overwhelmingly dominated by stars at approximately the same mass, i.e., the turnoff mass. Point *d* will not hold for IMFs that depart dramatically from the Salpeter IMF. Point *c* arises because CSPs have a range of turnoff masses that contribute to the integrated light. **Figure 4** shows the fractional contribution of stars of various masses to the total number of stars, stellar mass, and bolometric luminosity; the figure demonstrates quantitatively that low-mass stars dominate both the stellar mass and the number of stars in a galaxy but contribute only a few percent to the bolometric light of an old stellar population. At younger ages the light contribution from low mass stars is even less.

Tinsley (1980) demonstrated that the evolution in *M/L* for a passively evolving stellar population is sensitive to the logarithmic slope of the IMF, *x*, at the main sequence turnoff point. The logarithmic evolution of the luminosity per logarithmic time ($d\ln L/d\ln t$) scales linearly with *x*, at least for plausible values of *x* (see also van Dokkum 2008; Conroy, Gunn & White 2009). This dependency arises because the giant branch dominates the luminosity for all plausible values of *x*, and so the IMF determines the rate at which the giant branch is fed by turnoff stars. Steeper IMFs imply that the giant branch is more richly populated with time, and therefore the natural luminosity dimming is reduced. For sufficiently steep IMFs (e.g., $x \gtrsim 5$), the unevolving dwarfs would dominate the light, and so the integrated luminosity would be approximately constant over time.

It is somewhat less well appreciated that the IMF above 1 $M_\odot$ also strongly affects the shape of the SED of CSPs. In composite populations the SED is influenced by stars with a range of

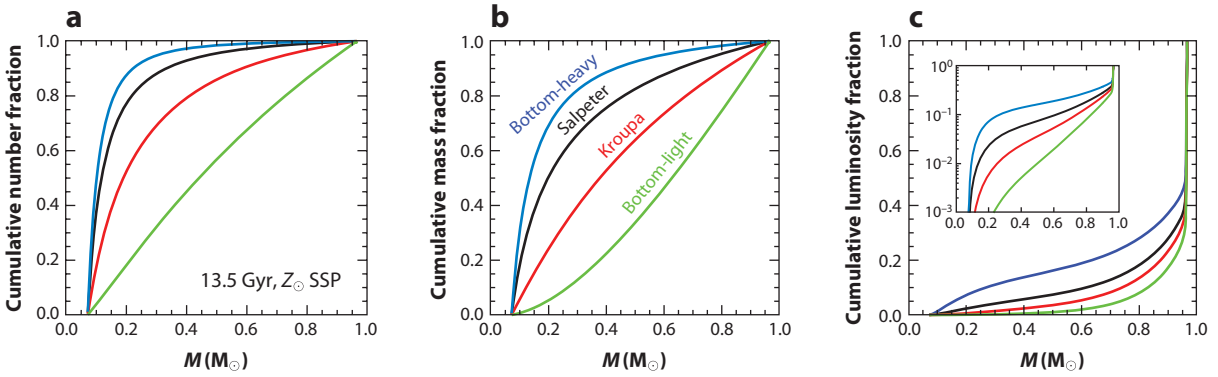

Figure 4

Fractional contribution to the total (*a*) number, (*b*) mass, and (*c*) bolometric luminosity as a function of stellar mass for a 13.5-Gyr solar metallicity model. Lines correspond to different initial mass functions (IMFs): a bottom-heavy IMF with logarithmic slope $x = 3.0$ (*blue line*); a Salpeter IMF ($x = 2.35$; *black line*); a Milky Way IMF (specifically a Kroupa IMF; *red line*); a bottom-light IMF [specifically of the form advocated by van Dokkum (2008); *green line*]. The inset in panel *c* shows the cumulative luminosity fraction in logarithmic units. Low-mass stars dominate the total number of and mass in stars but contribute a tiny fraction of the luminosity of old stellar populations. Abbreviation: SSP, simple stellar population.

masses (see Section 2.3), and so the IMF must play an important role (see, e.g., Pforr, Maraston & Tonini 2012).

2.2. Dust

Interstellar dust is a component of nearly all galaxies, especially those that are actively star-forming. Dust plays a dual role in SPS, both as an obscurer of light in the UV through NIR and as an emitter of light in the IR. For both historical and theoretical reasons, these two aspects are often modeled independently of one another. Indeed, they are sensitive to different properties of a galaxy (e.g., dust obscuration is highly sensitive to geometry, whereas dust emission is more sensitive to the interstellar radiation field), and so it is not unreasonable to decouple the modeling of these two components.

2.2.1. Attenuation. Dust grains obscure light by both absorbing and scattering starlight. From observations of individual stars, one can infer the total extinction along the line of sight by comparing an observed spectrum to the expected spectrum of the star in the absence of dust (the latter is typically obtained from models in conjunction with an estimated $T_{\rm eff}$ and $\log g$ of the source). Thus, extinction measures the total loss of light along a single line of sight. Observations in the Milky Way (MW) and Large and Small Magellanic Clouds (LMC and SMC, respectively) have been obtained for a number of sightlines, enabling construction of average extinction curves for these galaxies (Cardelli, Clayton & Mathis 1989; Pei 1992; Gordon & Clayton 1998). In the MW and LMC the only striking feature in the extinction curve is the broad absorption at 2,175 Å. This feature is absent in three out of four sightlines to the SMC, and it is weaker in the LMC than in the MW. The grain population responsible for this feature is not known, but polycyclic aromatic hydrocarbons (PAHs) are a leading candidate (Draine 2003). In general, dust extinction is a consequence of the optical properties of the grains and the grain size and shape distribution (Weingartner & Draine 2001).

When modeling SEDs of galaxies, the relevant concept is dust attenuation, which differs from extinction in two important respects: (*a*) light can be scattered both out of and into a given line

of sight, and (*b*) the geometrical distribution of dust with respect to the stars strongly affects the resulting SED (see Calzetti 2001 for an extensive discussion of these issues). The total dust attenuation in a galaxy can be estimated by analogy with how one estimates dust extinction: A spectrum of a galaxy is obtained and compared with the expected spectrum of the same galaxy in the absence of dust. For obvious reasons, estimating dust attenuation is considerably more complex than estimating dust extinction.

Although the shape of the dust attenuation curve depends on the star-dust geometry, grain size distribution, etc., in a complex manner, several general rules of thumb can be stated (see, e.g., Witt & Gordon 2000 for a more thorough discussion). The simplest dust geometry, that of a homogenous foreground screen, yields an attenuation curve whose shape depends only weakly on the total dust column density (the weak dependence arises from the scattered light component). More complex geometries generally yield attenuation curves that become grayer (i.e., shallower) as the column density increases. Clumpy interstellar media also result in grayer attenuation curves than their homogenous counterparts. In all cases, the total attenuation optical depth is less than the amount of extinction that would be produced by the same column density, because some scattered light is always returned to the line of sight. Finally, because the 2,175-Å dust feature is believed to be due to pure absorption, the effects of radiative transfer will cause this feature to respond differently to geometrical effects compared with the rest of the attenuation curve. The use of a single dust attenuation curve for analyzing a wide range of SED types is therefore without theoretical justification.

In practice, most SPS modelers include dust attenuation by fixing the shape of the attenuation curve and fitting for the normalization. Popular attenuation curves include the Calzetti law, the MW, LMC, and SMC extinction curves or the time-dependent attenuation model from Charlot & Fall (2000). The impact of the chosen attenuation curve on derived properties of galaxies will be discussed in later sections.

2.2.2. Emission. Beyond $\lambda \sim 10$ μm, the SEDs of normal galaxies are dominated by emission from dust grains. Mathis, Rumpl & Nordsieck (1977) were the first to postulate that the dust grain population is comprised of both silicate and carbonaceous grains. In modern theories, the carbonaceous grains are assumed to be PAHs when they are small and graphite when they are large (Draine 2003). The observed dust emission spectrum results from exposing these grains to a range of interstellar radiation field strengths.

A variety of models exist that combine grain size distributions and grain optical properties with models for starlight (or simply the radiation field) to predict IR emission (Desert, Boulanger & Puget 1990; Silva et al. 1998; Devriendt, Guiderdoni & Sadat 1999; Popescu et al. 2000; Dale et al. 2001; Jonsson 2006; Piovan, Tantalo & Chiosi 2006; Draine & Li 2007; Groves et al. 2008; Popescu et al. 2011). The modeling of PAH emission features (the most prominent being at 3.3 μm, 6.2 μm, 7.7 μm, 8.6 μm, and 11.3 μm) has become dramatically more sophisticated since the early attempts by Desert, Boulanger & Puget (1990), culminating in state-of-the-art models by Draine & Li (2007). At long wavelengths ($\lambda > 50$ μm) the emission is dominated by grains at a nearly steady temperature of ∼15–20 K and contributes ∼2/3 of the total IR luminosity. At shorter wavelengths the IR emission arises from single-photon heating of dust grains (including PAHs) and accounts for the remaining ∼1/3 of the total IR emission (see the review by Draine 2003 for details). The IR emission at the shortest wavelengths ($\lambda < 12$ μm) is supplied almost entirely by PAHs. In detail, these relative contributions will depend on the grain composition and size distribution and the interstellar radiation field.

The models listed above are not always well suited for interpreting large numbers of observed IR SEDs, because they contain a large number of parameters, require knowledge of the star-dust

ULIRG: ultraluminous infrared galaxy

geometry, and/or require radiative transfer calculations. Simpler models for dust emission have therefore been developed in parallel to the more complex ones. The IR templates of Chary & Elbaz (2001) and Dale et al. (2001) are widely used for estimating bolometric luminosities and *k*-corrections. These templates are based on sophisticated models but are constrained to match observations of normal star-forming and starburst [i.e., ultraluminous infrared galaxy (ULIRG)] galaxies. The resulting templates are functions of only one variable. For example, the Chary & Elbaz (2001) templates are a function of the total IR luminosity. Da Cunha, Charlot & Elbaz (2008) have developed a simple phenomenological model for dust emission that consists of a series of modified blackbodies for the thermal dust emission and for the emission from stochastically heated dust grains. In addition, they include an empirical spectrum of M17 to represent the PAH emission.

2.2.3. Dust around asymptotic giant branch stars. Stars experience very high mass-loss rates as they climb up the AGB (as high as $10^{-4}\,M_{\odot}$ year^{-1} in the superwind phase). The mass lost is observed to be dust-rich (Bedijn 1987). These stars are often heavily dust obscured in the optical and emit copiously in the IR; they are often so dusty that their SEDs peak at ∼10 μm (Bedijn 1987). Dust around AGB stars is important from the standpoint of SPS for two reasons: It will diminish the importance of AGB light in the optical and NIR, and it will contribute additional flux in the mid-IR beyond what would be expected from standard dust models (see, e.g., Kelson & Holden 2010).

Despite the obvious importance of AGB dust, this aspect is included in few SPS models. Notable exceptions include the models of Bressan, Granato & Silva (1998), Silva et al. (1998), Piovan, Tantalo & Chiosi (2003), and González-Lópezlira et al. (2010), which are all based on theoretical models for AGB stars, their mass-loss rates, and dust formation and composition. Even the use of presently available empirical libraries of AGB stellar spectra requires reddening the spectra to account for circumstellar dust (Lançon & Mouhcine 2002). Increasingly sophisticated radiative transfer models of dusty circumstellar envelopes are being developed (e.g., Sargent, Srinivasan & Meixner 2011; Srinivasan, Sargent & Meixner 2011; Groenewegen 2012). The outputs from these models should be incorporated into SPS codes as a standard practice.

2.3. Composite Stellar Populations

The SSPs discussed in Section 2.1 are the building blocks for more complex stellar systems. Composite stellar populations (CSPs) differ from simple ones in three respects: (*a*) they contain stars with a range of ages given by their SFH; (*b*) they contain stars with a range in metallicities as given by their time-dependent metallicity distribution function, $P(Z, t)$; and (*c*) they contain dust. These components are combined in the following way:

$$f_{\rm CSP}(t) = \int_{t'=0}^{t'=t} \int_{Z=0}^{Z_{\rm max}} \Big({\rm SFR}(t-t') P(Z, t-t') f_{\rm SSP}(t', Z) e^{-\tau_d(t')} + A\, f_{\rm dust}(t', Z) \Big)\, {\rm d}t'\, {\rm d}Z, \qquad (2)$$

where the integration variables are the stellar population age, t', and metallicity, Z. Time-dependent dust attenuation is modeled via the dust optical depth, $\tau_d(t')$, and dust emission is incorporated in the function $f_{\rm dust}$. The normalization constant A is set by balancing the luminosity absorbed by dust with the total luminosity reradiated by dust.

The SFH can in principle be arbitrarily complex, although simple forms are usually adopted. By far the most popular is the exponential, or τ model, where ${\rm SFR} \propto e^{-t/\tau}$. This form arises naturally in scenarios where the SFR depends linearly on the gas density in a closed-box model (Schmidt 1959). Recently, rising SFHs have become popular to explain the SEDs of high-redshift galaxies

(Maraston et al. 2010, Papovich et al. 2011). Rising SFHs at early times seem to be a natural consequence of galaxy evolution in a hierarchical Universe (Finlator, Davé & Oppenheimer 2007; Lee et al. 2010). Functional forms that incorporate an early phase of rising SFRs with late-time decay, such as SFR $\propto t^{\beta} e^{-t/\tau}$, may therefore become more popular among modelers.

The treatment of metallicity in CSPs is usually even more simplistic than the treatment of SFRs. The widely adopted simplification is to replace $P(Z, t)$ in Equation 2 with a δ-function. In other words, a single metallicity is assumed for the entire composite population. The impact of this simplification on the SPS modeling procedure has not been extensively explored.

The approach to Equation 2 outlined above is standard but not universal. A notable exception is the technique of fitting nonparametric SFHs and metallicity histories in either a predefined or adaptive set of age bins (Cid Fernandes et al. 2005, Ocvirk et al. 2006, Tojeiro et al. 2009). The latter approach is computationally expensive because as many as 30 parameters are simultaneously fit to the data. Very-high-quality data are also a prerequisite for nonparametric techniques. Nonetheless, they offer the promise of less biased reconstruction of the SFH and metallicity history of galaxies based solely on their SEDs.

Figure 5 presents some basic properties of CSPs, including the fractional flux contribution from stars in different evolutionary phases for three representative SFHs (**Figure 5*a–c***). At late times the RGB and red HB dominate the red and NIR flux of τ-model SFHs, as is well known. However, at young ages and/or for rising SFHs, the red and NIR are also influenced strongly by AGB stars, suggesting that the NIR can be susceptible to large uncertainties (due to uncertainties in the modeling of the AGB, as discussed in detail in later sections). **Figure 5*d*** shows the fractional flux contribution from stars more massive than 20 $M_{\odot}$ and 60 $M_{\odot}$ for a $\tau = 10$-Gyr SFH. Massive star evolution is uncertain owing to the complicating effects of rotation and binarity; thus **Figure 5*d*** provides a rough sense of the extent to which uncertainties in massive star evolution will affect SED modeling. Finally, **Figure 5*e*** shows the light-weighted age as a function of wavelength, again for a $\tau = 10$-Gyr SFH; the dashed line indicates the mass-weighted mean age. Already by 0.5 μm (approximately the V-band), the light-weighted age reaches its maximal value, again suggesting that going to redder restframe wavelengths is not providing substantial new information on the SFH. Notice also that the maximum light-weighted age never reaches the mass-weighted age. We return to this point in Section 4.

2.4. Nebular Emission

Although the effects of nebular emission on SEDs are not discussed in detail in this review, a brief overview of this component is given for completeness.

Nebular emission is comprised of two components: continuum emission consisting of free-free, free-bound, and two-photon emission, and recombination line emission. Several photoionization codes exist that make predictions for the nebular emission as a function of the physical state of the gas, including Cloudy (Ferland et al. 1998) and MAPPINGSIII (Groves, Dopita & Sutherland 2004). Other approaches can be taken to the modeling of nebular emission lines. For example, Anders & Fritze-von Alvensleben (2003) implement nonhydrogen emission lines based on observed line ratios as a function of metallicity. The nebular emission model must then be self-consistently coupled to a model for the starlight. Several groups have done this, with varying degrees of complexity, and with some including only nebular continuum, others only line emission, and others both (e.g., Leitherer et al. 1999; Charlot & Longhetti 2001; Panuzzo et al. 2003; Groves et al. 2008; Mollá, García-Vargas & Bressan 2009; Schaerer & de Barros 2010).

The effect of nebular emission on the SED is complex, especially when line emission is considered. As a general rule, nebular emission is more important at low metallicity and at young ages.

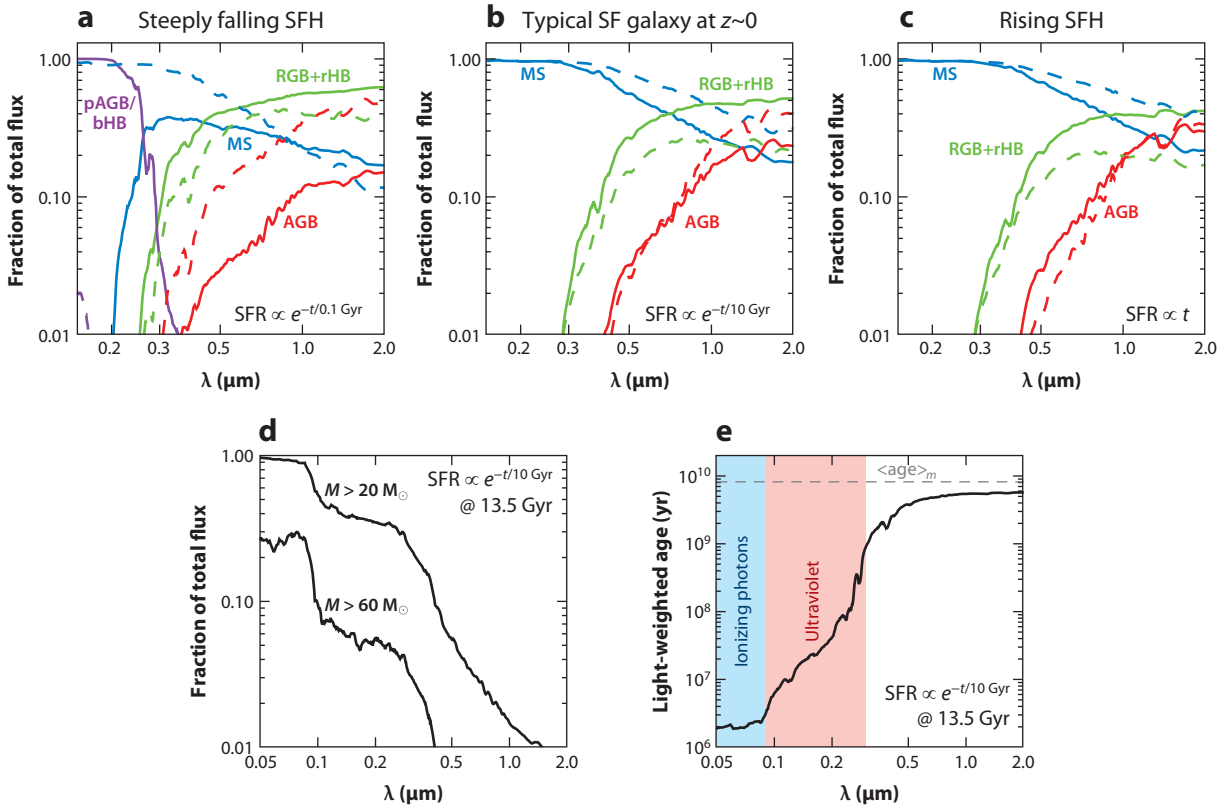

Figure 5

(*a–c*) Fractional contribution to the total flux from stars in various evolutionary phases for three different star-formation histories (SFHs). Panel *a* is representative of a galaxy that formed nearly all of its stars very rapidly at early times, panel *b* is representative of a typical star-forming galaxy at $z \sim 0$, and panel *c* may be representative of the typical galaxy at high redshift. Flux contributions are at 13 Gyr (*solid lines*) and 1 Gyr (*dashed lines*) after the commencement of star formation (SF); all models are solar metallicity, dust-free, and from FSPS (v2.3; Conroy, Gunn & White 2009). Labeled phases include the main sequence (MS), RGB, asymptotic giant branch [AGB, including the thermally pulsating (TP-)AGB], post-AGB (pAGB), and blue and the red horizontal branch (bHB and rHB). (*d*) Fractional flux contributions for stars more massive than 20 $M_\odot$ and 60 $M_\odot$ for the SFH shown in panel *b*. (*e*) Light-weighted age as a function of wavelength for the same SFH. The dashed line indicates the corresponding mass-weighted age. Abbreviations: FSPS, Flexible Stellar Population Synthesis; SFR, star-formation rate.

In such cases the contribution of nebular emission to broadband fluxes can be as high as 20–60% (Anders & Fritze-von Alvensleben 2003). Nebular emission will also be more important at high redshift because a feature with a fixed restframe EW will occupy a larger fraction of the filter band pass due to the redshifting of the spectrum. The effect of nebular emission therefore cannot be ignored at high redshift, where high-SFR, low-metallicity galaxies are common (Schaerer & de Barros 2010, Atek et al. 2011).

It is noteworthy that among the most widely used SPS codes, including those of Bruzual & Charlot (2003), Maraston (2005), PEGASE (Fioc & Rocca-Volmerange 1997), STARBURST99 (Leitherer et al. 1999), and FSPS (Flexible Stellar Population Synthesis) (Conroy, Gunn & White 2009), only PEGASE and STARBURST99 include nebular continuum emission, and only PEGASE includes both nebular continuum and line emission. As nebular emission is relatively

straightforward to implement (notwithstanding assumptions about the physical state of the gas), it should be a standard component of all SPS codes.

2.5. Fitting Models to Data

The SPS models described in this section are most frequently used to measure physical parameters of stellar populations. This is achieved by fitting the models to data, either in the form of broadband SEDs, moderate-resolution optical/NIR spectra, or spectral indices. The SSPs are usually taken as given, and the user then fits for a variety of parameters, including metallicity, dust attenuation, and one or more parameters for the SFH. If IR data are available, then additional variables must be considered. The fitting techniques vary but are generally limited to grid-based χ^2 minimization techniques. As the number of parameters increases, Markov Chain Monte Carlo techniques become increasingly more efficient (Conroy, Gunn & White 2009; Acquaviva, Gawiser & Guaita 2011). One must also be aware of the influence of the chosen priors on the derived parameters; in cases where parameters are poorly constrained, the prior can have a significant effect on the best-fit values (see, e.g., Kauffmann et al. 2003, Salim et al. 2007, Taylor et al. 2011 for discussion). Moreover, it is highly advisable to derive the best-fit parameters from the marginalized posterior distribution, rather than from the minimum of χ^2, since the likelihood surface can often be highly irregular (see, e.g., Bundy, Ellis & Conselice 2005; Taylor et al. 2011).

When fitting SEDs, it is important to remember that only the shape is being used to constrain the model parameters. In other words, the SED shape (or, more crudely, broadband colors) constrains parameters such as M/L, specific SFR (SSFR $\equiv$ SFR/M), dust attenuation, and metallicity. To obtain stellar masses one needs to multiply M/L by the observed luminosity and to obtain SFRs one then multiplies SSFR by M. This also holds true for M/L ratios and SSFRs inferred from EWs of emission lines, spectral indices, and full spectral fitting.

The reader is referred to Walcher et al. (2011) for further details on SED fitting techniques.

3. MASS-TO-LIGHT RATIOS AND STELLAR MASSES

3.1. Techniques and Uncertainties

There are three basic techniques for estimating the stellar mass-to-light ratio, M/L, of a galaxy: (*a*) using tabulated relations between color and M/L, (*b*) modeling broadband photometry, and (*c*) modeling moderate-resolution spectra. The first technique is the simplest to use as it requires photometry in only two bands and no explicit modeling. The other techniques require construction of a library of models and a means to fit those models to the data. How do these different techniques compare?

3.1.1. Color-based *M/L* ratios. The color-based M/L estimators have their origin in the pioneering work of Bell & de Jong (2001). These researchers used a preliminary version of the Bruzual & Charlot (2003) SPS model to chart out the relation between M/L and color as a function of metallicity and SFH. Remarkably, they found that variation in metallicity and SFH (parameterized as a τ model) moved galaxies along a well-defined locus in the space of M/L_B versus $B-R$, suggesting that the $B-R$ color could be a useful proxy for M/L_B. Perhaps most important, they demonstrated that the dust-reddening vector was approximately parallel to the inferred color-M/L relation, implying that dust should have only a second-order effect on derived stellar masses. They also investigated NIR colors and found much larger variation in M/L at fixed $I-K$, due mostly to variation in the SFH. Late bursts of SF complicate the interpretation of color-M/L relations

by driving the *M/L* ratios lower at fixed color compared with smoothly declining SFHs. Their analysis was for a fixed IMF; allowing for IMF variation will change the *M/L* while leaving the color basically unchanged. Bell & de Jong (2001) concluded that for a fixed IMF, assuming that large starbursts and low-metallicity systems are not common properties of galaxies and neglecting uncertainties in the SPS models, one could estimate *M/L* from a single color to an accuracy of ∼0.1–0.2 dex.

In subsequent work, Bell et al. (2003) analyzed the optical-NIR SEDs of ∼12,000 galaxies with SDSS and 2MASS photometry. They constructed a grid of SPS models with varying SFHs, including bursts, and metallicity. They did not allow for reddening due to dust. They derived best-fit *M/L* values from SED fitting and created new, observationally constrained color-*M/L* relations. The resulting $B-R$ versus M/L_B relation was similar to that of Bell & de Jong (2001), but the NIR relation was considerably more shallow than in the earlier work. At the bluest colors, the M/L_K ratios differed by ≈0.3 dex between the old and new relations. The difference arose due to a population of galaxies with blue observed colors and high inferred *M/L* ratios, which Bell et al. (2003) interpreted as being due to the lower metallicities allowed in their fitting procedure compared with the analytic models of Bell & de Jong. These differences are of some concern because the Bell et al. (2003) color-*M/L* relations are very widely used to derive "cheap" stellar mass estimates of galaxies.

Zibetti, Charlot & Rix (2009) revisited this issue with new SPS models from S. Charlot & G. Bruzual (in preparation). They followed a somewhat different approach compared with Bell et al. (2003) in that they constructed color-*M/L* relations directly from a library of model galaxies. This approach is sensitive to how one chooses to populate parameter space, as the resulting color-*M/L* relations are simple averages over the model space. In contrast, Bell et al. (2003) constructed color-*M/L* relations from only those models that provided good fits to observed optical-NIR photometry. Zibetti, Charlot & Rix (2009) allowed for dust attenuation, and they also allowed for larger mass fractions of stars formed in recent bursts compared with Bell et al. They found substantial differences in the $g-i$ color-*M/L* relation compared with Bell et al. (∼0.5 dex at the bluest colors), which they attributed to their allowance for much stronger bursts of star formation than allowed in Bell et al. (2003). Gallazzi & Bell (2009) also found a very different color-*M/L* relation compared with Bell et al. (2003), which they attributed to the different age distributions in their model library. Taylor et al. (2011) followed the philosophy of Bell et al. (2003) in fitting models to observed SEDs in order to derive color-*M/L* relations. They found systematic differences of order 0.1–0.2 dex compared with the Zibetti, Charlot & Rix relations, which they attributed mostly to their decision to select only those models that fit the photometric data, and also to the treatment of dust reddening.

Zibetti, Charlot & Rix (2009) found a large difference in M/L_H ratios estimated from $i-H$ colors between the new Charlot & Bruzual models and the previous version (Bruzual & Charlot 2003), with typical offsets of 0.2–0.4 dex. This difference is largely due to the different treatment of the TP-AGB evolutionary phase (see Section 3.2 for details). In contrast, optical color-*M/L* relations showed little difference between the two SPS models and also showed slightly less discrepancy with Bell et al. (2003). These researchers argued that optical color-*M/L* relations should generally be preferred to NIR-based ones owing to the larger impact of the uncertain TP-AGB phase in the NIR. Exceptions to this rule could be made for galaxies with very large amounts of dust reddening and/or very strong starbursts, in which cases the optical SED becomes a poor indicator of the SFH and hence *M/L*. The upshot is that NIR color-based *M/L* estimates should be treated with caution, as they are subject to large stellar evolution-based systematics. However, both optical and NIR-based *M/L* estimates will depend on the allowed range of SFHs and metallicities in the model library, with large systematics appearing for the bluest colors.

3.1.2. *M/L* from broadband and spectral fitting techniques. The modern era of SED fitting with SPS models was ushered in by Sawicki & Yee (1998) and Giallongo et al. (1998), who analyzed optical-NIR broadband photometry of high-redshift galaxies. The model grid by Sawicki & Yee (1998) consisted of an SFH that was either an instantaneous burst or a constant, and variation in metallicity and reddening. Subsequent modeling of broadband data has largely followed this approach, though with some differences in the choice of model SFHs (e.g., Sawicki & Yee 1998; Brinchmann & Ellis 2000; Papovich, Dickinson & Ferguson 2001; Shapley et al. 2001; Salim et al. 2007). Generically, when fitting broadband SEDs, one finds that stellar masses for "normal" galaxies (i.e., not including pathological SFHs) can be recovered at the ≈0.3 dex level (1σ uncertainty). This uncertainty does not include potential systematics in the underlying SPS models (see Section 3.2). Stellar masses appear to be the most robust parameter estimated from SED fitting (e.g., Papovich, Dickinson & Ferguson 2001; Shapley et al. 2001; Lee et al. 2009b; Muzzin et al. 2009; Wuyts et al. 2009). The reason for this is not fully understood, although it probably is at least partly due to the fact that the dust reddening vector is approximately parallel to SFH and metallicity variations in color-*M/L* diagrams (Bell & de Jong 2001). The choice of the SFH, in particular whether it is rising, declining, or bursty, can significantly change the best-fit stellar mass, by perhaps as much as 0.6 dex in extreme cases (Pforr, Maraston & Tonini 2012). A general rule of thumb is that *M/L* ratios estimated via simple SFHs (or single-age models) will be lower limits to the true *M/L* ratios (Papovich, Dickinson & Ferguson 2001; Shapley et al. 2001; Trager, Faber & Dressler 2008; Graves & Faber 2010; Pforr, Maraston & Tonini 2012). This is a consequence of the fact that young stars outshine older ones, making it relatively easy to "hide" old stellar populations in galaxies with a large number of young stars. This also explains why color-*M/L* relations are so uncertain for very blue colors. This general rule is not universal: The modeling of certain galaxy types may lead to systematic biases in the opposite direction (Gallazzi & Bell 2009). Partly for these reasons, stellar masses estimated for quiescent systems should be more reliable than for star-forming ones. Relatedly, Zibetti, Charlot & Rix (2009) demonstrated that stellar masses estimated for individual nearby galaxies based on a pixel-by-pixel analysis of colors are generally larger than those estimated from integrated colors. The differences are typically ∼0.05–0.15 dex, depending on galaxy type. This should not be surprising, especially for systems with star-forming disks and quiescent bulges, since the *M/L* ratio estimated from the integrated colors will tend to be biased low by the more luminous young stars in the star-forming component. Wuyts et al. (2012) performed a similar analysis on galaxies at $0.5 < z < 2.5$ with WFC3 *Hubble Space Telescope* (HST) photometry and found no systematic difference in stellar masses derived from resolved versus integrated light, although the fact that their galaxies were at high redshift means that they were probing spatial scales an order of magnitude larger than in Zibetti, Charlot & Rix (2009).

There has been some confusion in the literature regarding the importance of restframe NIR photometry for estimating stellar masses. First, as indicated in **Figure 5**, for smoothly varying SFHs, photometry at and redward of the *V*-band is sensitive to the same light-weighted age, and so redder bands do not provide stronger constraints on the mean stellar age. Taylor et al. (2011) analyzed mock galaxies and concluded that the addition of NIR data did not yield more accurate mass measurements. Taylor et al. also found that different SPS models produced good agreement in derived properties when NIR data were excluded from their fits but poor agreement when NIR data were included. These researchers also found much larger residuals in their SED fits when NIR data were included, suggesting that the models are still poorly calibrated in this regime. As discussed in Section 5.2, the NIR is at present probably most useful for constraining metallicities (within the context of a particular SPS model), and so NIR data may be useful in cases where there is a degeneracy between *M/L* and *Z*. In general, however, stellar mass estimates do not appear

to be strongly improved with the addition of NIR data, at least with presently available models. Exceptions to this rule may be made for galaxies with very high dust opacities.

As first emphasized by Bell & de Jong (2001) and Bell et al. (2003), some of the largest uncertainties in derived *M/L* ratios stem from uncertainties in the assumed SFHs, in particular the presence of bursty SF episodes. The consideration of the Balmer lines with other age and metallicity-sensitive features, such as the 4,000-Å break (D_n4000), can constrain the burstiness of the SFH. Optical spectra therefore offer the possibility of providing stronger constraints on the *M/L* ratio. Kauffmann et al. (2003) modeled the Hδ and D_n4000 spectral features measured from SDSS spectra in order to constrain SFHs and *M/L* ratios. They obtained 95% confidence limits on stellar masses of ∼0.2 dex and ∼0.3 dex for quiescent and star-forming galaxies, respectively. Again, these are statistical uncertainties because the underlying SPS model and other aspects such as the adopted parameterization of the SFH were held fixed. Chen et al. (2012) employed principal component analysis (PCA) to model the optical spectra of massive galaxies in SDSS. These researchers found systematic uncertainties in the recovered stellar masses of order ∼0.1 dex, depending on the assumed metallicity, dust model, and SFH. They also demonstrated that their PCA technique was capable of measuring parameters at much lower S/N than direct fitting to selected spectral indices. They determined statistical uncertainties on their mass measurements to be ∼0.2 dex, which they showed to be comparable to the formal errors estimated from modeling broadband photometry. This result is in agreement with Gallazzi & Bell (2009), who argued that for galaxies with simple SFHs and lacking dust, the uncertainty on the derived masses is not much larger when using color-based estimators compared with spectroscopic-based estimators. With regard to estimating *M/L*, the real value of spectra appears to be restricted to galaxies with unusual SFHs.

The comparison of spectroscopically based and photometrically based stellar masses is informative because the approaches suffer from different though by no means orthogonal systematics. The most obvious difference is with regard to dust: Spectroscopic masses are much less sensitive to dust attenuation than photometric masses. Drory et al. (2004) compared their own photometrically derived masses to the spectroscopic masses from Kauffmann et al. (2003). They found a root mean square scatter of ∼0.2 dex between the two estimates, with a modest systematic trend that correlated with Hα EW. Blanton & Roweis (2007) estimated photometric stellar masses via a technique that is similar to PCA except that the templates are constrained to be nonnegative and are based on an SPS model. They compared their derived stellar masses to those of Kauffmann et al. and found good agreement, with systematic trends between the two restricted to $\lesssim$0.2 dex.

Figure 6 shows a comparison of stellar masses for the same galaxies estimated with different fitting techniques, SPS models, and priors (Moustakas et al. 2012). The galaxies included in this figure are predominantly "normal" star-forming and quiescent $z \sim 0$ galaxies. For these galaxies, the mean absolute differences between various mass estimators is less than 0.2 dex, which is in agreement with other work on the systematic uncertainties in stellar masses of normal galaxies.

3.2. Uncertainties in *M/L* Due to Stellar Evolution Uncertainties

Maraston et al. (2006) were the first to draw attention to the sensitivity of derived stellar masses to uncertain stellar evolutionary phases, in particular the TP-AGB. The Maraston (2005) SPS model predicts much more luminosity arising from TP-AGB stars than in previous models (e.g., Fioc & Rocca-Volmerange 1997, Bruzual & Charlot 2003). At ages where the TP-AGB phase is most prominent ($\sim 3 \times 10^8 - 2 \times 10^9$ year), Maraston's model predicts approximately a factor of two more flux at >1 μm compared with earlier work. Maraston et al. (2006) found that her SPS model implied a factor of two smaller stellar mass, on average, compared with masses derived with the

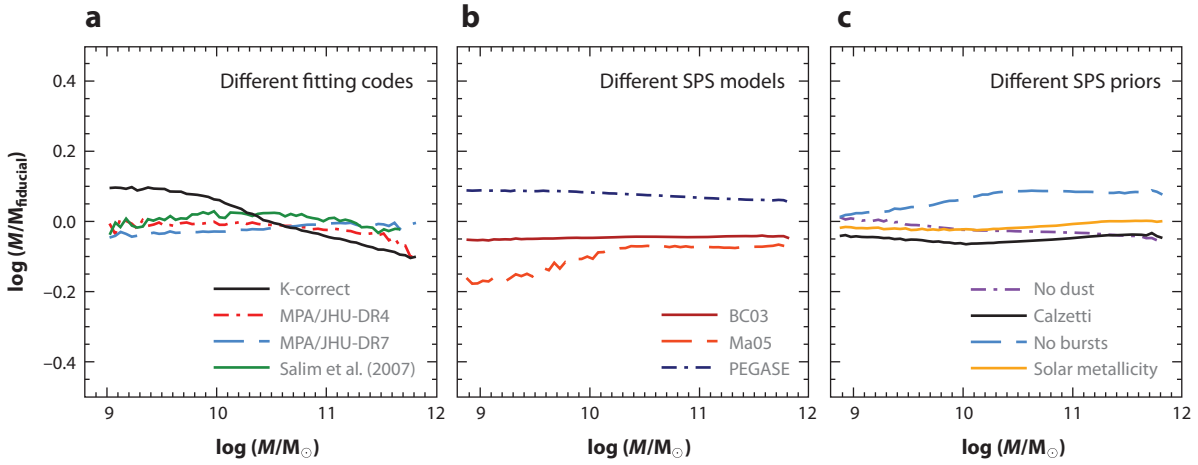

Figure 6

Comparison of different (*a*) fitting codes, (*b*) stellar population synthesis (SPS) models, and (*c*) priors on derived stellar masses. The fiducial masses are based on fitting SDSS and GALEX photometry of $z \sim 0$ galaxies using the `iSEDfit` code (Moustakas et al. 2012), with simple stellar populations (SSPs) from FSPS (Conroy, Gunn & White 2009), including dust attenuation, a range in metallicities, and star-formation histories with both smooth and bursty components. Panel *a* compares stellar mass catalogs produced by different groups/codes. K-correct and MPA/JHU-DR7 are based on SDSS photometry, MPA/JHU-DR4 on SDSS spectral indices, and Salim et al. (2007) on SDSS and GALEX photometry. Panel *b* shows the effect of different SPS models (i.e., different SSPs), and panel *c* shows the effect of varying the priors on the model library. The mean systematic differences between mass estimators are less than ± 0.2 dex. Figure courtesy of J. Moustakas (Moustakas et al. 2012). Abbreviations: FSPS, Flexible Stellar Population Synthesis; SDSS, Sloan Digital Sky Survey.

Bruzual & Charlot (2003) SPS model for galaxies at $z \sim 2$. When the fits excluded the possibility of dust reddening, Maraston's model provided a better fit to the optical-NIR SEDs than previous models, whereas when dust was allowed, the quality of the fits became indistinguishable, although the offsets in best-fit masses remained.

Subsequent work has largely confirmed the sensitivity of estimated stellar masses to the adopted SPS model (Kannappan & Gawiser 2007; Wuyts et al. 2007; Cimatti et al. 2008; Conroy, Gunn & White 2009; Longhetti & Saracco 2009; Muzzin et al. 2009). Essentially all work on this topic has focused on comparing Maraston's model to Bruzual & Charlot's, where the difference in TP-AGB treatment is probably the most significant, though not the only, difference (other differences include different RGB temperatures and different treatments for core convective overshooting). Many researchers have found a difference of a maximum factor of ∼2–3 in derived M/L ratios between the two models, especially when NIR data were included. Kannappan & Gawiser (2007) showed that the differences between Maraston's and Bruzual & Charlot's models are relatively modest ($\lesssim$1.3) when NIR data are excluded. Conroy, Gunn & White (2009) constructed a new SPS model in which the luminosity contribution from the TP-AGB phase could be arbitrarily varied. These researchers isolated the importance of the TP-AGB phase and confirmed previous work indicating that the adopted weight given to this phase in the models can have a large modulating effect on the stellar mass.

The contribution of TP-AGB stars to the integrated light peaks at $\sim 3 \times 10^8 - 2 \times 10^9$ year, depending on metallicity, and so the importance of this phase to modeling SEDs will depend on the SFH of the galaxy. It was for this reason that Maraston et al. (2006) focused their efforts on quiescent galaxies at $z \sim 2$; at this epoch even a quiescent galaxy will have a typical stellar age no older than several gigayears. In addition to high-redshift quiescent galaxies, Lançon et al. (1999)

suggested that poststarburst galaxies should harbor large numbers of TP-AGB stars because their optical spectra show strong Balmer lines, indicative of large numbers of 10^8–10^9-year-old stars. This fact was exploited by Conroy & Gunn (2010), Kriek et al. (2010), and Zibetti et al. (2012) to constrain the TP-AGB contribution to the integrated light. These researchers find evidence for a low contribution from TP-AGB stars, and in particular, they argue that Maraston's models predict significantly too much flux in the NIR for these objects.

The situation with TP-AGB stars is extremely complex owing to the fact that this phase is so sensitive to age and metallicity. Moreover, using galaxy SEDs to constrain the importance of this phase is difficult because many parameters must be simultaneously constrained (metallicity, SFH, dust, etc.). A case in point is the analysis of high-redshift galaxies, where Maraston et al. (2006) found large differences in the quality of the fit of Bruzual & Charlot models, depending on whether or not dust was included in the fits (as an aside, if these galaxies do have copious numbers of TP-AGB stars, then one may expect them to also contain dust, because these stars are believed to be efficient dust factories). It is also worth stressing that the conclusion to the TP-AGB controversy may not be an either/or situation in the sense that some models may perform better for some ranges in age and metallicity, whereas other models may perform better in different regions of parameter space. Ultimately of course we desire models that perform equally well over the full range of parameter space, and this requires a continual evolution and improvement of SPS models.

There are other aspects of stellar evolution that are poorly constrained, including convective overshooting, blue stragglers, the HB, and even the temperature of the RGB. The propagation of these uncertainties into derived properties such as *M/L* ratios is only just beginning (e.g., Conroy, Gunn & White 2009). For example, Melbourne et al. (2012) have demonstrated that the latest Padova isochrones fail to capture the observed flux originating from massive core helium burning stars as observed in nearby galaxies. These stars are very luminous and can dominate the NIR flux of young stellar populations ($\lesssim$300 Myr).

Finally, it is worth stressing that the effect of TP-AGB stars is limited to galaxies of a particular type, in particular those that are dominated by stars with ages in the range $\sim 3 \times 10^8 - 2 \times 10^9$ year. Examples include poststarburst galaxies, which are rare at most epochs, or quiescent galaxies at $z \gtrsim 2$. For typical galaxies at $z \sim 0$, the treatment of this phase seems to be of little relevance for estimating stellar masses, at least on average, as is evident in **Figure 6**.

3.3. Stellar Masses at High Redshift

Galaxies with high SFRs can in principle contain a large population of "hidden" older stars, as these stars have high *M/L* ratios. Papovich, Dickinson & Ferguson (2001) found that their data allowed for significantly larger stellar masses when two-component SFH models (young + old) were compared with their fiducial single-component models (a median difference of a factor of $\approx$3, with extreme cases differing by an order of magnitude). This issue becomes more severe at higher redshifts because the typical SFRs are higher and because of the increasing possibility of rising SFHs (to be discussed in detail in Section 4). This makes the analysis of high-redshift-galaxy SEDs much more complicated.

However, at the highest redshifts ($z \gtrsim 6$), the analysis of SEDs may actually become simpler. At $z = 8$, the age of the Universe is only $\approx$640 Myr, and if one presumes that galaxy formation commences after $z \approx 20$, then even the oldest stars at $z = 8$ will be no more than $\approx$460 Myr old. The oldest possible main sequence turnoff stars will thus be A-type stars. Put another way, the *M/L* ratio in the blue (*U*- through *V*-bands) at 13 Gyr is 4.5–15 times higher for an instantaneous burst of SF compared with a constant SFH, whereas the *M/L* ratio for these two SFHs differs by the more modest 2.5–5 at 500 Myr. So there is some expectation that "hidden" mass will be

less hidden when modeling SEDs at the highest redshifts. This expectation appears to be borne out by detailed modeling. Finkelstein et al. (2010) analyzed the SEDs of $z \sim 7$–8 galaxies and concluded that even allowing for the possibility of extreme amounts of old stars (90% by mass), the best-fit stellar masses increased by no more than a factor of two compared with a fiducial single-component SFH (see also Curtis-Lake et al. 2013).

At even higher redshifts ($z \gtrsim 10$), the analysis of galaxy SEDs may become even simpler, at least with regard to estimating stellar masses. At sufficiently high redshifts the age of the oldest possible stars will eventually become comparable to the SF timescale probed by the restframe UV ($\sim 10^8$ year at ~2,500 Å; see **Figure 5**). The measured SFR will thus be averaged over roughly the entire age of the galaxy, implying that a reasonable estimate of the stellar mass can be obtained by multiplying the UV-derived SFR with the age of the Universe. This may in fact explain the unexpectedly strong correlation between stellar mass and UV luminosity at $z > 4$ reported by González et al. (2011). However, at the highest redshifts other difficulties arise, including accounting for the effects of very high EW emission lines and the reliability of the underlying models at very low metallicities.

3.4. Summary

M/L ratios for most galaxies with normal SEDs are probably accurate at the ~0.3 dex level, for a fixed IMF, with the majority of the uncertainty dominated by systematics (depending on the type of data used). Galaxies with light-weighted ages in the range of ~0.1–1 Gyr will have more uncertain *M/L* ratios, with errors as high as factors of several, owing to the uncertain effect of TP-AGB stars and perhaps other stars in advanced evolutionary phases. Galaxies that have very young light-weighted ages (e.g., high-redshift and starburst galaxies) will also have very uncertain *M/L* ratios because of the difficulty in constraining their past SFHs. Uncertainties due to dust seem to be subdominant to other uncertainties, at least for standard reddening laws and modest amounts of total attenuation. Essentially all stellar masses are subject to an overall normalization offset due to both the IMF and the uncertain contribution from stellar remnants. Owing to the lingering model uncertainties in the NIR (e.g., from TP-AGB and cool core helium burning stars), it may be advisable to derive physical parameters by modeling the restframe UV-optical (see, e.g., the discussion in Taylor et al. 2011).

4. STAR-FORMATION RATES, HISTORIES, AND STELLAR AGES

4.1. Measuring Star-Formation Rates

The practice of measuring SFRs from monochromatic indicators (and combinations thereof) is well established (see, e.g., the reviews of Kennicutt 1998, Kennicutt & Evans 2012). A wide variety of relations have been established between SFRs and the UV, Hα, Pα, 24-μm luminosity, total IR luminosity, radio continuum luminosity, and even the X-ray flux. As they are not the focus of the present review, only a few brief remarks will be given regarding monochromatic SFR indicators. Each indicator is sensitive to a different SFR timescale, with ionizing radiation (as probed by, e.g., the recombination lines) being sensitive to the shortest timescale, $\sim 10^6$ year, and the UV and total IR being sensitive to longer timescales, e.g., $\sim 10^8$ year. In detail, the UV and IR are sensitive to a range of SF timescales, depending on wavelength and SFH. In the IR this sensitivity arises because shorter wavelengths are probing dust heated mostly by HII regions, whereas FIR photons are sensitive to dust heated by both old and young stars. Among the recombination lines, "redder is better" because dust attenuation will be less severe at longer wavelengths, and so Pα should be

preferred over Hα. For reference, an attenuation of 1 mag in the V-band implies an attenuation of only 0.15 mag at Pα, for standard attenuation curves. The optical and UV SFR indicators require correction for dust when used on their own. For this reason, mixed SFR indicators have become popular, usually via the combination of UV and IR or Hα and IR indicators (Calzetti et al. 2007, Kennicutt et al. 2007).

Estimating SFRs from SED fitting is very challenging for several reasons: (*a*) the age-dust-metallicity degeneracy makes it difficult to reliably measure ages and hence SFRs unless high quality data are available (see Section 6), and (*b*) the choice of priors on the dust model and SFH library imposes often severe biases on the resulting ages and SFRs. These difficulties were recognized early on in the study of high-redshift galaxies (Sawicky & Yee 1998; Papovich, Dickinson & Ferguson 2001) and are still relevant today.

Brinchmann et al. (2004) measured SFRs for SDSS galaxies by modeling a suite of optical emission lines. Their model included variation in the total metallicity, dust attenuation, ionization parameter, and dust-to-metals ratio. As the SDSS is a fiber-based survey, these researchers had to make a correction for the fact that the spectra sample only a fraction of the galaxy light. In addition, they modeled the stellar continuum in order to subtract any absorption features under the emission lines. Salim et al. (2007) analyzed a comparably sized sample of $z \sim 0$ galaxies, focusing on UV photometry from the *Galaxy Evolution Explorer* (GALEX) and optical photometry from SDSS. These researchers fit the data to SPS models with a range of SFHs (including exponentially declining SFHs and superimposed starbursts), metallicities, and dust attenuation. They presented a direct comparison of their SED-based SFRs and the emission line–based SFRs from Brinchmann et al. (2004). The result is shown in **Figure 7**. Although the overall agreement is good, there is a systematic trend, with stellar mass resulting in offsets of ~0.2 dex at the low- and high-mass ends. Salim et al. explored the origin of this offset and concluded that the different derived dust attenuation optical depths between the two methods were the source of the discrepancy. They further speculated that in most cases it was the emission line–based dust attenuation values that

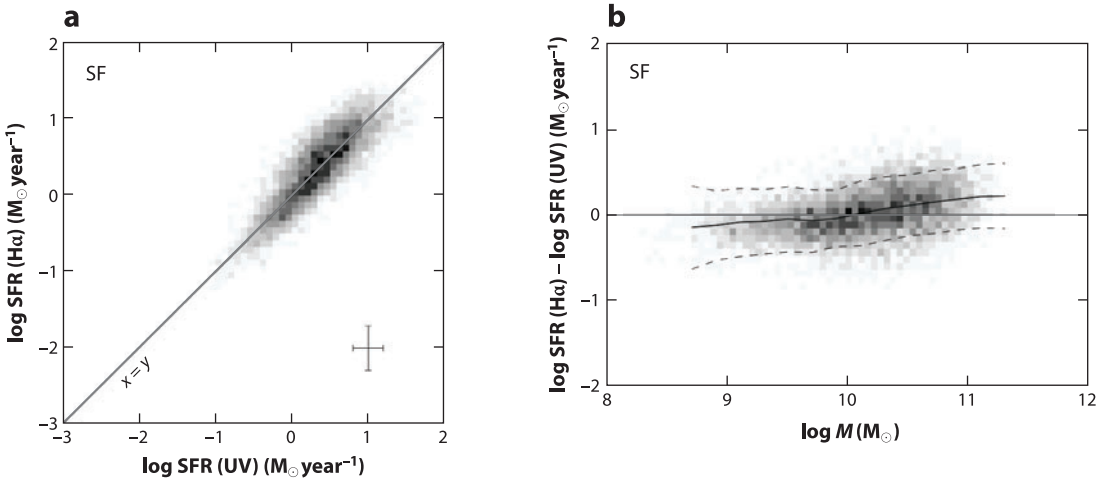

Figure 7

(*a*) Comparison of star-formation rates (SFRs) estimated from emission lines (Hα; Brinchmann et al. 2004) and from modeling the UV-optical spectral energy distributions (UV; Salim et al. 2007) of star-forming galaxies at $z \sim 0$. (*b*) Difference between SFR estimators as a function of stellar mass. There is a systematic trend between the two estimators, which may be due to modeling differences and/or the uncertainty in extrapolating the fiber-based Hα SFRs to the total galaxy. Adapted from Salim et al. (2007).

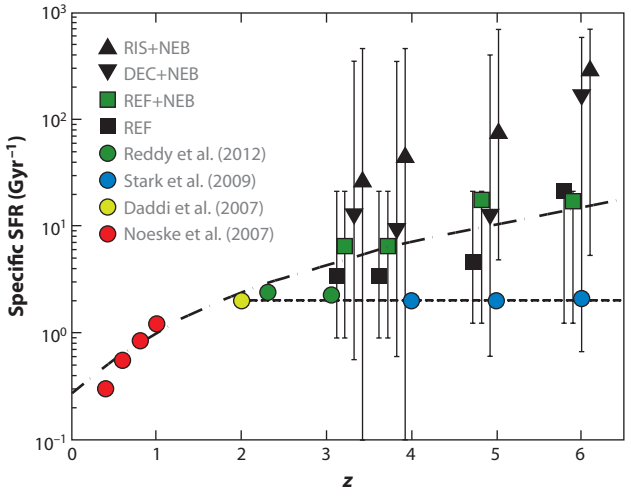

Figure 8

Specific star-formation rates (SFRs) for galaxies with stellar masses of $10^{9.5}$ $M_\odot$ as a function of redshift. The black and green symbols reflect different assumptions regarding the star-formation history (REF, RIS, and DEC for constant, rising, and declining, respectively) and the correction for emission lines (NEB). Error bars reflect 68% confidence limits. From de Barros, Schaerer & Stark (2012).

were more accurate, and therefore also the SFRs. Salim et al. (2007) also demonstrated that for galaxies with low SFRs and/or galaxies with emission line ratios indicative of AGN activity, the UV-based SFRs tended to be more reliable than those estimated by Brinchmann et al. These results suggest that SFRs based on modeling UV-optical SEDs carry systematic uncertainties at the $\lesssim$0.3 dex level.

Wuyts et al. (2011) compared the SFRs of galaxies at $z \sim 3$ computed with three different techniques: Hα-based SFRs, SED-fitting-based SFRs, and a mixed SFR indicator based on the UV and IR emissions. For SFRs $\lesssim$100 $M_\odot$ year^{-1}, these researchers found that the three indicators agreed reasonably well (no systematic offsets were detected), provided that extra attenuation was included toward HII regions when modeling the Hα-based SFRs. They also found that at the highest SFRs ($\gtrsim$100 $M_\odot$ year^{-1}) the SED-based values tended to underpredict the SFR, compared with the mixed indicator (see also Santini et al. 2009). They argued that this was because of their assumption of a uniform dust screen, and at high column density this becomes an increasingly poor representation of reality.

At high redshift the effect of nebular emission lines becomes an additional source of systematic uncertainty in the modeling and can significantly affect the best-fit SFRs. The impact of emission lines is larger at higher redshift because of three effects: (*a*) specific SFRs are higher, (*b*) metallicities are lower, and (*c*) the redshifting of the spectrum implies that a line of given EW comprises a larger fraction of the flux through a filter. In **Figure 8**, the specific SFR for galaxies with a mass of $10^{9.5}$ $M_\odot$ is shown as a function of redshift for various choices regarding the contribution of emission lines to the observed broadband fluxes. Evidently the inclusion or not of emission lines in the modeling can change the derived specific SFRs in a redshift-dependent manner, by a factor of roughly two in the most extreme cases (see also Labbé et al. 2012, Pacifici et al. 2012).

4.2. Light-Weighted Mean Ages

The mean stellar ages of galaxies are another important probe of the SFH. Mass-weighted ages offer a direct probe of the integrated SFH, whereas light-weighted ages are more directly measurable

from SEDs. Mass-weighted ages will always be larger than light-weighted ones, owing to the fact that young stars outshine older stars. As discussed further in the next section, the mass-weighted ages of actively star-forming galaxies turn out to be highly sensitive to the assumed model SFH used in the SED fitting. Due to the fact that light-weighting is highly nonlinear, light-weighted ages computed from spatially resolved photometry will tend to be older than ages computed from integrated photometry, as demonstrated by Wuyts et al. (2011).

The mean ages of quiescent galaxies have been estimated largely via the modeling of spectral features, including D_n4000 and the Lick indices. A widely adopted procedure is to fit single-age SSPs to the Lick indices in order to estimate ages. In this approach it is the hydrogen Balmer lines that provide the primary constraint on the age, as these lines are strongest in A-type stars and thus for populations with ages of $\approx 10^8$–10^9 year. The derived ages are sometimes referred to as SSP-equivalent ages in order to highlight the fact that no attempt is made to model CSPs. A number of researchers have demonstrated that these derived ages are lower limits to the true mass-weighted and light-weighted ages (Trager et al. 2000a; Serra & Trager 2007; MacArthur, González & Courteau 2009; Trager & Somerville 2009). As emphasized by Trager & Somerville (2009), this fact implies that any observed trend of SSP-equivalent ages with other parameters such as velocity dispersion will be stronger than the true underlying mass-weighted trend. The SSP-equivalent ages are younger than even light-weighted ages largely because of the sensitivity of the Balmer lines to ∼1-Gyr-old stars. Trager & Somerville (2009) concluded that SSP-equivalent ages are mostly measuring residual star formation over ∼1 Gyr timescales.

These conclusions are not restricted to the analysis of spectral indices. Ferreras et al. (2009) estimated mean ages of early-type galaxies at $z \sim 1$ by fitting models to HST grism spectra. The ages estimated from single-age models showed almost no correlation with ages estimated with composite models. Likewise, MacArthur, González & Courteau (2009) performed full spectrum fitting on a sample of nearby galaxies and found only a modest correlation between ages derived from single-age models and light-weighted ages derived from composite models.

It is widely believed that the Hβ index is the ideal age indicator because it is largely insensitive to metallicity and abundance patterns (Worthey 1994; Tripicco & Bell 1995; Korn, Maraston & Thomas 2005). However, as noted by Worthey (1994) and later by de Freitas Pacheco & Barbuy (1995), Maraston & Thomas (2000), and Lee, Yoon & Lee (2000), the Balmer lines are also sensitive to the presence of blue HB stars, and there will therefore be some ambiguity in determining ages from Hβ without additional constraints on the presence of such stars. However, Trager et al. (2005) demonstrated that although the inferred ages of the oldest stellar populations ($\gtrsim$10 Gyr) are susceptible to uncertainties of 2–5 Gyr owing to the presence of blue HB stars, the ages of intermediate-age populations (∼1–10 Gyr) are rather less affected by blue HB stars. This is because the Balmer lines increase so strongly with decreasing age that very large quantities of blue HB stars would have to be present in old stellar populations to reproduce the high observed Hβ EWs. As an example, Thomas et al. (2005) found that they could reproduce the highest Hβ EWs in their sample with a model in which 50% of the old metal-rich stars had blue HB stars. In this two-component model, the component with blue HB stars needed a metallicity that was 0.2–0.4 dex higher than the other component. Percival & Salaris (2011) also found that models with very extreme HB populations and old ages could masquerade as a relatively young population with ages as young as ∼3 Gyr, based on Hβ EWs. There is no compelling evidence supporting the existence of a population of blue HB stars in metal-rich, quiescent galaxies large enough to explain the full range of Hβ EWs. However, it is reasonable to assume that there will be a population of blue HB stars in such systems, and they will affect the derived stellar ages.

The higher-order Balmer lines are promising because they will be even more sensitive to warm/hot stars than Hβ. In principle, then, the consideration of multiple Balmer lines should

provide constraints on multiple age components and/or allow for the separation of age and blue HB effects (Schiavon et al. 2004, Schiavon 2007, Serra & Trager 2007). However, the potential power of the higher-order Balmer lines is tempered by the fact that these features are more sensitive to metallicity and abundance ratios than Hβ (Thomas, Maraston & Korn 2004; Korn, Maraston & Thomas 2005). Schiavon (2007) analyzed the Hβ, Hγ, and Hδ indices measured from stacked SDSS early-type galaxy spectra with a variety of composite models, including varying blue HB stars, blue stragglers, and multiage populations. He concluded that small fractions of young/intermediate-age stellar populations, perhaps in the form of extended SFHs, were the most likely scenario to explain the observed trends. This proposal is similar, though not identical, to the "frosting" of young stars proposed by Trager et al. (2009a) in order to explain the observed correlations between velocity dispersion, age, metallicity, and abundance pattern.

There exist other proposed methods for constraining multiage components based on spectral indices. Rose (1984) proposed a CaII index that is sensitive to the Hϵ Balmer line. Leonardi & Rose (1996) demonstrated that this index in conjunction with Hδ can break the "age-strength degeneracy," referring to the age and strength of a recent burst of star formation. Smith, Lucey & Hudson (2009) used this diagnostic to argue against a frosting of small fractions of young stars (<1 Gyr) to explain the young apparent ages for quiescent galaxies in the Shapley supercluster. Kauffmann et al. (2003) considered both the Hδ and D_n4000 spectral features in an attempt to measure two-component SFHs (in particular, a burst of SF and an underlying τ model SFH). Galaxies with a sizable mass fraction formed in a recent burst of SF are significant outliers in the Hδ-D_n4000 plane, and so strong constraints on the burst fraction can be obtained in this way. Percival & Salaris (2011) argued that the CaII Rose index and the MgII feature near 2,800 Å could also be used to separate age from blue HB effects.

Renzini & Buzzoni (1986) suggested that the onset of the AGB in ∼0.1–1-Gyr-old populations could be used to age-date galaxies in the NIR. Subsequent modeling efforts by Maraston (2005) confirmed that NIR spectral features attributable to oxygen- and carbon-rich AGB stars vary strongly over the age range ∼0.1–1 Gyr and may be used as an independent constraint on the presence of intermediate-age populations in galaxies. In principle, the very strong sensitivity of AGB evolution to mass (age) and metallicity suggests that they should be good clocks. However, their sensitivity to mass and metallicity is due to poorly understood physics, including convection and mass-loss, and so the calibration of an AGB-based clock is quite uncertain. Miner, Rose & Cecil (2011) attempted to use NIR spectral features to place constraints on the ages of M32 and NGC 5102 based on Maraston's models. They found broad qualitative agreement between NIR-based ages and CMD-based ages. Future quantitative modeling of the optical-NIR spectra will be required to assess the utility of AGB-sensitive spectral indices as age indicators.

Finally, it is also worth emphasizing that it is fundamentally very difficult to measure ages for systems older than ∼9 Gyr because evolution in the isochrones is so slow at late times. For example, at solar metallicity between 9–13.5 Gyr, the RGB changes by only ≈50 K, whereas the main sequence turnoff point changes by ≈230 K. Very accurate models and very high-quality data are required to distinguish such small temperature variations. In theory, the UV should be much more sensitive to age at late times owing to the onset of an extended (blue) HB (Yi et al. 1999). In the context of a particular model, the UV colors become very sensitive to age for ages $\gtrsim$7 Gyr. The problem with this chronometer is that it is very sensitive to the uncertain physical inputs, such as the mass-loss prescription and the helium abundance, and also to the underlying distribution of stellar metallicities (Yi, Demarque & Oemler 1997). These uncertainties will render absolute ages unreliable, although relative ages (or simply the rank-ordering of galaxies by age) are probably more robust.

4.3. Which Model Star-Formation Histories to Use?

Papovich, Dickinson & Ferguson (2001) recognized that SED modeling suffered from a fundamental limitation, namely, that the young stars, being so bright, tend to outshine the older, less luminous stars. This outshining effect was known to result in underestimated stellar masses when single-component SFH models were used (e.g., Papovich, Dickinson & Ferguson 2001; Daddi et al. 2004; Shapley et al. 2005; Lee et al. 2009b; Pforr, Maraston & Tonini 2012), but its effect on recovered SFRs and ages remained relatively less well explored until recently. Lee et al. (2009b) analyzed the SEDs of high-redshift mock galaxies and concluded that the use of single-component exponentially decreasing SFHs (τ models) resulted in underestimated SFRs and overestimated mean ages (by factors of 2 for both parameters). They attributed this shortcoming to the fact that the mock galaxies tended to have rising SFHs in contrast to the declining model SFHs. Subsequent work by Lee et al. (2010), Maraston et al. (2010), Wuyts et al. (2011), and Pforr, Maraston & Tonini (2012) largely confirmed these findings and further concluded that models with rising SFHs tend to provide a better fit to observed high-redshift SEDs and produce SFRs in better agreement with other indicators. Relatedly, the choice of the allowed range of each SFH parameter (i.e., the prior) can significantly affect the inferred best-fit SFRs and ages (e.g., Lee et al. 2010, Wuyts et al. 2011).

Figure 8 shows a specific example of the effect of the adopted SFH parameterization on SFRs, with the specific SFR shown as a function of redshift at a reference stellar mass of $10^{9.5}$ $M_{\odot}$. At high redshift the scatter between the RIS, DEC, and REF models is entirely due to the choice of the assumed SFH (rising, declining, or constant, respectively). At the highest redshifts these different choices result in a change in specific SFRs of more than an order of magnitude.

There has been some difference in opinion regarding which functional form one should adopt for the rising SFHs. Maraston et al. (2010) and Pforr, Maraston & Tonini (2012) advocated exponentially increasing SFHs, whereas Lee et al. (2010) advocated delayed τ models of the form SFR $\propto t e^{-t/\tau}$. The data do not presently favor one functional form over the other. The basic conclusion to draw from these analyses is that the model SFH library must be sufficiently diverse to allow for a wide range in SFH types. Model SFHs that are too restricted will inevitably lead to biased results. The criterion for sufficiently diverse SFHs will depend on the galaxy type in question and has not been thoroughly examined in a general sense. At present, all that can be stated with confidence is that for certain SED types, especially highly star-forming galaxies, great care must be taken when constructing the model library of SFHs.

Another option is to use a library of SFHs drawn from semianalytic or hydrodynamic models of galaxy formation. This technique was introduced by Finlator, Davé & Oppenheimer (2007), who analyzed SEDs of six high-redshift galaxies with SFHs drawn from their hydrodynamic simulations. The advantage of this approach is that the model SFH library is more likely to contain realistic SFHs (with rising and falling SFHs, multiple bursts, etc.) than simple analytic models. Recently, Pacifici et al. (2012) explored a similar technique using SFHs from a semianalytic model rather than a hydrodynamic simulation. The advantage of using a semianalytic model is that a much larger range of SFHs can be computed in a given amount of computational time. As with any other SFH library, the results can be sensitive to the choice of priors. In this case, the prior is in some sense the reliability of the model in producing a realistic range of SFHs. A possible disadvantage of this approach is that it can be much more difficult to quantify the influence of this prior on the derived physical properties than when using analytic SFH libraries.

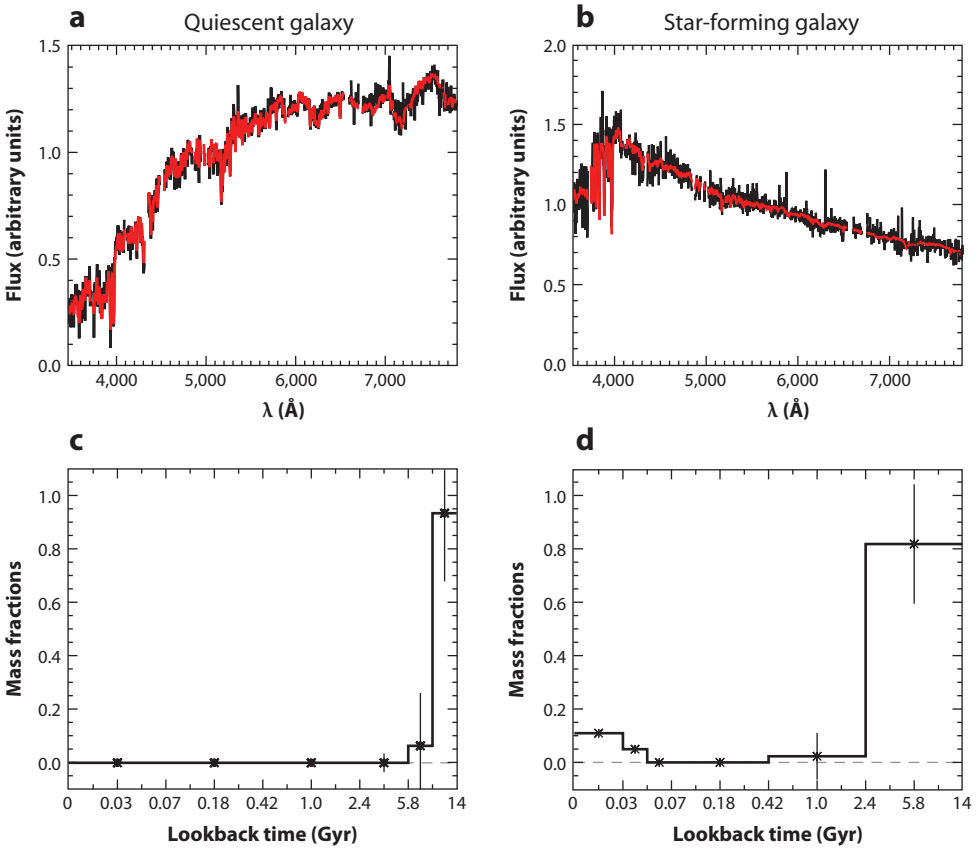

Figure 9

Example fits to the optical spectrum of a quiescent and a star-forming galaxy with VESPA (Tojeiro et al. 2009). The star-formation histories (SFHs) are estimated nonparametrically, with an age binning that is adaptive, depending on the S/N and information content of the spectrum. (*a*,*b*) The best-fits are shown (*red line* is the model; *black line* is the data; emission lines have been excluded from the fits). (*c*,*d*) Recovered SFHs are plotted as the mass fraction formed within each age bin. Figure courtesy of R. Tojeiro.

4.4. Nonparametric Star-Formation Histories

When modeling SEDs, one typically must adopt some parameterization of the SFH, and it is this step that clearly introduces a number of poorly quantified systematics. An appealing solution to this problem is to model SEDs with nonparametric SFHs. This is precisely the approach taken by several groups, including MOPED (Heavens, Jimenez & Lahav 2000), STARLIGHT (Cid Fernandes et al. 2005), STECMAP (Ocvirk et al. 2006), VESPA (Tojeiro et al. 2007), ULySS (Koleva et al. 2009), and MacArthur, González & Courteau (2009). In the simplest implementation one specifies a fixed set of age bins and then fits for the fraction of mass formed within each bin. More sophisticated algorithms utilize adaptive age binning that depends on the SED type and S/N (e.g., Tojeiro et al. 2007). In all cases one is engaging in full spectrum fitting (in the restframe optical; for an example of the technique, see **Figure 9**). In principle, one could use such codes to fit broadband SEDs, but the fits would likely be seriously underconstrained. These methods have been tested in a variety of ways, and it appears that they are capable of recovering complex

SFHs remarkably well, at least when the mock galaxies are built with the same SPS models as used in the fitting routines (Ocvirk et al. 2006, Tojeiro et al. 2007, Koleva et al. 2009). Not surprisingly, the requirements on the data quality are demanding: A wide wavelength coverage, high spectral resolution, and high S/N (typically >50 Å^{-1}) are required in order to robustly recover complex SFHs (Ocvirk et al. 2006, Tojeiro et al. 2007). In addition, there are clear systematics in the recovered SFHs owing to different SPS models, particularly for the SFHs at ages of ∼0.1–1 Gyr (Tojeiro et al. 2009, 2011). This is perhaps related to the different treatment of AGB stars and/or core convective overshooting among SPS models. Moreover, present implementations of nonparametric SFH recovery utilize SPS models that only allow variation in metallicity and age—the abundance pattern is fixed to the solar value. When fitting to spectra, this practice can introduce additional systematics because many of the features that are being fit are sensitive to the detailed abundance pattern of the system.

There have been few comparisons between the SFHs derived via nonparametric methods with more conventional techniques. Tojeiro et al. (2009) compared SFRs estimated with VESPA to emission line–based SFRs from Brinchmann et al. (2004). No obvious discrepancies were found, but further detailed analyses would be desirable. Moreover, there appears to be no published work comparing the mean stellar ages (or some other moment of the SFH) between these various techniques.

4.4.1. Star-formation histories from color-magnitude diagrams versus star-formation histories from integrated light. Ideally, one would like an independent constraint on the SFH to compare against the SFH derived from integrated light spectra. Unfortunately, no direct tests of this sort have been performed to date. The most robust method for determining SFHs is via the modeling of resolved CMDs of the stars within galaxies. This technique is well developed and has recently been applied by Weisz et al. (2011) to a large sample of dwarf galaxies in the local volume compiled by the ACS Nearby Galaxy Treasury Survey (ANGST; Dalcanton et al. 2009). Leitner (2012) compared the SFHs derived by Weisz et al. (2011) to the SFHs derived from integrated light spectra by Tojeiro et al. (2009). The result is shown in **Figure 10**. The dwarf galaxies from the ANGST Survey have masses slightly lower than the lowest mass bin in the integrated light sample, and it is worth emphasizing that there is no overlap between the two samples. And yet the dwarfs have SFHs comparable to the highest mass bin in the integrated light sample. There are many complications in making this comparison, not the least of which is the question of whether or not nearby dwarfs are representative of the cosmological average. Nonetheless, the difference in the qualitative trend derived from CMD-based and integrated light-based SFHs is striking and worthy of further study.

4.5. Low-Level Star Formation

Probing low levels of star formation in galaxies is challenging because at low levels classic SF indicators can become contaminated by other processes. At low luminosities emission lines can be influenced by low-level AGN activity and they become difficult to measure on top of the strong absorption features in the continuum; dust emission can be due to heating from old stars (rather than tracing the formation of new stars); and UV light can be attributed to hot evolved low-mass stars. The former two indicators have been effectively abandoned as low-level SF indicators, whereas the third, UV light, still holds some promise.

It is beyond the scope of this review to discuss in detail the complications in interpreting UV (especially FUV) emission from predominantly quiescent systems, but a few remarks will serve to round out this section. The reader is referred to O'Connell (1999) for a thorough review

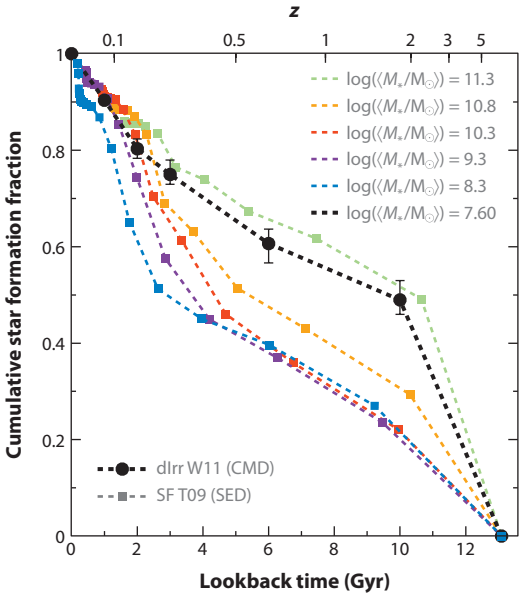

Figure 10

Comparison of star-formation histories (SFHs) estimated from integrated light spectral energy distributions (SEDs) to those estimated from color-magnitude diagrams (CMDs) for star-forming (SF) galaxies. The SED-based SFHs are based on SDSS spectra, as derived in Tojeiro et al. (2009), and binned by stellar mass. The CMD-based SFHs are from Weisz et al. (2011), based on data from the ANGST survey, and are for low-mass dwarf irregulars. It is striking that the CMD-based SFHs for low-mass dwarfs look closer to the SED-based SFHs for the most massive galaxies. Adapted from Leitner (2012). Abbreviations: ANGST, ACS Nearby Galaxy Treasury Survey; SDSS, Sloan Digital Sky Survey.

and to Yi (2008) for a recent update. Low-level UV emission from galaxies can be due to either young massive stars or hot evolved low-mass stars. The latter category includes extreme HB stars, post-AGB stars, AGB-Manqué stars, etc. Extreme HB stars are known to exist in essentially all low-metallicity and some high-metallicity globular clusters. Post-AGB stars should exist at all metallicities, and AGB-Manqué stars are thought to occur only in special circumstances. It is very difficult to predict the specific numbers of these stars as a function of metallicity and time, and it is for this reason that low levels of UV flux are so difficult to interpret. The recent catalog of evolved hot stars in Galactic globular clusters by Schiavon et al. (2012) may help to calibrate the models for these advanced evolutionary phases.

There have been several important developments since the review by O'Connell (1999), which are mainly due to progress provided by HST and GALEX. It is now clear that galaxies on the optically defined red sequence (e.g., in $B-V$ or $g-r$ color space) frequently harbor low levels of star formation, at the rate of $\sim 0.1 - 1\,M_\odot$ year^{-1} (Yi et al. 2005, Kaviraj et al. 2007, Salim & Rich 2010, Salim et al. 2012, Fang et al. 2012), although for the most massive galaxies SF levels appear to be even lower. The implication is that optical SEDs are not sensitive to specific SF at levels of $\lesssim 10^{-11}$ year^{-1}. It is also now quite clear that optically defined red sequence galaxies have a wide range of UV colors, from those with low levels of star formation to those that are extremely red. It has become common practice to define a somewhat arbitrary UV-optical color boundary in order to separate star forming from quiescent galaxies (Yi et al. 2005, Jeong et al. 2009). Of course, such a practice does not provide an answer to the question of how low SFRs actually are in the reddest galaxies. Instead it signals the difficulty in measuring SFRs for such red systems because any UV

flux becomes easily confused with hot evolved low-mass stars. Further progress can be made by directly resolving luminous young stars and star clusters in nearby galaxies. This was the strategy taken by Ford & Bregman (2013), who observed four nearby elliptical galaxies with HST. These researchers argued that the galaxies in their sample have present specific SFRs in the range of 10^{-14}–10^{-16} year^{-1}, far below what can be reliably probed via SED modeling. UV spectroscopic features may also aid in distinguishing hot evolved low-mass stars from hot upper main sequence stars (O'Connell 1999).

4.6. Summary

Measuring the detailed SFH of a galaxy from its observed SED is one of the holy grails of SPS modeling. Unfortunately, two unrelated physical effects make this task very difficult in practice: (*a*) high mass stars are so luminous that they dominate the SEDs of star-forming galaxies, easily outshining the more numerous, older, lower mass stars, and (*b*) at late times isochrones evolve very little, so it is difficult in practice to distinguish an ∼8 Gyr population from an ∼12 Gyr one. The first effect implies that light-weighted ages will always underestimate the true mass-weighted age. It also implies that the priors on the model SFHs can strongly influence the best-fit parameters. Nonparametric SFH reconstruction methods offer the best hope of providing unbiased results, but they require data of very high quality. As a general rule of thumb, optical SEDs are sensitive to specific SFRs as low as 10^{-11} year^{-1} and UV fluxes are sensitive to levels as low as 10^{-12} year^{-1}, whereas resolved UV photometry is in principle sensitive to specific SFRs down to at least $\lesssim 10^{-14}$ year^{-1}. SED-based SFRs are probably accurate at the factor of two level (at a fixed IMF), except for extreme systems where uncertainties can be much larger. There appears to be little consensus on the accuracy of light-weighted and mass-weighted stellar ages derived from SED fitting.

5. STELLAR METALLICITIES AND ABUNDANCE PATTERNS

5.1. The Age-Metallicity Degeneracy

The metallicity, Z, affects the SED in two distinct ways: (*a*) an increase in metallicity results in lower effective temperatures, including a cooler main sequence and giant branch, and (*b*) at fixed $T_{\rm eff}$, an increase in metallicity results in stronger spectroscopic absorption features and generally redder colors. Both of these effects contribute to the overall reddening of an SED with increasing metallicity. In addition to the overall metal content, the detailed elemental abundance pattern is imprinted on the SED, especially in the strength of spectral absorption features.

Age will also tend to redden the SED through the effect of age on the isochrones. Worthey (1994) studied the degeneracy between age and metallicity in detail using his SPS models and concluded that at ages >5 Gyr neither broadband colors nor most spectral indices were able to reliably separate age from metallicity. Worthey introduced his "3/2 rule," whereby an increase/decrease in the population age by a factor of three is almost perfectly degenerate with an increase/decrease in metallicity by a factor of two. He identified a small number of spectral indices that were unusually sensitive to age, including the hydrogen Balmer lines, and several indices that were unusually sensitive to metallicity, including the Fe4668 and Fe5270 indices (see also O'Connell 1980, Rabin 1982, Rose 1985 for early attempts at separating age and metallicity). Worthey therefore demonstrated conclusively that the age-metallicity degeneracy could be broken by jointly considering a handful of carefully chosen indices. He also pointed out that the age-metallicity degeneracy is less severe at low metallicity, where the turnoff point and giant branch have very different age sensitivity at fixed metallicity.

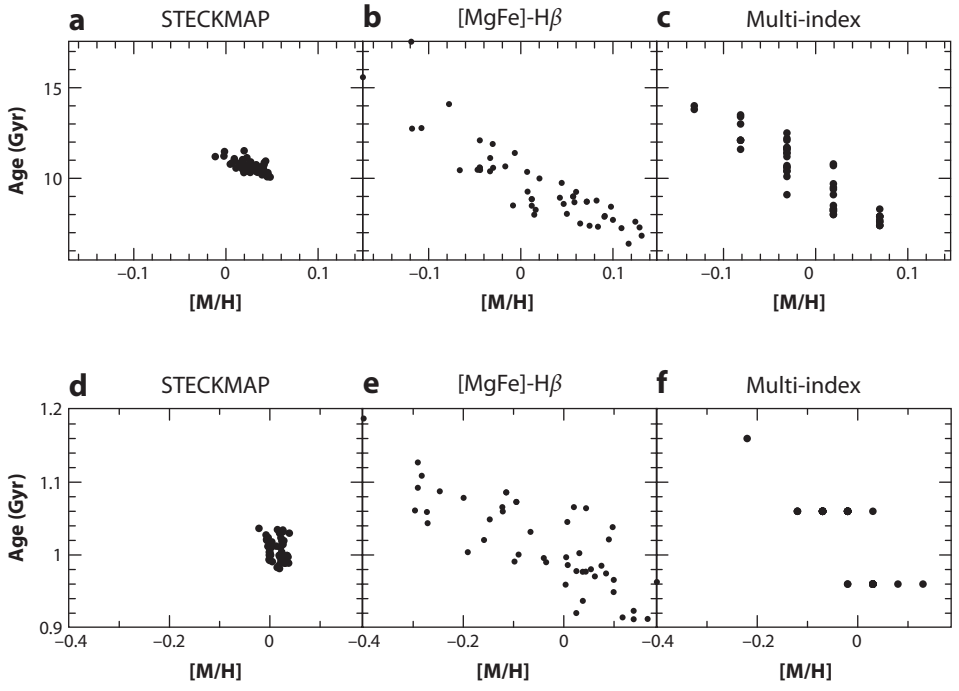

Figure 11

Illustration of the age-metallicity degeneracy in spectra of modest S/N. Three techniques are compared: (*a*,*d*) the full spectrum fitting technique of Ocvirk et al. (2006), (*b*,*e*) classic two-index fitting, and (*c*,*f*) multi-index fitting. Results are shown for a mock galaxy with S/N = 50 Å^{-1}, [M/H] = 0.0, and an age of (*a*,*b*,*c*) 10 Gyr and (*d*,*e*,*f*) 1 Gyr. Each point represents the best fit for a single realization of the mock galaxy spectrum. From Sánchez-Blázquez et al. (2011).

It has long been appreciated that a clean separation of age and metallicity can be achieved with Lick indices only for data of very high S/N ($\gtrsim$100 Å^{-1}; Trager et al. 2000b, Kuntschner 2000). **Figure 11** demonstrates that an age-metallicity degeneracy persists when exploiting Lick indices at lower S/N. In contrast, full spectral fitting offers a much more robust separation of age and metallicity at moderate to low S/N (at least within the context of an underlying set of model SSPs; see MacArthur, González & Courteau 2009; Sánchez-Blázquez et al. 2011). This is simply a consequence of the fact that much more information is available in the full optical spectrum than can be captured by a limited number of spectral indices.

5.2. Photometric Metallicities

The age-metallicity degeneracy discussed in Worthey (1994) strictly applies to systems that are coeval with ages >5 Gyr; models at younger ages were not considered by Worthey. In subsequent work it became clear that the broadband optical-NIR colors of CSPs could separate age and metallicity effects. The physics underlying the idea is that blue colors probe the age-sensitive main sequence turnoff point whereas red/NIR colors probe the metallicity-sensitive giant branches. Bell & de Jong (2000) and MacArthur et al. (2004), among others, showed that age and metallicity vectors were nearly orthogonal in optical-NIR colors (e.g., $B-R$ versus $R-H$). These researchers therefore concluded that estimates of stellar metallicities were possible from photometric data

alone, for systems whose light-weighted ages were not too old. Eminian et al. (2008) showed that galaxies grouped by spectroscopically derived ages and metallicities separate relatively well in $g-r$ versus $Y-K$ color-color space. Notice that this statement does not depend on the predicted model colors, thereby providing strong evidence that separation of age and metallicity is at least in principle possible based on broadband optical-NIR data alone.

Lee et al. (2007) investigated the model uncertainties associated with separating age and metallicity based on broadband colors. They echoed previous work in that the young populations in composite stellar models dominate the light and therefore allow a separation of age and metallicity effects when optical-NIR colors are employed. However, they also emphasized that different SPS models produce very different age-metallicity vectors in color-color space, a point also emphasized by Eminian et al. (2008). The result is that age and metallicity can be separately constrained within the context of a particular SPS model, but the derived ages and metallicities will vary from model to model. The underlying cause of this problem is that the NIR light is heavily influenced by AGB stars for populations of moderate age, and so different treatments of this uncertain evolutionary phase cause substantial differences in the age-metallicity grids. Because of the difficulty in measuring metallicities from photometric data, many SPS studies simply treat metallicity as a nuisance parameter to be marginalized over. Other studies take the even simpler approach of fixing the metallicity to the solar value. The danger in making the latter simplification is that assumptions in the assumed metallicity will generally affect other parameters of interest, such as the stellar mass, dust opacity, and SFR (see, e.g., Wuyts et al. 2009; Marchesini et al. 2009; Muzzin et al. 2009; Pforr, Maraston & Tonini 2012).

5.3. Spectroscopic Metallicities

The more robust approach to estimating stellar metallicities is to employ spectroscopic features. Optical spectra of galaxies are rich in atomic and molecular absorption features that are readily apparent even at low spectral resolution ($R \sim 1{,}000$). For a fixed population age, the strengths of the absorption features will depend not only on the overall metallicity, Z, but also on the detailed elemental abundance pattern. In general, this greatly complicates interpretation of absorption features and spectral indices. However, with the aid of models that allow for variation in both metallicity and abundance pattern, one can search for combinations of features that are relatively robust against abundance pattern variations. Thomas, Maraston & Bender (2003b) refined a proposal by González (1993) of an index comprised of magnesium and iron lines that is almost entirely insensitive to the level of α enhancement, [α/Fe], and is therefore a relatively robust tracer of Z. The index is defined as $[\mathrm{MgFe}]' \equiv \sqrt{\mathrm{Mg}\, b\,(0.72\,\mathrm{Fe5270} + 0.28\,\mathrm{Fe5335})}$, where Mg b, Fe5270, and Fe5335 are Lick indices defined in Worthey et al. (1994). The power of this index, and others like it (see, e.g., Bruzual & Charlot 2003), is that variable abundance pattern models are then not required to measure total metallicities from galaxy spectra. However, a significant caveat to this approach is the assumption that abundance patterns in galaxies can be described by two parameters: [Fe/H], and [α/Fe]. In reality, analyses of high-resolution stellar spectra in the Galaxy consistently demonstrate that the α elements do not vary in lock-step (Edvardsson et al. 1993; Venn et al. 2004; Fulbright, McWilliam & Rich 2007). This means that the true total metallicity, Z, can only be accurately estimated if the detailed abundance patterns are known.

Gallazzi et al. (2005) applied the idea that [MgFe]$'$ is insensitive to [α/Fe] (assuming that the α elements, C and N all vary in lock-step) to the analysis of 175,000 galaxies from the SDSS with the aide of the Bruzual & Charlot (2003) SPS models. Several age-sensitive and Z-sensitive spectral indices were used in their analysis. They derived light-weighted stellar metallicities for individual

galaxies with statistical errors as low as 0.1 dex for the highest S/N spectra. These researchers also explored a variety of systematic effects and concluded that these could add ∼0.1 dex systematic uncertainty to the error budget on Z. Probably the dominant systematic in the results of Gallazzi et al., and others based on similar techniques, is the assumption that the α elements and C and N all vary in lock-step.

Another technique is to fit the entire optical spectrum with models that allow for variation in age and total metallicity, and to simply ignore the possibility that the observed spectrum may have nonsolar abundance patterns. This approach has become increasingly common as automated spectral fitting codes garner wider use. Tojeiro et al. (2011) fit stacked spectra of luminous red galaxies from SDSS as a function of luminosity and redshift with the VESPA code. Remarkably, they found essentially no variation in Z with galaxy luminosity (though the sample was restricted to very luminous galaxies), and for the Conroy, Gunn & White (2009) and Maraston (2005) SPS models there was no evolution in Z with redshift over the interval $0.1 < z < 0.5$. When the Bruzual & Charlot (2003) models are employed, VESPA favored higher metallicities at higher redshift. Variation in the best-fit metallicity between SPS models points toward systematic uncertainties in the models at the ∼0.2-dex level.

Koleva et al. (2008) investigated the accuracy of full spectrum fitting codes at recovering metallicities. They considered both the ability of one SPS model to recover the known metallicity of a second model and the ability of an SPS model to recover the known metallicities of Galactic globular clusters. They concluded that the high-resolution version of the Bruzual & Charlot (2003) model carries large systematic uncertainties owing to its use of the STELIB stellar library. STELIB does not sample a wide enough range in metallicity, and so metallicities derived from the Bruzual & Charlot models will carry large uncertainties. The other models tested, including the Vazdekis/MILES and PEGASE-HR models, reproduced the known globular cluster metallicities to an accuracy of ≈0.14 dex.

The most robust method for estimating stellar metallicities is with models that self-consistently include abundance pattern variation. Such models have existed for the Lick indices since the late 1990s, whereas models for the full optical-NIR spectrum have only recently become available (Coelho et al. 2007, Walcher et al. 2009, Conroy & van Dokkum 2012a).

Trager et al. (2000a,b) modeled three spectral indices with SPS models that allowed for variation in abundance patterns. Trager et al. focused on fitting for the age, total metallicity, Z, and enhancement ratio, [α/Fe]. In practice, they grouped elements into two types, the depressed and the enhanced group, with the latter comprised of α elements except Ca, plus C and N, whereas the former comprised the iron-peak elements and Ca. In subsequent work, Thomas et al. (2005) modeled the same set of spectral indices as in Trager et al., though with their own SPS models and with an expanded dataset. Their conclusions largely echoed those of Trager et al., with the novel finding that at fixed velocity dispersion galaxies in denser environments appeared to be more metal-rich than galaxies in less dense environments.

As discussed in Section 4, most analyses of Lick indices fit single-age models to the data. Serra & Trager (2007) and Trager & Somerville (2009) considered the effect of multiple age components in the fitting of the Lick indices of mock galaxies and found that the derived metallicities agreed well with the light-weighted mean metallicities when the youngest component was older than ∼3 Gyr. For young components with ages of 1–3 Gyr, there was a slight bias in the sense that the derived metallicities were ∼0.1 dex higher than the true light-weighted mean metallicities. These researchers did not consider components younger than 1 Gyr.

Total metallicities estimated with models that include abundance pattern variation are the most robust but also the most restricted. Models such as those by Thomas et al., Conroy & van Dokkum, Worthey, or Schiavon are limited to ages >1 Gyr and are therefore routinely applied

only to early-type galaxies. A major area for future growth in this field is the extension of these models to younger ages in order to model galaxies of all types.

5.4. Elemental Abundance Patterns

Wallerstein (1962) was the first to show that nonsolar abundance patterns were common among metal-poor stars in the Galaxy. It was therefore natural to wonder if other galaxies harbored nonsolar abundance patterns. Early data suggested that magnesium may vary more than iron among the early-type galaxies (O'Connell 1976, Peterson 1976, Peletier 1989), but it was with the availability of new, relatively high-quality spectral synthesis models that Worthey, Faber & Gonzalez (1992) were able to firmly establish that the [Mg/Fe] ratio varied within the early-type galaxy population. The discovery of nonsolar abundance patterns has been one of the most significant discoveries afforded by population synthesis models. The ratio between the abundance of α elements and iron-peak elements, [α/Fe], is considered to be particularly valuable as it provides insight into the SFH of galaxies (Tinsley 1979). Following the development of models that allowed for arbitrary variation in abundance patterns, the measurement of abundance ratios became routine. Particular attention has been paid to [Mg/Fe], in large part because it is the most readily measurable abundance ratio in moderate-resolution spectra, thanks to the numerous strong FeI features and the Mg *b* feature at 5,200 Å (**Figure 3**).

As discussed above, Trager et al. (2000a,b) presented the first systematic investigation of abundance patterns in early-type galaxies. They found enhancement ratios, [α/Fe], generally in excess of zero, with a strong correlation with velocity dispersion. As Trager et al. fit only Hβ, Mg *b*, and two iron indices, their [α/Fe] is in reality a statement about [Mg/Fe]. Since then, numerous researchers, using different SPS models, have all reached the same conclusion that [Mg/Fe] exceeds zero and increases with galaxy velocity dispersion (Thomas et al. 2005; Schiavon 2007; Graves, Faber & Schiavon 2009; Smith et al. 2009; Johansson, Thomas & Maraston 2012).

As noted in the previous section, early studies grouped elements into two classes, enhanced and depressed, and so only the total metallicity and the enhancement factor could be measured from the data (Trager et al. 2000a, Thomas et al. 2005). More recent work has allowed for the abundance of a larger number of elements to vary, including C, N, Ca, and Ti (see Schiavon 2010 for a complementary review to the one presented below).

The calcium abundance is most commonly measured from the CaI line at 4,227 Å, as probed by the Ca4227 Lick index (**Figure 3**). Other regions of the spectrum with strong sensitivity to calcium abundance include the CaII H and K lines and the triplet of CaII lines at 8,600 Å (CaT). The calcium abundance in early-type galaxies has been described as a puzzle because its abundance does not seem to track magnesium, despite the fact that they are both α elements. This was noted qualitatively in the early work of Vazdekis et al. (1997) and Trager et al. (1998) and quantified with variable abundance models by Thomas, Maraston & Bender (2003a). The CaT feature is weaker than even solar-scaled models, for reasons that will be discussed in Section 7. Schiavon (2007) and Johansson, Thomas & Maraston (2012) fit the Ca4227 index (along with others) of early-type galaxies from SDSS and find [Ca/Fe] values close to zero.

Carbon and nitrogen abundances can be measured from the NH, CH, C_2, and CN molecular absorption features in the blue spectral region (**Figure 3**). Kelson et al. (2006) were the first to probe the C and N content of early-type galaxies based on Lick indices. Schiavon (2007) measured [C/Fe] and [N/Fe] from Lick indices as a function of early-type galaxy luminosity based on stacked spectra from SDSS. He found that the abundance of these elements increased significantly with increasing luminosity. Johansson, Thomas & Maraston (2012) reached similar conclusions based on analysis of individual early-type galaxies in SDSS. The NH feature at ≈3,360 Å is in principle

a powerful probe of [N/Fe] because it is sensitive only to N (unlike CN). To date, this feature has not been extensively utilized, both because it is near the atmospheric transmission cutoff and thus difficult to observe and because variable abundance models are not well developed in this spectral region. Nonetheless, several researchers have investigated empirical trends of this feature with other properties of early-type galaxies, with mixed results (Davidge & Clark 1994, Ponder et al. 1998, Serven et al. 2011).

Moderate-resolution spectra of early-type galaxies respond strongly to changes in the abundances of Fe, Mg, C, N, Ca, and Ti, and thus these elements are the most easily measured. However, the optical and NIR spectrum of an old stellar population contains information on many more elements. In a forward-looking study, Serven, Worthey & Briley (2005) considered the spectral response due to variation in the abundance of 23 separate elements and concluded that for S/N = 100 spectra and a galaxy velocity dispersion of $\sigma = 200$ km s^{-1}, one could in principle measure the abundance of C, N, O, Na, Mg, Al, Si, Ca, Sc, Ti, V, Cr, Mn, Fe, Co, Ni, Sr, and Ba. Of course, as the effects are often quite subtle, all relevant systematics must be well controlled. As a first step toward extracting these more subtle features, Conroy, van Dokkum & Graves (2013) reported measurements of the abundances of the neutron-capture elements Sr and Ba from analysis of moderate-resolution spectra of nearby early-type galaxies. Studies such as these should provide important new clues to the formation histories of old stellar systems.

Attention here has focused exclusively on early-type galaxies with little or no ongoing star formation, and for good reason. The hot massive stars that dominate the SEDs of actively star-forming galaxies have generally weak metal absorption lines, especially in the optical-NIR, and so their presence acts primarily to dilute the strength of the metal lines of the older, cooler stars. More fundamentally, models simply do not presently exist to study the abundance patterns of actively star-forming galaxies.

5.4.1. What about oxygen? Oxygen is the most abundant element in the Universe after hydrogen and helium. Its abundance relative to iron, [O/Fe], is therefore a critical variable in both stellar interior models (VandenBerg & Bell 2001) and stellar atmospheres. There are no transitions of atomic oxygen visible in moderate-resolution spectra, but molecules involving oxygen (including TiO, H_2O, CO, and OH) do create significant features in the optical-NIR spectra of cool stars. TiO is the only molecule with transitions in the optical (beginning at ≈4,500 Å), and unfortunately the work on response functions of the Lick indices to abundance changes have neglected TiO line lists from their computations (Tripicco & Bell 1995; Korn, Maraston & Thomas 2005). The situation with oxygen is quite complex because CO has the highest dissociation potential of any molecule, and thus increasing the abundance of oxygen has a cascading effect on other species. For example, increasing oxygen causes more carbon to be consumed by the formation of CO, which in turn causes a decrease in the concentration of CN and C_2. The oxygen abundance must therefore be known, or assumed, before one can interpret other spectral features. The OH lines in the *H*-band probably afford the most direct constraint on the oxygen abundance, but these features have not been exploited because of a lack of available models. This limitation has now been overcome with the variable abundance ratio models of Conroy & van Dokkum (2012a) that extend to the *K*-band. The upshot is that direct constraints on the photospheric abundance of oxygen in other galaxies presently do not exist, but they are possible with newly available models. This presents a significant limitation to present models because of the strong effect of oxygen on the effective temperatures, etc., of stars. More troubling is the observation that in the Galactic bulge the abundances of oxygen and magnesium do not track each other (Fulbright, McWilliam & Rich 2007). In fact, bulge stars with [Fe/H] > 0 have [O/Fe] < 0.2, [Si/Fe] < 0.2, [Ca/Fe] < 0.2, and [Ti/Fe] < 0.2, whereas [Mg/Fe] ∼ 0.3 for the same stars. The lesson to draw from the Galactic

bulge is that one should be very cautious in using [Mg/Fe] as a tracer of [α/Fe]. Because of these uncertainties surrounding oxygen, Thomas et al. (2005) investigated its effect on their analysis of Lick indices. They concluded that if oxygen is in reality decoupled from the other α elements (e.g., [O/Mg] is nonzero), then the ages and [Fe/H] and [Mg/Fe] abundances are largely unchanged with respect to their standard model where oxygen tracks the other α elements. However, these researchers only considered the effect of oxygen on the stellar spectra; they did not consider the nontrivial effect of oxygen on the isochrones (Dotter et al. 2007). Further work is clearly needed regarding the important role of oxygen in SPS models.

5.4.2. *Z* versus [Fe/H]. The iron abundance, [Fe/H], is often regarded as a proxy for the total metallicity, *Z*, but as discussed above, the correspondence between these two quantities breaks down for nonsolar abundance patterns. As shown in Trager et al. (2000b), the relation between [*Z*/H] and [Fe/H] can be parameterized by $[Z/H] = [Fe/H] + A[\alpha/Fe]$. The constant A depends on the detailed abundance pattern; for models in which all α elements and carbon and nitrogen are grouped together, $A = 0.93$, whereas for models with $[O/Fe] = [C/Fe] = 0, A = 0.77$. It needs to be emphasized here that formulae such as the one presented above only apply in the simple case in which all α elements vary in lock-step and carbon and nitrogen either are solar-scaled or vary with α. This is probably not a good approximation to reality. From the modeling perspective, some have chosen to enhance or depress element groups at fixed *Z* (e.g., Trager et al. 2000b; Thomas, Maraston & Bender 2003b), whereas others have chosen to fix [Fe/H] as other elements vary (e.g., Schiavon 2007; Conroy & van Dokkum 2012a). The choice would be rather arbitrary and inconsequential were it not for the fact that most models adopt a fixed set of isochrones as the abundances are varied. The important question is, then, whether isochrones vary with abundance pattern more at fixed *Z* or fixed [Fe/H]. At least for variation in [O/Fe], Dotter et al. (2007) have demonstrated that the isochrones vary in $T_{\rm eff}$ by approximately the same absolute amount (though with a different sign) when the variation is computed at fixed *Z* or fixed [Fe/H]. The disadvantage, at least conceptually, of computing models at fixed *Z* is that a variation in one element forces variation in another so that *Z* is held constant.

5.5. The Low-Metallicity Tail

Stars within the Galaxy have a wide range of metallicities, and so one might expect other massive galaxies to harbor stars of varying metallicity. This expectation was confirmed with resolved CMDs of nearby early-type galaxies (e.g., Grillmair et al. 1996, Harris & Harris 2000, Monachesi et al. 2011). The difference between a monometallic, metal-rich stellar population and one that includes even a small fraction of metal-poor stars will be most apparent in the UV range. This occurs for two reasons: At low metallicity the main sequence turnoff point is considerably hotter than at solar metallicity, and at low metallicity stellar populations are observed to contain significant numbers of blue HB stars. The closed box model of galactic chemical evolution predicts that ≈10% of the stars in an evolved galaxy will have $[Fe/H] < -1$. Old stellar populations with $[Fe/H] \lesssim -1$ can be expected to harbor blue HB stars (by analogy with the Galactic globular clusters), and thus there will be a large difference in the UV between a closed box metallicity distribution function and one that is monometallic.

Bressan, Chiosi & Fagotto (1994) constructed spectrophotometric evolutionary models for elliptical galaxies and found that closed box models produced an excess of UV flux compared with observations. They argued that the failure of the model was due to the excess of metal-poor stars and concluded that real early-type galaxies contain a more narrowly peaked metallicity distribution function. This conclusion mirrors the observation in the Solar Neighborhood, where fewer

low-metallicity stars are observed than predicted by the closed box model (this is known as the G-dwarf problem; Tinsley 1980). Worthey, Dorman & Jones (1996) arrived at a similar conclusion from analysis of a UV-optical spectrum of M31 and spectral indices for a sample of early-type and S0 galaxies. These researchers argued for a metal-poor component that was a factor of 2–3 lower than predicted by the closed box model. From the analysis of Lick indices of a sample of early-type galaxies, Greggio (1997) also concluded that a closed box model for the metallicity distribution failed to reproduce the data.

Although it is reasonably clear that early-type galaxies contain fewer low-metallicity stars than predicted by the closed box model, the more general task of measuring the detailed metallicity distribution function, or even the fraction of low-metallicity stars from integrated light measurements, is much more complex. As discussed in Section 4.5, the UV spectral region is sensitive to minority populations of hot stars of many types, including metal-poor main sequence stars, young stars, and exotic and uncertain evolutionary phases such as blue stragglers, extreme HB stars, and post-AGB stars. The latter two are very hot and so are more influential at $\lambda < 2{,}000$ Å, where the UV upturn phenomenon in early-type galaxies exists. From consideration of the mid-UV ($2{,}000$ Å $< \lambda < 4{,}000$ Å) spectra of M31 and other nearby galaxies, Worthey, Dorman & Jones (1996) argued for metal-poor fractions $\leq$5%. Maraston & Thomas (2000) modeled the mid-UV spectra of four nearby galaxies and found metal-poor fractions $\leq$6%, and Lotz, Ferguson & Bohlin (2000) argued in favor of small but nonzero fractions of metal-poor stars. Maraston & Thomas (2000) also highlight the point, first raised by Greggio (1997), that known metallicity gradients within galaxies, when combined with projection effects, will "contaminate" nuclear spectra of galaxies with metal-poor stars. It is notable that Maraston & Thomas (2000) find evidence for a spread in metal-poor fractions, ranging from 0–6%. This suggests that one should include the metal-poor fraction as an additional free parameter when fitting the mid-UV spectral range of early-type galaxies. Care must be taken when interpreting these fractions because the definition of metal-poor varies, although it generally refers to metallicities at least as low as [Fe/H] $\lesssim -1.5$. The problem boils down to the fact that the hot star fraction can be measured from UV (and perhaps blue spectral) data, but it is very challenging to convert this hot star population to a fraction of metal-poor stars owing to uncertainties in advanced phases of stellar evolution.

For actively star-forming galaxies essentially nothing is known regarding their internal distribution of metallicities, as the young stars overwhelm the subtle UV features signaling the presence or absence of low-metallicity stars.

5.6. Summary

The technique of measuring metallicities and abundance patterns from old stellar systems is well established. The age-metallicity degeneracy can be robustly broken by considering the hydrogen Balmer lines in conjunction with iron features in moderate-resolution optical spectra. Abundance ratios including [Mg/Fe], [C/Fe], [N/Fe], and [Ca/Fe] are now routinely measured from optical spectra. Other elements including O, Na, Si, Sc, Ti, V, Cr, Mn, Co, Ni, Sr, and Ba should also be measurable from high S/N optical-NIR spectra of old stellar systems, and models are presently being developed to extract this information. It is possible to measure metallicities based on photometric data, but the derived values depend on the underlying SPS model and on various assumptions like the form of the SFH. Photometric metallicities are therefore probably accurate only in a relative sense. Spectroscopic metallicities seem to be accurate at the ~0.2-dex level, with model systematics again being the dominant source of error. There is clearly information on the distribution of stellar metallicities within galaxies, and previous work suggests that it is possible to measure at least the low-metallicity tail of the distribution. Further modeling is required to

understand precisely how much information on the metallicity distribution function is available in the SEDs of quiescent galaxies.

6. DUST

6.1. Total Dust Attenuation

There exist four primary techniques for measuring dust attenuation in galaxies. (*a*) As the obscuring effects of dust increase with decreasing wavelength, multiwavelength analysis (including moderate-resolution spectra) of the UV-NIR SED can yield constraints on the total dust attenuation. (*b*) One can exploit the fact that the Balmer line ratio Hα/Hβ (sometimes referred to as the Balmer decrement) in the absence of dust can be computed from first principles and depends only weakly on the temperature of the gas (Osterbrock 1989). Comparison of the observed to the intrinsic ratio provides a measurement of the attenuation toward HII regions. (*c*) Energy conservation demands that whatever photons are absorbed in the UV/optical must be reradiated in the IR. The ratio of IR to UV luminosity (often referred to as IRX) therefore provides a measure of the total dust absorption. (*d*) A sufficiently luminous background source with a known intrinsic spectrum can provide a constraint on the attenuation in the foreground galaxy. This last technique is not discussed here, as it falls outside the scope of what one can learn from the SEDs of galaxies.

Techniques *a*–*c* provide complementary constraints on the dust within galaxies. This was most clearly demonstrated in the work of Calzetti, Kinney & Storchi-Bergmann (1994), who analyzed the reddening in a sample of 39 starburst and blue compact galaxies from both the Balmer line ratio Hα/Hβ and the slope of the UV continuum. These researchers found that the dust optical depth measured from the Balmer lines was nearly twice that estimated from the continuum (sometimes referred to as the 1:2 rule). They speculated that this could occur if young hot stars are embedded in dusty natal clouds, whereas older stars are subject to attenuation only from the diffuse ISM. Charlot & Fall (2000) later provided a detailed model for dust absorption that adopted this physical picture wherein young stars are embedded in their natal dusty clouds, and in addition, all stars experience dust attenuation due to the diffuse ISM. In this two-component model one must specify a transition time, after which the natal cloud is dispersed (typically taken to be 10^7 year), and attenuation curves for both the natal cloud and the diffuse ISM. In the standard implementation, both curves are taken to be power laws with the same exponent ($\tau_d \propto \lambda^{-0.7}$), and the normalization of the natal cloud attenuation curve is taken to be twice that of the diffuse ISM. The Charlot & Fall dust model is widely employed when modeling dusty SEDs.

In subsequent work, Meurer, Heckman & Calzetti (1999) compared the UV continuum slope, β, to the ratio between FIR and UV flux, $\log(L_{IR}/L_{UV}) \equiv$ IRX, and concluded that the starburst galaxies formed a well-defined sequence in the IRX-β plane (**Figure 12**). With additional assumptions about the underlying stellar populations and dust attenuation curve, these researchers were able to relate IRX (and hence β) to the total FUV dust attenuation. The resulting Meurer relation has been widely used to estimate the dust attenuation in distant galaxies for which only measurements of β are available. However, many subsequent studies have cast doubt on the practice of using β to estimate UV dust attenuation. Bell et al. (2002) noted that the relationship between β and UV attenuation measured in HII regions in the LMC differed from the Meurer relation. Kong et al. (2004) demonstrated that although dust content was the main variable responsible for the Meurer relation, other stellar population parameters, particularly the recent SFH, drive galaxies to other locations in the IRX-β plane (see also Boquien et al. 2012). The underlying extinction curve and star-dust geometry also play an important role in determining where galaxies lie in this plane (Charlot & Fall 2000; Kong et al. 2004; Panuzzo et al. 2007; Conroy, Schiminovich & Blanton 2010).

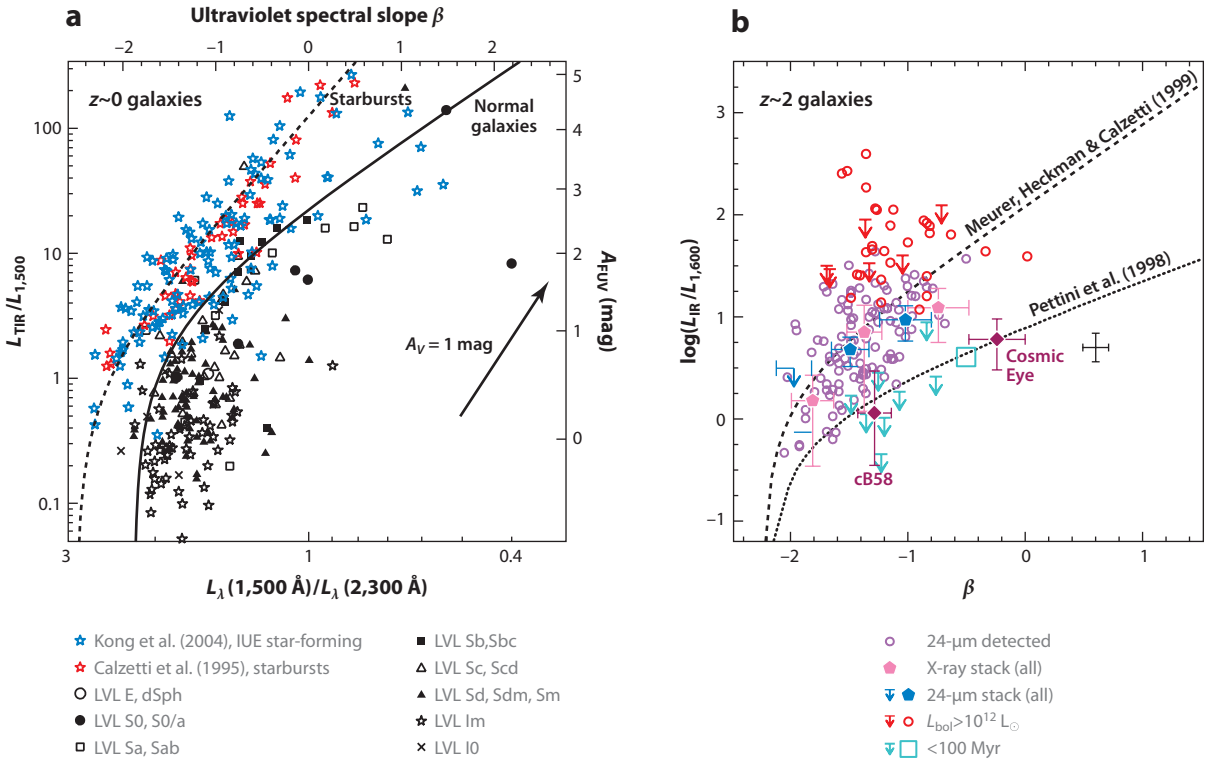

Figure 12

The IRX-β relation at (*a*) $z = 0$ from the Local Volume Legacy Survey (LVL) (Dale et al. 2009) and at (*b*) $z \sim 2$ (Reddy et al. 2010). The starburst relation (Meurer, Heckman & Calzetti 1999) is shown as a dashed line in both panels. (*a*) Symbols indicate starburst and star-forming galaxies, along with galaxies split by morphological type. (*b*) Symbols indicate galaxies selected in several different ways, either as having a young light-weighted age and high bolometric luminosity, or on the basis of X-ray or 24-μm fluxes. There is an overall trend that redder UV slopes correspond to higher IRX values. However, the more striking impression is the tremendous scatter in IRX at fixed β, especially in the region of the diagram where most galaxies reside, at $-2 < \beta < -1$.

Based on UV-IR photometry of 1,000 galaxies, Johnson et al. (2007) cast further doubt on the utility of the IRX-β relation for estimating dust content. Their conclusion rested partly on the observation that the relation defined by normal star-forming galaxies is so steep that even small errors in β will translate into large errors on IRX. **Figure 12** shows the IRX-β relation for galaxies from the Local Volume Legacy Survey (Dale et al. 2009), and the IRX-β relation for $z \sim 2$ galaxies from Reddy et al. (2010). It is clear that although galaxies of a particular type define their own IRX-β relations, the overall galaxy population presents a complicated picture. Fortunately, as multiwavelength datasets become increasingly common, the estimation of dust content from crude measures such as the IRX-β relation will give way to more robust techniques.

SED fitting of UV-NIR data has become remarkably common in the past decade. In nearly all cases the dust content is a parameter included in the fit, although the derived dust opacities are rarely discussed, most likely because the dust opacity is a relatively poorly constrained quantity when data only reach the NIR. As an example of the difficulty in constraining the dust opacity from broadband data, Salim et al. (2007) fit UV-NIR photometry to models and were able to recover *V*-band dust opacities with an uncertainty of ∼0.4 mag. Furthermore, there was only a weak correlation between the dust opacity derived from broadband data and the opacity derived from

emission lines via Brinchmann et al. (2004). Some of the difference can be attributed to aperture effects and real differences in the opacity measured from emission lines and stellar continua, but overall, the weak correlation confirms that dust content measured from broadband data is quite uncertain. Poorly constrained dust opacities appear to be a generic result of the modeling of UV-NIR broadband SEDs (e.g., Papovich, Dickinson & Ferguson 2001; Shapley et al. 2006; Kriek et al. 2008; Taylor et al. 2011).

Broadband UV-NIR data do not provide strong constraints on dust attenuation because of the well-known degeneracy between age and dust (e.g., Papovich, Dickinson & Ferguson 2001). This degeneracy can be broken, and stronger constraints on the dust opacity can be obtained, when either spectroscopic or FIR data are available. Spectroscopic data offer an estimate of the mean stellar age and metallicity independent of dust content because narrow spectroscopic features are relatively immune to overall changes in the continuum shape. Kauffmann et al. (2003) exploited this technique to measure mean ages of $\sim 10^5$ SDSS galaxies from Hδ and the 4,000-Å break. With the ages thus constrained, an estimate of the dust attenuation could be obtained by comparing the model colors with the observed ones. This study was limited primarily by the fact that the SDSS spectra sample a modest fraction of the total galaxy, and so a correction must be made for this aperture effect (ongoing and future planned integral field unit surveys such as CALIFA and MaNGA will remedy this limitation). Narrowband photometric surveys also offer the promise of separately constraining age and dust attenuation, primarily because of the strongly age-sensitive D_n4000 spectral feature, which is so strong that it can be probed with low-resolution data (e.g., Whitaker et al. 2010, Pérez-González et al. 2013). FIR data can also provide a robust measurement of the total dust attenuation because they significantly reduce the degeneracy between age and dust (e.g., Burgarella, Buat & Iglesias-Páramo 2005; Noll et al. 2009a).

Wuyts et al. (2007) and Williams et al. (2009) pioneered the use of restframe optical-NIR color-color diagrams (specifically $U-V$ versus $V-J$; commonly referred to as the UVJ diagram) to efficiently separate quiescent and star-forming galaxies. The UVJ diagram has since become a popular tool for separating these two galaxy types, especially at high redshift where data are limited. In a broad sense, the UVJ diagram allows one to break the age-dust degeneracy, but only in the sense of separating quiescent and dusty star-forming galaxies. Within the star-forming sequence, the age-dust degeneracy is still manifest when only broadband information is available.

Extremely blue UV continua can place strong constraints on the amount of dust in the system. Bouwens et al. (2012) and Finkelstein et al. (2012) measured the UV continuum slopes of high-redshift galaxies and found that β systematically decreases toward higher redshift and fainter galaxy luminosities. At the highest redshifts and faintest luminosities, they find $-2.0 < \beta < -2.5$, which not only suggests that these galaxies are dust-free but also begins to place interesting constraints on their stellar populations. The models of Schaerer (2003) reach such blue slopes only at very young ages ($\sim 10^6$ year) and/or very low metallicities ($<10^{-3}\ Z_\odot$), and the inclusion of nebular continuum emission, which presumably must be present whenever stars of these young ages are still alive, sets a lower limit to the UV continuum slope of $-2.5 < \beta < -3.0$, depending on the details of the SFH. Clearly, more data probing the restframe UV at very high redshifts would be valuable.

6.2. Constraints on the Attenuation Curve

Calzetti, Kinney & Storchi-Bergmann (1994) estimated a mean attenuation curve from 39 starburst and blue compact galaxies based on UV-optical spectra. By assuming that their sample was comprised of galaxies with the same underlying stellar populations, they were able to construct average attenuation curves by comparing galaxies with high and low Balmer line ratios, i.e., by

comparing dusty to dust-free galaxies. The resulting average attenuation curve, measured over ≈1,200 –8,000 Å, was grayer (shallower) than either the MW or LMC extinction curve and lacked the broad 2,175-Å dust feature visible in the MW and LMC. The derived curve is now referred to as the Calzetti attenuation law and is widely used when modeling the broadband SEDs of galaxies.

The Calzetti law was estimated from a relatively small sample of unusual (i.e., starburst and blue compact) galaxies at $z = 0$, and so one may wonder to what extent it is applicable to other systems. As noted in the previous section, the IRX-β relation is sensitive to the attenuation curve. The large range in β at a fixed IRX, evident in **Figure 12**, suggests considerable variation in the attenuation curve, but interpretation of the IRX-β plane is complicated by the additional variables affecting IRX and β.

Progress can be made by estimating stellar population parameters such as the SFH and metallicity independently of the dust content (e.g., via narrow spectral features). With such quantities in hand, one can exploit the technique pioneered by Calzetti and collaborators by computing ratios of SEDs of more to less dusty galaxies with the same underlying stellar populations. Johnson et al. (2007) estimated mean attenuation curves in this way for galaxies as a function of the 4,000-Å break strength and stellar mass. The curves were constrained from broadband FUV-NIR photometry and were consistent both with a simple power law, $\tau_d \propto \lambda^{-0.7}$ and with the Calzetti law. Wild et al. (2011) exploited a similar technique using pairs of galaxies with similar gas-phase metallicities, specific SFRs and inclinations, and significantly different Balmer decrements to construct attenuation curves from broadband FUV-NIR data. These researchers found significant variation in the mean attenuation curve as a function of specific SFR, inclination, and stellar mass surface density, based on a sample of 20,000 $z \sim 0$ star-forming galaxies. They also found variation in the ratio between dust opacity in the stellar continuum and in the nebular line emission, implying that the 1:2 rule of Calzetti, Kinney & Storchi-Bergmann (1994)—one unit of continuum opacity for every two units of line opacity—is not universal. Buat et al. (2012) modeled the UV-FIR SEDs of galaxies at $1 < z < 2$, allowing for variation in the dust attenuation curve. They found evidence for a steeper attenuation curve (i.e., faster rise in the UV) than the Calzetti law in 20–40% of their sample.

6.2.1. The 2,175-Å dust feature. The absence of the 2,175-Å dust feature from the Calzetti attenuation law is striking given its ubiquity in the MW and LMC. Witt & Gordon (2000) were able to reproduce the Calzetti law in their radiative transfer models only by assuming SMC-type dust, i.e., by adopting an underlying extinction curve that lacked the 2,175-Å dust feature. In contrast, Granato et al. (2000) were able to reproduce the Calzetti law in their radiative transfer models with MW-type dust. In their model the star-dust geometry plays a central role in shaping the starburst attenuation curve. Their molecular clouds are optically thick, and so the attenuation curve is determined primarily by the fraction of stars inside molecular clouds as a function of age (see also Panuzzo et al. 2007). Fischera & Dopita (2011) were able to reproduce a Calzetti-like attenuation curve if the carrier responsible for the 2,175-Å dust feature (e.g., PAHs) was destroyed at high column density.

In all radiative transfer dust models, the expectation is that normal star-forming galaxies should show evidence for the 2,175-Å dust feature provided that the underlying grain population is similar to the MW or LMC. Owing to a paucity of restframe UV spectra of star-forming galaxies, it has proved difficult to verify this expectation. Burgarella, Buat & Iglesias-Páramo (2005) analyzed the UV-FIR SEDs of 180 star-forming galaxies and concluded that the data required an attenuation curve with a 2,175-Å dust feature that was on average weaker than observed in the MW extinction curve. Noll et al. (2009b) presented stacked restframe UV spectra of $z \sim 2$ star-forming galaxies and found strong evidence for the presence of the 2,175-Å dust feature in a subsample of their objects.

Conroy, Schiminovich & Blanton (2010) analyzed UV-NIR photometry of $z \sim 0$ star-forming galaxies as a function of inclination and found evidence for a 2,175-Å dust feature with a strength slightly weaker than observed in the MW extinction curve. Hoversten et al. (2011) analyzed medium-band UV photometry from the *Swift* UV/Optical Telescope and found evidence for a prominent 2,175-Å bump in M81. Wild et al. (2011) found evidence in their derived attenuation curves for the presence of the 2,175-Å dust feature, with a slight tendency for galaxies with higher specific SFRs to have lower bump strengths. Wijesinghe et al. (2011) compared dust-corrected SFRs estimated from Hα and the UV and found agreement only when the 2,175-Å feature was removed from the attenuation curve, but these researchers did not consider variation in the shape of the attenuation curve. Buat et al. (2012) found evidence that the 2,175-Å dust feature is present in 20% of their sample, with an amplitude that is half the strength found in the MW extinction curve. Similar to Wild et al., they found an anticorrelation between bump strength and specific SFR. The emerging consensus appears to be that the 2,175-Å dust feature is present in the typical star-forming galaxy over the redshift range $0 < z < 2$, with a strength that is generally lower than in the MW extinction curve and increases with increasing inclination and decreasing specific SFR. The absence of the dust feature in the Calzetti law may then simply be a reflection of the fact that the galaxies in the Calzetti sample have unusually high specific SFRs. An outstanding question is whether these trends are due to varying star-dust geometries or changes in the underlying grain population. As emphasized in Conroy, Schiminovich & Blanton (2010) and elsewhere, these results have consequences for interpreting the IRX-β relation, as β is frequently measured over a wavelength range that includes the 2,175-Å dust feature.

6.3. Physical Dust Properties

The IR emission by dust grains provides strong constraints on a variety of physical properties of a galaxy, including the bolometric luminosity, dust temperature(s), dust mass, and relative abundance of PAH molecules (or more generally, the grain size distribution). A constraint on the bolometric luminosity helps to break the age-dust degeneracy in the UV-NIR, as discussed in the previous section. The other parameters provide clues to the nature of dust in galaxies and its spatial relation to the stars and gas.

It has long been recognized that constraints on the dust mass and dust temperatures require data beyond the peak in the thermal dust emission spectrum at ~100 μm. The SCUBA bolometer array at the James Clerk Maxwell Telescope, operating at 450 μm and 850 μm, has been extremely influential in this field, and now the SPIRE instrument onboard the *Herschel Space Observatory*, operating at 250–500 μm, promises to revolutionize the field by dramatically increasing sample sizes over a wide range in redshifts. With data obtained for the SCUBA Local Universe Galaxy Survey, Dunne et al. (2000) and Dunne & Eales (2001) constrained dust masses and temperatures for 104 nearby galaxies. The data favored models that contained both cold and warm dust components (at ~20 K and ~40 K, respectively). They also found that dust masses estimated with single-temperature models were on average lower by a factor of ~2 compared with two-temperature models, and the two-temperature dust masses yielded dust-to-gas ratios in agreement with measurements in the Galaxy.

Draine et al. (2007) presented a thorough analysis of the IR SEDs of galaxies from the SINGS survey of 65 nearby galaxies. These researchers analyzed data from *Spitzer*, IRAS, and SCUBA with the physical dust models of Draine & Li (2007). The model considers grain populations exposed to a variety of starlight intensities and includes both thermal emission and single photon heating of dust particles. In addition, the fraction of dust mass contained in PAH molecules is a free variable. Draine et al. confirmed the results of previous work that the submillimeter data,

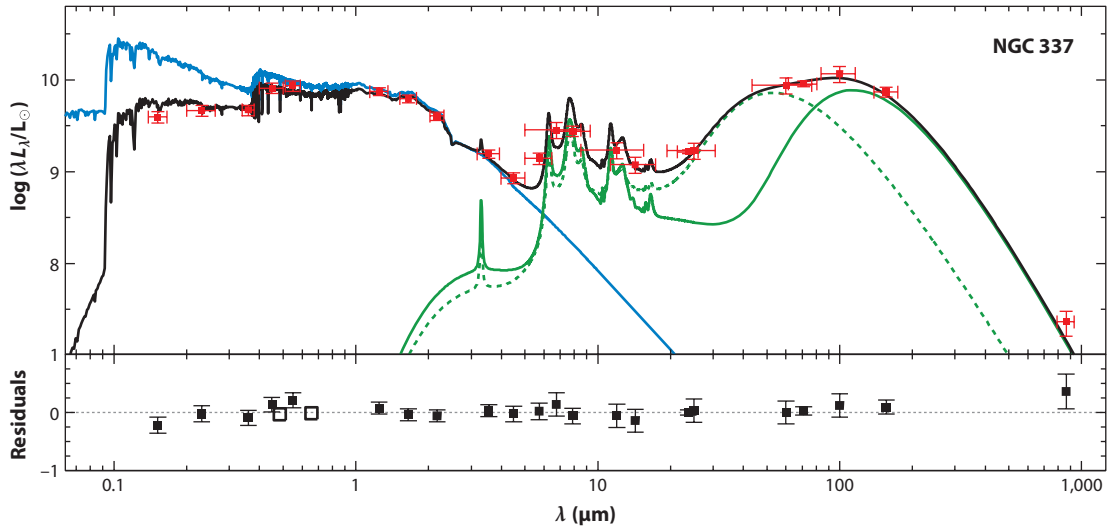

Figure 13

Model fit to the far-ultraviolet through far-infrared spectral energy distribution of NGC 337. The black line is the best-fit model. Also shown are the unattenuated model starlight (*blue line*) and the dust emission separated into dust in the diffuse interstellar medium (*solid green line*) and dust in birth clouds (*dotted green line*). Figure courtesy of E. da Cunha (da Cunha, Charlot & Elbaz 2008).

provided by SCUBA, were essential for deriving dust masses with an uncertainty of <50%. They also derived strong constraints on the fraction of dust mass in PAHs, the interstellar radiation field strength in the diffuse ISM, and the flux-weighted mean radiation field strength averaged over the galaxy. The well-sampled spectral coverage from the mid-IR through the submillimeter was essential in order to separately constrain each of these components.

Dale et al. (2012) analyzed FIR and submillimeter photometry for SINGS galaxies from *Herschel* in conjunction with previously available 2MASS, *Spitzer*, IRAS, ISO, and SCUBA data. These researchers modeled the SEDs with the Draine & Li (2007) dust model, both with and without the *Herschel* data. They found modest differences (factors of ≈1.6 on average) in the best-fit dust masses, PAH mass fractions, and fraction of dust emission arising from the diffuse ISM when the FIR and submillimeter data were either included or excluded. They also demonstrated that dust masses estimated via simple modified blackbody fits significantly underestimated the dust masses (by factors of ≈3 in the worst cases), with the underestimation becoming more severe as bluer wavelengths were included in the fits. The *Herschel* data are of such high quality that simplistic, modified blackbody dust models are no longer capable of providing adequate fits to the data.

da Cunha, Charlot & Elbaz (2008) developed a phenomenological model for the UV-FIR SEDs of galaxies based on the Bruzual & Charlot (2003) SPS models for starlight, the Charlot & Fall (2000) dust attenuation model, and dust emission comprised of multiple components including an empirical spectrum for the PAH emission, warm and cold thermal dust emission, and emission from stochastically heated grains (**Figure 13**). Based on tests with mock galaxies, they concluded that a variety of parameters could be constrained within the context of their model, including the temperature of the cold dust component, the fractional contribution of the cold dust to the total FIR emission, and the total dust mass. They analyzed the same SINGS galaxies as did Draine et al. and derived dust masses that agreed to within 50%, demonstrating that dust masses can be reliably measured with reasonably well-sampled mid-IR, FIR, and submillimeter data.

Galliano, Dwek & Chanial (2008) employed the dust model of Zubko, Dwek & Arendt (2004) to constrain a variety of parameters, including the total dust mass, fraction of dust mass in PAHs, fraction of dust luminosity originating from photodissociation regions, and gas-phase metallicity. Galliano, Dwek & Chanial measured these and other parameters for 35 galaxies with optical, IR, and submillimeter photometry and mid-IR spectroscopy. There is broad overall agreement between Draine et al. (2007) and Galliano, Dwek & Chanial (2008) in the trend of PAH mass fraction versus gas-phase metallicity, although detailed object-by-object comparisons would be fruitful. As discussed extensively by Draine & Li (2007), the optical properties of the PAH molecules are uncertain and have in many cases been tuned to fit extragalactic data. It would therefore be valuable to compare the results obtained from dust models that assume different treatments of the uncertain PAH properties.

6.4. Cosmic Evolution of IR Spectral Energy Distributions

Measuring the cosmic evolution of IR SEDs is important not only for constraining models of galaxy evolution but also because local IR SED templates are frequently employed to interpret high-redshift data. For example, the local templates are often used to convert 24-μm observations of high-redshift galaxies to SFRs. If IR SEDs at fixed $L_{\rm bol}$ evolve with time, then it would considerably complicate the interpretation of higher redshift data.

Pope et al. (2006) presented evidence that the SEDs of ULIRGs at $z \sim 2$ peak at longer wavelengths than local ULIRGs, implying that the dust temperature in high-redshift ULIRGs is on average ∼5 K cooler than local ULIRGs. Muzzin et al. (2010) analyzed high-quality data for two $z \sim 2$ ULIRGs and found that these galaxies contained colder dust than local ULIRGs, in agreement with Pope et al. (2006). Muzzin et al. showed that the SED shapes of their ULIRGs were well fit by the $z = 0$ Chary & Elbaz (2001) templates that were an order of magnitude less luminous than their $z \sim 2$ galaxies. In other words, the $z \sim 2$ ULIRGs had SED shapes that were similar to local luminous IR galaxies (LIRGs). Exploiting the power of *Herschel* data, Hwang et al. (2010) estimated dust temperatures by fitting modified blackbodies to the data and found evidence for slightly cooler, by 2–5 K on average, dust temperatures at $z \sim 1$ for galaxies with $L_{\rm IR} > 10^{11}\ L_{\odot}$. Daddi et al. (2007) compared restframe 8-μm luminosities of $z \sim 2$ galaxies to local templates and found evidence for excess mid-IR emission for galaxies with $L_{8\,\mu{\rm m}} > 10^{11}\ L_{\odot}$. This mid-IR excess problem was confirmed by Papovich et al. (2007) and later by Elbaz et al. (2010) with *Herschel* data. It is noteworthy that the problem only appears at $z > 1.5$. Bolometrically luminous high-redshift galaxies thus have colder dust and more flux in the mid-IR compared with galaxies at the same $L_{\rm bol}$ at $z = 0$. The mid-IR excess problem has important implications for the common practice of estimating SFRs for galaxies at $z \sim 2$ with *Spitzer* 24-μm observations (i.e., restframe ∼8 μm). The sign of the excess is such that SFRs estimated by extrapolating observed 24-μm flux with local templates will tend to overestimate the true SFRs, by factors of several in the most extreme cases (e.g., Papovich et al. 2007).

Elbaz et al. (2011) investigated the origin of the differences between high and low redshift IR SEDs with very deep *Herschel* observations. They argued that it is the distribution of SED types that is changing at high luminosity as a function of redshift. At low redshift, high-luminosity systems (i.e., ULIRGs) are predominantly starbursts and compact, whereas at higher redshift ULIRGs are mostly the high-luminosity extensions of normal star-forming galaxies. Local ULIRGs therefore have hotter dust temperatures and a depressed emission component from PAHs in the mid-IR compared with distant ULIRGs, because the former are compact starbursts whereas the latter are normal, extended star-forming galaxies (see also Rujopakarn et al. 2012, who reached similar conclusions). The physical origin of this result is not yet fully understood, but a plausible

explanation is that compact starbursts have harder and more intense radiation fields. The radiation field obviously has a direct influence on the dust temperature, and it may also modulate the dust mass fraction in PAHs and therefore the mid-IR luminosity (Voit 1992, Madden et al. 2006, Draine et al. 2007).

6.5. Summary

The Calzetti attenuation curve works remarkably well at describing the mean attenuation properties of star-forming galaxies over most of cosmic history. However, closer scrutiny of the data reveals variation in the attenuation curve of galaxies as a function of galaxy properties, as expected on theoretical grounds. In contrast to the Calzetti attenuation curve for starburst galaxies, the 2,175-Å dust feature is common in normal star-forming galaxies, with a strength that is weaker than observed in the MW extinction curve. The IRX-β relation should be used with caution, as there is evidently no universal relation for all galaxies. In addition, the relation is so steep over the range in β where most galaxies reside that estimating dust opacity in this way is highly unreliable. Dust masses can be measured to an accuracy of ∼50% when FIR and submillimeter data are available. Physical dust models, such as the model of Draine & Li (2007), are capable of extracting a variety of parameters from the global SEDs of galaxies, including the fraction of dust mass in PAHs, the fraction of dust emission due to photodissociation regions versus the diffuse ISM, and the typical interstellar radiation field strength heating the dust grains (or alternatively, the typical dust temperature). Further work is needed to sort out which derived parameters are robust and which are dependent on uncertain components of the model. Below $L_{\rm bol} \sim 10^{11}\ L_{\odot}$, the IR SEDs of galaxies evolve little over the interval $0 < z < 2$. At higher luminosities there is a marked shift such that high-redshift ULIRGs have more mid-IR flux and a colder dust component that peaks at longer wavelengths. A plausible explanation for this trend is that ULIRGs at high redshift are at the massive end of the normal star-forming galaxy sequence, whereas ULIRGs in the local Universe are unusual, compact star-bursting systems.

7. THE INITIAL MASS FUNCTION

7.1. Constraints from Spectral Energy Distributions

The stellar IMF is of fundamental importance for many areas of astrophysics. The form of the IMF is well constrained in the Galactic disk (Salpeter 1955, Miller & Scalo 1979, Kroupa 2001, Chabrier 2003). However, it is not clear whether the IMF has had the same form over all of cosmic time and in all environments. The low mass end is of particular importance, as ∼60–80% of the stellar mass density in the Universe is in the form of stars with masses $<0.5\ M_{\odot}$. Low-mass stars are very faint and so contribute only a few percent to the integrated light of an old population. For this reason, when fitting the SEDs of galaxies, an IMF is typically assumed, and so the IMF is one of the largest sources of systematic uncertainty in studies of extragalactic stellar populations.

It has been known since at least the 1960s that dwarf-sensitive and, to a lesser degree, giant-sensitive spectral features could be used to count the number of low-mass stars in the integrated light of old stellar populations (e.g., Spinrad 1962; Spinrad & Taylor 1971; Whitford 1977; Frogel et al. 1978; Frogel, Persson & Cohen 1980; Vazdekis et al. 1996; Schiavon, Barbuy & Singh 1997; Schiavon et al. 1997; Schiavon, Barbuy & Bruzual 2000). This idea is limited to quiescent systems because the massive stars associated with ongoing star formation would dramatically outshine the faint low-mass stars. The fundamental difficulty then, as now, is the separation of abundance effects from giant-to-dwarf ratio effects. Both effects can change the strength of the gravity-sensitive lines.

Spinrad & Taylor (1971) concluded that the nuclei of the nearby galaxies M31, M32, and M81 are dominated by dwarfs, with an implied $M/L = 44$. These conclusions were based on photoelectric scanner observations reaching to 1 μm. Subsequently, Cohen (1978) measured the IMF-sensitive NaI, CaT, FeH, and TiO features in the nucleus of M31 and M32 and concluded that an IMF comparable to that of the Solar Neighborhood was favored, along with metallicity enhancement in M31. Faber & French (1980) also measured the strength of the NaI doublet in M31 and M32 and instead argued for a dwarf-rich IMF, along the lines of Spinrad & Taylor (1971), with $M/L_B = 28$. Frogel et al. (1978) analyzed optical-NIR colors and the CO band head at 2.3 μm for 51 early-type galaxies and concluded that dwarf-rich IMFs were inconsistent with the data and favored models with $M/L_V < 10$. With updated detector technology and more sophisticated models, Carter, Visvanathan & Pickles (1986) argued against dwarf-rich IMFs on the basis of the NaI, CaT, TiO, and FeH features in 14 elliptical and lenticular galaxies. Their results implied mass-to-light ratios of $M/L \sim 6$. In a series of articles, Hardy, Couture, and collaborators (Hardy & Couture 1988, Delisle & Hardy 1992, Couture & Hardy 1993) analyzed the IMF features NaI and FeH for on the order of a dozen galaxies and concluded that dwarf-rich IMFs were strongly disfavored. Measurements of the FeH band at 1 μm (also known as the Wing-Ford band) were particularly important, as this feature becomes very strong for IMF exponents steeper than Salpeter (Whitford 1977).

Early work aimed at measuring the IMF from integrated light spectra suffered from serious limitations, including (*a*) the lack of accurate stellar evolution calculations across the main sequence and through advanced evolutionary phases; (*b*) the use of empirical stellar spectra collected from the Solar Neighborhood, which implied that the effect of nonsolar abundance ratios could not be adequately assessed; and (*c*) poor NIR detector technology, which made it very difficult to measure red spectra at the subpercent-level precision necessary to measure the low-mass IMF in integrated light. These limitations contributed to the wide range of reported IMF exponents and mass-to-light ratios noted above. In the past two decades, each of these limitations has been significantly reduced, though not eliminated. Stellar evolution calculations have improved dramatically since the 1970s; the response of stellar spectra to elemental abundance variations has been studied in detail (e.g., Tripicco & Bell 1995; Korn, Maraston & Thomas 2005; Serven, Worthey & Briley 2005; Conroy & van Dokkum 2012a); and NIR detector technology has steadily improved.

The debate over IMF variation was renewed by Saglia et al. (2002) and Cenarro et al. (2003), who independently reported an anticorrelation between the strength of the IMF-sensitive CaT index and velocity dispersion for elliptical galaxies. Comparison to SPS models with solar-scaled abundance ratios required dwarf-rich IMFs, with an exponent of $\alpha \approx 4$ at the highest dispersions (compared with the Salpeter value of 2.35). Saglia et al. (2002) argued against this interpretation, as such a steep IMF would imply $M/L \approx 40$, well in excess of newly available dynamical constraints. Worthey, Ingermann & Serven (2011) investigated several calcium-sensitive spectral features and concluded that a modest decrease in [Ca/Fe] with velocity dispersion could also explain the observed trends. Worthey, Ingermann & Serven (2011) also noted that such dwarf-rich IMFs would yield optical-NIR colors (e.g., $V-K$) much redder than even the reddest observed early-type galaxies.

An IMF different from the Galactic disk (often referred to as a nonuniversal IMF) was also reported by van Dokkum & Conroy (2010) based on the analysis of high S/N spectra extending to 1 μm for eight massive galaxies in the Coma and Virgo clusters. These data were of extremely high quality thanks to new detector technology installed on the Low-Resolution Imaging Spectrometer (LRIS) instrument at the Keck Telescope. The data were interpreted with new models limited to solar-scaled abundance patterns. Dwarf-rich IMFs were favored, with an IMF exponent in the range $2.3 < x < 3$. It is worth pausing here to note that the meaning of dwarf-rich has evolved

over the years. In the 1970s, dwarf-rich IMFs indicated mass-to-light ratios exceeding 20, often reaching as high as 40. With the IMF in the Solar Neighborhood now well established (Kroupa 2001, Chabrier 2003), the reference point has shifted. Now, dwarf-rich IMFs are those that contain relatively more low-mass stars than found in the Solar Neighborhood and would indicate, among other implications, a nonuniversal IMF. In this sense, the Salpeter IMF is dwarf-rich as it contains more low-mass stars than the Kroupa (2001) IMF for the Solar Neighborhood.

Conroy & van Dokkum (2012b) were the first to analyze high-quality absorption line spectra of 34 early-type galaxies and the nuclear bulge of M31 with a model that allowed for both IMF variation and abundance pattern variation (in addition to variation in age and several nuisance parameters). The model, presented in Conroy & van Dokkum (2012a), allows for variation in the abundance pattern of 11 elements and is based on the latest isochrone tables and the MILES and IRTF stellar libraries. Conroy & van Dokkum (2012b) simultaneously fit the full blue and red galaxy spectra to their models, including the classic IMF-sensitive features NaI, CaT, and FeH, as well as IMF-sensitive features in the blue spectral region. An example fit to a massive early-type galaxy is shown in **Figure 14**. These researchers argued that the models favor IMFs that become progressively more dwarf-rich (i.e., more bottom heavy) for more massive and more α-enhanced galaxies. Over the full sample, the mass-to-light ratios predicted by their best-fit IMFs vary by only a factor of 3 at fixed age and metallicity. The IMF variation advocated by Conroy & van Dokkum (2012b) is thus much subtler than previous claims for dwarf-rich IMFs. The best-fit mass-to-light ratios do not violate dynamical constraints. Similar conclusions were reached by Smith, Lucey & Carter (2012) based on the analysis of 1-μm spectroscopy of 92 galaxies in the Coma cluster and by Spiniello et al. (2012), who analyzed indices sensitive to NaI and TiO for a sample of early-type galaxies.

Meanwhile, there have been several less direct arguments favoring top-heavy (or bottom-light) IMFs in some types of galaxies and in some phases of a galaxy's evolution. Tinsley (1980) suggested that a constraint on the IMF near the turnoff mass could be obtained by comparing the evolution of the *M/L* ratio and color of passively evolving galaxies. Van Dokkum (2008) applied this idea to the evolution of galaxies on the fundamental plane and found evidence that the IMF is flatter than the MW IMF at $\sim$1 $M_\odot$ in early-type galaxies. However, van Dokkum & Conroy (2012) demonstrated that when galaxies are compared at fixed velocity dispersion, as opposed to fixed stellar mass, the evolution in the fundamental plane is consistent with the standard Salpeter slope at $\sim$1 $M_\odot$ (see also Kelson et al. 2001, Holden et al. 2010). Numerous researchers have demonstrated that the evolution of the cosmic SFR and cosmic stellar mass density are mutually inconsistent but can be brought into agreement by adopting a top-heavy IMF (Hopkins & Beacom 2006; Davé 2008; Wilkins, Trentham & Hopkins 2008). However, recent improvement in the modeling of the data, including luminosity-dependent dust corrections, rising SFHs, and revised values of the faint end slope of the mass function have reconciled the cosmic star formation and mass densities derived with standard IMFs (Reddy & Steidel 2009; Papovich et al. 2011; Behroozi, Wechsler & Conroy 2013). A third argument in favor of top-heavy IMFs is the apparent inability of galaxy formation models to reproduce the observed number of luminous submillimeter galaxies (Baugh et al. 2005). Here, too, recent observations and more sophisticated models have significantly reduced the tension between models and data (Hayward et al. 2012). It thus appears that much of the evidence originally favoring a top-heavy IMF at certain epochs and under certain conditions can now be explained by more mundane effects.

7.2. Summary

Extremely dwarf-rich IMFs are now routinely ruled out by both sophisticated SPS models and dynamical constraints, and earlier evidence for top-heavy IMFs has not held up to further scrutiny.

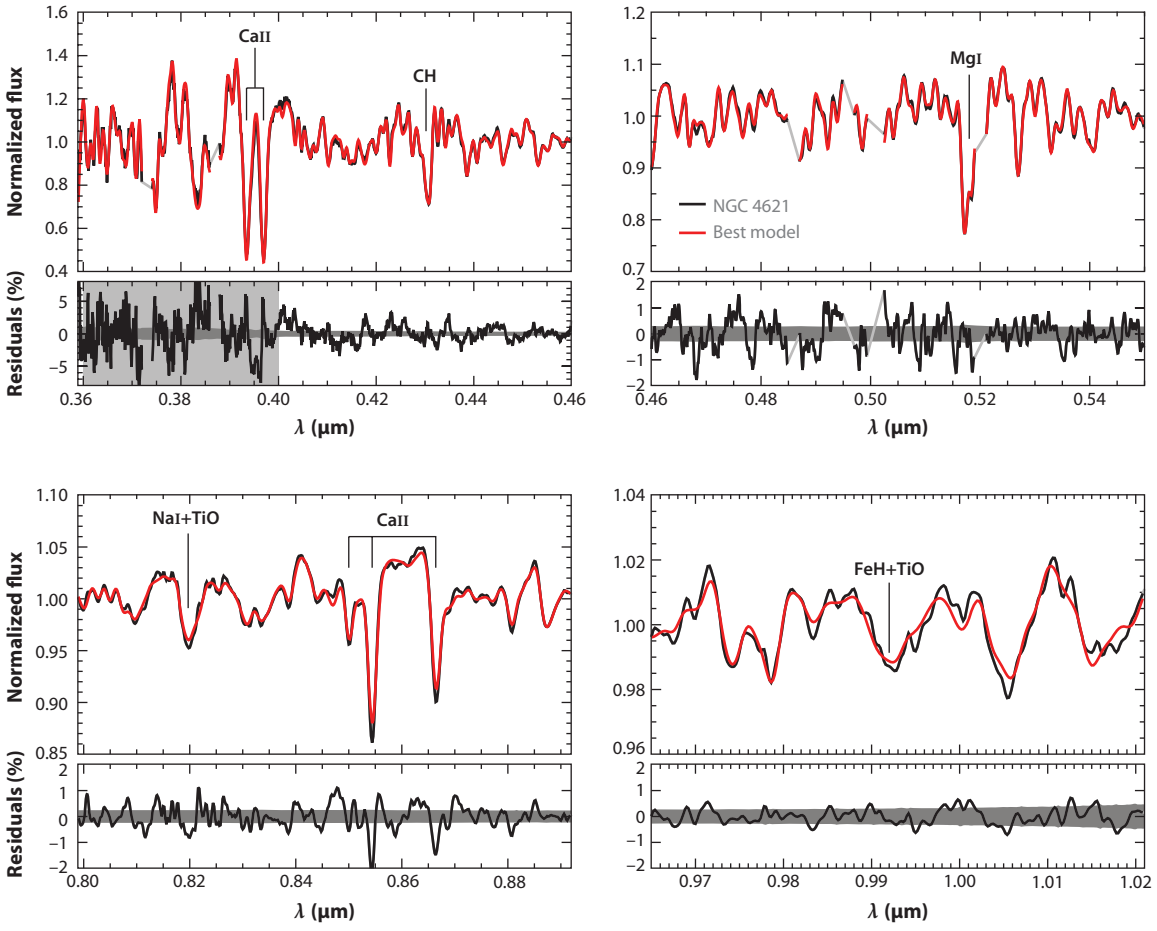

Figure 14

Comparison of the best-fit model and observed spectrum for NGC 4621, a massive early-type galaxy. Both data and model have been continuum normalized. The S/N is indicated as a gray shaded band; the data at <4,000 Å were not included in the fit but are included here for completeness. The model has 21 free parameters, including the abundance of 11 elements and the shape of the low-mass initial mass function (IMF). The root mean square difference between the model and data is 0.8%. IMF-sensitive features include the NaI doublet at 0.82 μm, the CaII triplet at ≈0.86 μm, and the FeH band head (i.e., the Wing-Ford band) at 0.99 μm. The best-fit *M/L* is twice as large as would be expected for a Milky Way IMF, suggesting that the IMF is not universal. Adapted from Conroy & van Dokkum (2012b).

However, more modest IMF variations appear to be supported by the data, at the level of a factor of 2–3 in *M/L*. It is intriguing that constraints on the IMF based solely on dynamical modeling also favor a mild steepening (i.e., relatively more low-mass stars) with increasing velocity dispersion (Auger et al. 2010; Graves & Faber 2010; Treu et al. 2010; Thomas et al. 2011; Cappellari et al. 2012; Dutton, Mendel & Simard 2012; Dutton et al. 2013a,b; Sonnenfeld et al. 2012; Spiniello et al. 2012). As both dynamical and stellar population–based techniques suffer from nonnegligible but largely orthogonal systematics, the most promising direction for future constraints will come from joint analyses of the same systems with SPS and dynamical techniques.

8. CONCLUDING REMARKS

The goal of this review has been to summarize what we have learned about galaxies from their panchromatic SEDs using the tools of SPS. By way of concluding, I would like to turn toward the future and highlight areas where additional work is needed to make SED modeling both a more firmly quantitative science and also an effective engine for new discoveries. In short, and not surprisingly, the future requires better data, better models, better comparison of models to data, and a better understanding of what is in principle knowable from the analysis of galaxy SEDs.

A clear theme of this review has been the power of combining broadband data with moderate-resolution spectra. The SDSS has been a revolutionizing force in this regard, as it has provided high-quality photometry and optical spectra for over one million objects. The great drawback of the SDSS is that it is fiber-based and thus the spectra only sample the central 3 arcsec (in diameter) of galaxies. This drawback will be alleviated with integral field unit spectroscopic surveys of nearby galaxies, including the recently completed SAURON survey (Bacon et al. 2001), the ongoing ATLAS3D survey (Cappellari et al. 2011) of 260 early-type galaxies, the CALIFA survey of ∼600 galaxies (Sánchez et al. 2012), and the proposed MaNGA survey of a mass-limited sample of ∼10,000 galaxies. Such surveys will provide high-quality spectra that are well matched to the broadband data. Restframe NIR spectra will be a new frontier for SPS studies as next generation NIR facilities become operational, including ground-based spectrographs (FIRE, FMOS, KMOS, MOSFIRE, FLAMINGOS-2, etc.), and the eventual launch of the *James Webb Space Telescope*. High-quality models are only now being developed to interpret such data. In addition to spectra, narrow-band photometry will also be a valuable addition to the landscape, as pioneered by the COMBO-17 survey (Wolf et al. 2004) and now utilized by surveys such as ALHAMBRA (Moles et al. 2008), the NEWFIRM Medium-Band Survey (Whitaker et al. 2011), and SHARDS (Pérez-González et al. 2013). Grism data will also help bridge the gap between broadband photometry and moderate-resolution spectra, as demonstrated by the 3D-HST survey (Brammer et al. 2012). In addition to these object-by-object surveys, the construction of composite SEDs from galaxies spanning a range of redshifts allows for the creation of very-high-quality and well-sampled SEDs that will be invaluable for SPS studies (Assef et al. 2008, Kriek et al. 2011).

Another theme of this review has been the growing realization that uncertainties in the SPS models are becoming a critical limiting factor to the interpretation of galaxy SEDs. The challenge here is not simply to enumerate the uncertainties but rather to identify areas where clear progress can be made. As a first step, all SPS models should include contributions from nebular emission and dust around AGB stars, as these processes are known to occur and the incorporation of such effects into the models is reasonably straightforward, even if the details are uncertain. Panchromatic models (i.e., FUV-FIR coverage) should also become standard both because IR data are now widely available and because sophisticated dust emission models are well developed (e.g., Draine & Li 2007). The stellar atmospheric and synthetic spectral models will benefit from new asteroseismology measurements from the *Kepler* mission, interferometric observations (e.g., by CHARA), and new very-high-resolution UV-NIR spectral atlases of nearby stars across the HR diagram (Bagnulo et al. 2003, Lebzelter et al. 2012). Perhaps the most vexing issues lie with the stellar evolution uncertainties, as obvious calibrating data are lacking. The well-known problem is that although globular clusters are the canonical testing ground for stellar evolution, metal-rich clusters are rare, and so the models tend to be poorly constrained precisely in the metallicity range most relevant for modeling galaxies. Moreover, the largest uncertainties are associated with fast evolutionary phases, and so stars in such phases will be rare in all but the most massive star clusters. Efforts to constrain uncertain stellar evolutionary phases from the SEDs of galaxies is promising because the right metallicity ranges are probed and there are sufficient numbers of stars

to overcome Poisson noise, but the obvious complexity of dealing with CSPs makes this approach challenging (e.g., Kriek et al. 2010, MacArthur et al. 2010, Zibetti et al. 2012). The Panchromatic Hubble Andromeda Treasury survey (Dalcanton et al. 2012) is an HST program covering ∼1/3 of M31's star-forming disk in six filters. It promises to provide new and powerful constraints on luminous and advanced stellar evolutionary phases at moderately high metallicities.

More accurate models and higher-quality data will necessitate a more sophisticated approach to comparing the two. Presently, model fitting is something of an art, owing to the fact that large regions of parameter space are often severely underconstrained, which implies that the choice of priors on the model parameters can have a large impact on the derived results. A few basic guidelines should be followed to ensure that results are robust. For example, one should not simply fix a parameter to a particular value because it is underconstrained. Moreover, because the likelihood surface often contains multiple peaks and valleys and is frequently computed on a coarse grid, the best-fit parameters ought not be chosen based on the minimum of χ^2 (see, e.g., Taylor et al. 2011). Rather, the full posterior distributions should be used to derive best-fit values and associated uncertainties. The choice of priors needs to be considered carefully, and in fact, the model space should probably depend on the type of data being fit, the redshift of the object, and even its spectral type (quiescent versus star-forming versus peculiar). As the number of parameters increases, Markov Chain Monte Carlo techniques will see more widespread use owing to their efficient exploration of parameter space. With regard to the modeling of moderate-resolution spectra, the analysis of spectral indices should eventually give way to full spectral fitting as the latter not only allows for the extraction of more information but also allows the modeler to visually inspect the fits in a way that is not possible when only EWs are extracted from the data. This is important for identifying model systematics and areas for future improvement.

Finally, further work is needed to understand what is knowable, in principle, from the modeling of galaxy SEDs. Yet to be thoroughly explored are questions such as, How many discrete SF episodes can be measured from high-quality optical spectra? How many moments of the metallicity distribution function can be extracted from SEDs? Can the detailed dust attenuation curve be measured with sufficiently high-quality data on an object-by-object basis? Addressing these questions will be difficult because they depend sensitively on the quality of the data, the SED type, and the reliability of the models. Fitting routines such as STARLIGHT, STECMAP, and VESPA that attempt a nonparametric recovery of the SFH and metallicity distribution function offer what are probably the most reliable tools to explore these questions. Theoretical studies aimed at understanding what is "knowable" will help guide the next generation of surveys aimed at studying the detailed physical properties of galaxies.

DISCLOSURE STATEMENT

The author is not aware of any affiliations, memberships, funding, or financial holdings that might be perceived as affecting the objectivity of this review.

ACKNOWLEDGMENTS

I would like to thank my collaborators for the continuous lively conversations that have helped form my views on this topic. I would also like to thank the researchers who generously shared their figures for this review, and especially Elisabete da Cunha, John Moustakas, Naveen Reddy, and Rita Tojeiro for providing new or modified figures. Stéphane Charlot, Daniel Dale, Sandy Faber, Jerome Fang, Ricardo Schiavon, Rita Tojeiro, and Scott Trager are thanked for very useful

comments on an earlier version of this manuscript. Finally, I would like to thank Roselyn Lowe-Webb for her patience in managing this manuscript through the production process.

LITERATURE CITED

Acquaviva V, Gawiser E, Guaita L. 2011. *Ap. J.* 737:47
Allard F, Hauschildt PH. 1995. *Ap. J.* 445:433–50
Allard F, Homeier D, Freytag B. 2011. In *16th Cambridge Workshop on Cool Stars, Stellar Systems, and the Sun*, ed. C Johns-Krull, MK Browning, AA West, *ASP Conf. Ser.* 448:91–98. San Francisco: ASP
Alongi M, Bertelli G, Bressan A, Chiosi C. 1991. *Astron. Astrophys.* 244:95–106
Alonso A, Arribas S, Martinez-Roger C. 1996. *Astron. Astrophys.* 313:873–90
Alvarez R, Lançon A, Plez B, Wood PR. 2000. *Astron. Astrophys.* 353:322–34
Anders P, Fritze-von Alvensleben U. 2003. *Astron. Astrophys.* 401:1063–70
Ardila DR, Van Dyk SD, Makowiecki W, Stauffer J, Song I, et al. 2010. *Ap. J. Suppl.* 191:301–39
Aringer B, Girardi L, Nowotny W, Marigo P, Lederer MT. 2009. *Astron. Astrophys.* 503:913–28
Asplund M, Grevesse N, Sauval AJ, Scott P. 2009. *Annu. Rev. Astron. Astrophys.* 47:481–522
Assef RJ, Kochanek CS, Brodwin M, Brown MJI, Caldwell N, et al. 2008. *Ap. J.* 676:286–303
Atek H, Siana B, Scarlata C, Malkan M, McCarthy P, et al. 2011. *Ap. J.* 743:121
Auger MW, Treu T, Gavazzi R, Bolton AS, Koopmans LVE, Marshall PJ. 2010. *Ap. J. Lett.* 721:L163–67
Bacon R, Copin Y, Monnet G, Miller BW, Allington-Smith JR, et al. 2001. *MNRAS* 326:23–35
Bagnulo S, Jehin E, Ledoux C, Cabanac R, Melo C, et al. 2003. *The Messenger* 114:10–14
Baraffe I, Chabrier G, Allard F, Hauschildt PH. 1998. *Astron. Astrophys.* 337:403–12
Barber RJ, Tennyson J, Harris GJ, Tolchenov RN. 2006. *MNRAS* 368:1087–94
Bastian N, Covey KR, Meyer MR. 2010. *Annu. Rev. Astron. Astrophys.* 48:339–89
Baugh CM, Lacey CG, Frenk CS, Granato GL, Silva L, et al. 2005. *MNRAS* 356:1191–200
Bedijn PJ. 1987. *Astron. Astrophys.* 186:136–52
Behroozi PS, Wechsler RH, Conroy C. 2013. *Ap. J.* 770:57
Bell EF, de Jong RS. 2000. *MNRAS* 312:497–520
Bell EF, de Jong RS. 2001. *Ap. J.* 550:212–29
Bell EF, Gordon KD, Kennicutt RC Jr, Zaritsky D. 2002. *Ap. J.* 565:994–1010
Bell EF, McIntosh DH, Katz N, Weinberg MD. 2003. *Ap. J. Suppl.* 149:289–312
Bertelli G, Bressan A, Chiosi C, Fagotto F, Nasi E. 1994. *Astron. Astrophys. Suppl.* 106:275–302
Bertone E, Buzzoni A, Chávez M, Rodríguez-Merino LH. 2004. *Astron. J.* 128:829–41
Bessell MS, Brett JM, Scholz M, Wood PR. 1991. *Astron. Astrophys. Suppl.* 89:335–66
Bessell MS, Brett JM, Wood PR, Scholz M. 1989. *Astron. Astrophys. Suppl.* 77:1–30
Bica E, Alloin D. 1986. *Astron. Astrophys.* 162:21–31
Blackwell DE, Shallis MJ. 1977. *MNRAS* 180:177–91
Blanton MR, Moustakas J. 2009. *Annu. Rev. Astron. Astrophys.* 47:159–210
Blanton MR, Roweis S. 2007. *Astron. J.* 133:734–54
Bloecker T. 1995. *Astron. Astrophys.* 299:755
Boquien M, Buat V, Boselli A, Baes M, Bendo GJ, et al. 2012. *Astron. Astrophys.* 539:A145
Bouwens RJ, Illingworth GD, Oesch PA, Franx M, Labbé I, et al. 2012. *Ap. J.* 754:83
Boyajian TS, McAlister HA, van Belle G, Gies DR, ten Brummelaar TA, et al. 2012a. *Ap. J.* 746:101
Boyajian TS, von Braun K, van Belle G, McAlister HA, ten Brummelaar TA, et al. 2012b. *Ap. J.* 757:112
Brammer GB, van Dokkum PG, Franx M, Fumagalli M, Patel S, et al. 2012. *Ap. J. Suppl.* 200:13
Bressan A, Chiosi C, Fagotto F. 1994. *Ap. J. Suppl.* 94:63–115
Bressan A, Granato GL, Silva L. 1998. *Astron. Astrophys.* 332:135–48
Brinchmann J, Charlot S, White SDM, Tremonti C, Kauffmann G, et al. 2004. *MNRAS* 351:1151–79
Brinchmann J, Ellis RS. 2000. *Ap. J. Lett.* 536:L77–80
Bruzual G. 1983. *Ap. J.* 273:105–27
Bruzual G, Charlot S. 1993. *Ap. J.* 405:538–53
Bruzual G, Charlot S. 2003. *MNRAS* 344:1000–28

Buat V, Noll S, Burgarella D, Giovannoli E, Charmandaris V, et al. 2012. *Astron. Astrophys.* 545:A141
Bundy K, Ellis RS, Conselice CJ. 2005. *Ap. J.* 625:621–32
Burgarella D, Buat V, Iglesias-Páramo J. 2005. *MNRAS* 360:1413–25
Burstein D, Faber SM, Gaskell CM, Krumm N. 1984. *Ap. J.* 287:586–609
Calzetti D. 2001. *Publ. Astron. Soc. Pac.* 113:1449–85
Calzetti D, Bohlin RC, Kinney AL, Storchi-Bergmann T, Heckman TM. 1995. *Ap. J.* 443:136–51
Calzetti D, Kinney AL, Storchi-Bergmann T. 1994. *Ap. J.* 429:582–601
Calzetti D, Kennicutt RC, Engelbracht CW, Leitherer C, Draine BT, et al. 2007. *Ap. J.* 666:870–95
Cappellari M, Emsellam E, Krajnović D, McDermid RM, Scott N, et al. 2011. *MNRAS* 413:813–36
Cappellari M, McDermid RM, Alatalo K, Blitz L, Bois M, et al. 2012. *Nature* 484:485–88
Cardelli JA, Clayton GC, Mathis JS. 1989. *Ap. J.* 345:245–56
Carter D, Visvanathan N, Pickles AJ. 1986. *Ap. J.* 311:637–50
Casagrande L, Ramírez I, Meléndez J, Bessell M, Asplund M. 2010. *Astron. Astrophys.* 512:A54
Cassisi S. 2004. In *Variable Stars in the Local Group*, *IAU Colloq. 193*, ed. DW Kurtz, KR Pollard. *ASP Conf. Ser.* 310:489–97. San Francisco: ASP
Cassisi S, Marín-Franch A, Salaris M, Aparicio A, Monelli M, Pietrinferni A. 2011. *Astron. Astrophys.* 527:A59
Cenarro AJ, Cardiel N, Gorgas J, Peletier RF, Vazdekis A, Prada F. 2001. *MNRAS* 326:959–80
Cenarro AJ, Gorgas J, Vazdekis A, Cardiel N, Peletier RF. 2003. *MNRAS* 339:L12–16
Cenarro AJ, Peletier RM, Sánchez-Blázquez P, Selam SO, Taloba E, et al. 2007. *MNRAS* 374:664–90
Chabrier G. 2003. *Publ. Astron. Soc. Pac.* 115:763–95
Chabrier G, Baraffe I. 1997. *Astron. Astrophys.* 327:1039–53
Charlot S. 1996. In *From Stars to Galaxies: The Impact of Stellar Physics on Galaxy Evolution*, ed. C Leitherer, U Fritze-von-Alvensleben, J Huchra. *ASP Conf. Ser.* 98:275–86. San Francisco: ASP
Charlot S, Bruzual AG. 1991. *Ap. J.* 367:126–40
Charlot S, Fall SM. 2000. *Ap. J.* 539:718–31
Charlot S, Longhetti M. 2001. *MNRAS* 323:887–903
Charlot S, Worthey G, Bressan A. 1996. *Ap. J.* 457:625
Chary R, Elbaz D. 2001. *Ap. J.* 556:562–81
Chen Y, Trager S, Peletier R, Lançon A. 2011. *J. Phys. Conf. Ser.* 328:012023
Chen YM, Kauffmann G, Tremonti CA, White S, Heckman TM, et al. 2012. *MNRAS* 421:314–32
Cid Fernandes R, Mateus A, Sodré L, Stasińska G, Gomes JM. 2005. *MNRAS* 358:363–78
Cimatti A, et al. 2008. *Astron. Astrophys.* 482:21–42
Coelho P, Barbuy B, Meléndez J, Schiavon RP, Castilho BV. 2005. *Astron. Astrophys.* 443:735–46
Coelho P, Bruzual G, Charlot S, Weiss A, Barbuy B, Ferguson JW. 2007. *MNRAS* 382:498–514
Cohen JG. 1978. *Ap. J.* 221:788–96
Conroy C, Gunn JE. 2010. *Ap. J.* 712:833–57
Conroy C, Gunn JE, White M. 2009. *Ap. J.* 699:486–506
Conroy C, Schiminovich D, Blanton MR. 2010. *Ap. J.* 718:184–98
Conroy C, van Dokkum PG. 2012a. *Ap. J.* 747:69
Conroy C, van Dokkum PG. 2012b. *Ap. J.* 760:71
Conroy C, van Dokkum PG, Graves GJ. 2013. *Ap. J. Lett.* 763:L25
Cordier D, Pietrinferni A, Cassisi S, Salaris M. 2007. *Astron. J.* 133:468–78
Couture J, Hardy E. 1993. *Ap. J.* 406:142–57
Curtis-Lake E, McLure RJ, Dunlop JS, Schenker M, Rogers AB, et al. 2013. *MNRAS* 429:302–22
da Cunha E, Charlot S, Elbaz D. 2008. *MNRAS* 388:1595–617
Daddi E, Cimatti A, Renzini A, Vernet J, Conselice C, et al. 2004. *Ap. J. Lett.* 600:L127–30
Daddi E, Dickinson M, Morrison G, Chary R, Cimatti A, et al. 2007. *Ap. J.* 670:156–72
Dalcanton JJ, Williams BF, Lang D, Lauer TR, Kalinari JS, et al. 2012. *Ap. J. Suppl.* 200:18
Dalcanton JJ, Williams BF, Seth AC, Dolphin A, Holtzman J, et al. 2009. *Ap. J. Suppl.* 183:67–108
Dale DA, Helou G, Contursi A, Silbermann NA, Kolhatkar S. 2001. *Ap. J.* 549:215–27
Dale DA, Cohen SA, Johnson LC, Schuster MD, Calzetti D, et al. 2009. *Ap. J.* 703:517–56
Dale DA, Aniano G, Engelbracht CW, Hinz JL, Krause O, et al. 2012. *Ap. J.* 745:95
Davé R. 2008. *MNRAS* 385:147–60

Davidge TJ, Clark CC. 1994. *Astron. J.* 107:946–57
de Barros S, Schaerer D, Stark DP. 2012. *Astron. Astrophys.* Submitted (arXiv:1207.3663)
de Freitas Pacheco JA, Barbuy B. 1995. *Astron. Astrophys.* 302:718
Delisle S, Hardy E. 1992. *Astron. J.* 103:711–27
Desert F, Boulanger F, Puget JL. 1990. *Astron. Astrophys.* 237:215–36
Devriendt JEG, Guiderdoni B, Sadat R. 1999. *Astron. Astrophys.* 350:381–98
Dotter A, Chaboyer B, Ferguson JW, Lee H-C, Worthey G, et al. 2007. *Ap. J.* 666:403–12
Dotter A, Chaboyer B, Jevremović D, Kostov V, Baron E, Ferguson JW. 2008. *Ap. J. Suppl.* 178:89–101
Draine BT. 2003. *Annu. Rev. Astron. Astrophys.* 41:241–89
Draine BT, Dale DA, Bendo G, Gordon KD, Smith JDT, et al. 2007. *Ap. J.* 663:866–94
Draine BT, Lee HM. 1984. *Ap. J.* 285:89–108
Draine BT, Li A. 2007. *Ap. J.* 657:810–37
Drory N, Bender R, Feulner G, Hopp U, Maraston C, et al. 2004. *Ap. J.* 608:742–51
Dunne L, Eales S, Edmunds M, Ivison R, Alexander P, Clements DL. 2000. *MNRAS* 315:115–39
Dunne L, Eales SA. 2001. *MNRAS* 327:697–714
Dutton AA, Macciò AV, Mendel JT, Simard L. 2013a. *MNRAS* 432:2496–511
Dutton AA, Mendel JT, Simard L. 2012. *MNRAS* 422:L33
Dutton AA, Treu T, Brewer BJ, Marshall PJ, Auger MW, et al. 2013b. *MNRAS* 428:3183–95
Edvardsson B, Andersen J, Gustafsson B, Lambert DL, Nissen PE, Tomkin J. 1993. *Astron. Astrophys.* 275:101
Elbaz D, Dickinson M, Hwang HS, Díaz-Santos T, Magdis G, et al. 2011. *Astron. Astrophys.* 533:A119
Elbaz D, Hwang HS, Magnelli B, Daddi E, Aussel H, et al. 2010. *Astron. Astrophys.* 518:L29
Eldridge JJ, Izzard RG, Tout CA. 2008. *MNRAS* 384:1109–18
Eldridge JJ, Stanway ER. 2012. *MNRAS* 419:479–89
Eminian C, Kauffmann G, Charlot S, Wild V, Bruzual G, et al. 2008. *MNRAS* 384:930–42
Faber SM. 1972. *Astron. Astrophys.* 20:361–74
Faber SM. 1977. In *Evolution of Galaxies and Stellar Populations*, ed. BM Tinsley, RB Larson, p. 157. New Haven, CT: Yale Univ. Obs.
Faber SM, French HB. 1980. *Ap. J.* 235:405–12
Fanelli MN, O'Connell RW, Burstein D, Wu CC. 1992. *Ap. J. Suppl.* 82:197–245
Fang JJ, Faber SM, Salim S, Graves GJ, Rich RM. 2012. *Ap. J.* 761:23
Ferland GJ, Korista KT, Verner DA, Ferguson JW, Kingdon JB, Verner EM. 1998. *Publ. Astron. Soc. Pac.* 110:761–78
Ferreras I, Pasquali A, Malhotra S, Rhoads J, Cohen S, et al. 2009. *Ap. J.* 706:158–69
Finkelstein SL, Papovich C, Giavalisco M, Reddy NA, Ferguson HC, et al. 2010. *Ap. J.* 719:1250–73
Finkelstein SL, Papovich C, Salmon B, Finlator K, Dickinson M, et al. 2012. *Ap. J.* 756:164
Finlator K, Davé R, Oppenheimer BD. 2007. *MNRAS* 376:1861–78
Fioc M, Rocca-Volmerange B. 1997. *Astron. Astrophys.* 326:950–62
Fischera J, Dopita M. 2011. *Astron. Astrophys.* 533:A117
Fluks MA, Plez B, The PS, de Winter D, Westerlund BE, Steenman HC. 1994. *Astron. Astrophys. Suppl.* 105:311–36
Ford HA, Bregman JN. 2013. *Ap. J.* 770:137
Frogel JA. 1988. *Annu. Rev. Astron. Astrophys.* 26:51–92
Frogel JA, Persson SE, Cohen JG. 1980. *Ap. J.* 240:785–802
Frogel JA, Persson SE, Matthews K, Aaronson M. 1978. *Ap. J.* 220:75–97
Fulbright JP, McWilliam A, Rich RM. 2007. *Ap. J.* 661:1152–79
Gallazzi A, Bell EF. 2009. *Ap. J. Suppl.* 185:253–72
Gallazzi A, Charlot S, Brinchmann J, White SDM, Tremonti CA. 2005. *MNRAS* 362:41–58
Galliano F, Dwek E, Chanial P. 2008. *Ap. J.* 672:214–43
Giallongo E, D'Odorico S, Fontana A, Cristiani S, Egami E, et al. 1998. *Astron. J.* 115:2169–83
Girardi L, Bressan A, Bertelli G, Chiosi C. 2000. *Astron. Astrophys. Suppl.* 141:371–83
González JJ. 1993. *Line strength gradients and kinematic profiles in elliptical galaxies*. PhD thesis. Univ. Calif., Santa Cruz
González V, Labbé I, Bouwens RJ, Illingworth G, Franx M, Kriek M. 2011. *Ap. J. Lett.* 735:L34

González Delgado RM, Cerviño M, Martins LP, Leitherer C, Hauschildt PH. 2005. *MNRAS* 357:945–60
González-Lópezlira RA, Bruzual-A G, Charlot S, Ballesteros-Paredes J, Loinard L. 2010. *MNRAS* 403:1213–38
Gordon KD, Clayton GC. 1998. *Ap. J.* 500:816
Granato GL, Lacey CG, Silva L, Bressan A, Baugh CM, et al. 2000. *Ap. J.* 542:710–30
Graves GJ, Faber SM. 2010. *Ap. J.* 717:803–24
Graves GJ, Faber SM, Schiavon RP. 2009. *Ap. J.* 693:486–506
Gregg MD, Silva D, Rayner J, Worthey G, Valdes F, et al. 2006. In *The 2005 HST Calibration Workshop: Hubble After the Transition to Two-Gyro Mode*, ed. AM Koekemoer, P Goudfrooij, LL Dressel, p. 209. Washington, DC: Natl. Aeronaut. Space Adm.
Greggio L. 1997. *MNRAS* 285:151–66
Grillmair CJ, Lauer TR, Worthey G, Faber SM, Freedman, et al. 1996. *Astron. J.* 112:1975
Groenewegen MAT. 2012. *Astron. Astrophys.* 543:A36
Groves B, Dopita MA, Sutherland RS, Kewley LJ, Fischera J, et al. 2008. *Ap. J. Suppl.* 176:438–56
Groves BA, Dopita MA, Sutherland RS. 2004. *Ap. J. Suppl.* 153:9–73
Gunn JE, Stryker LL. 1983. *Ap. J. Suppl.* 52:121–53
Han Z, Podsiadlowski P, Maxted PFL, Marsh TR. 2003. *MNRAS* 341:669–91
Han Z, Podsiadlowski P, Maxted PFL, Marsh TR, Ivanova N. 2002. *MNRAS* 336:449–66
Hardy E, Couture J. 1988. *Ap. J. Lett.* 325:L29–31
Harris GLH, Harris WE. 2000. *Astron. J.* 120:2423–36
Hayward CC, Narayanan D, Keres D, Jonsson P, Hopkins PF, et al. 2013. *MNRAS* 428:2529–47
Heap SR, Lindler D. 2011. In *16th Cambridge Workshop on Cool Stars, Stellar Systems, and the Sun*, ed. C Johns-Krull, MK Browning, AA West, *ASP Conf. Ser.* 448:887–91. San Francisco: ASP
Heavens AF, Jimenez R, Lahav O. 2000. *MNRAS* 317:965–72
Heger A, Fryer CL, Woosley SE, Langer N, Hartmann DH. 2003. *Ap. J.* 591:288–300
Holden BP, van der Wel A, Kelson DD, Franx M, Illingworth GD. 2010. *Ap. J.* 724:714–29
Hopkins AM, Beacom JF. 2006. *Ap. J.* 651:142–54
Hoversten EA, Gronwall C, Vanden Berk DE, Basu-Zych AR, Breeveld AA, et al. 2011. *Astron. J.* 141:205
Hwang HS, Elbaz D, Magdis G, Daddi E, Symeonidis M, et al. 2010. *MNRAS* 409:75–82
Jeong H, Yi SK, Bureau M, Davies RL, Falcón-Barroso J, et al. 2009. *MNRAS* 398:2028–48
Johansson J, Thomas D, Maraston C. 2012. *MNRAS* 421:1908–26
Johnson BD, Schiminovich D, Seibert M, Treyer M, Bartin DC, et al. 2007. *Ap. J. Suppl.* 173:392–403
Jones LA. 1999. *Differential spectral synthesis of low-luminosity elliptical galaxies.* PhD thesis. Univ. North Carol.
Jonsson P. 2006. *MNRAS* 372:2–20
Kalirai JS, Hansen BMS, Kelson DD, Reitzel DB, Rich RM, Richer HB. 2008. *Ap. J.* 676:594–609
Kannappan SJ, Gawiser E. 2007. *Ap. J. Lett.* 657:L5–8
Kauffmann G, Heckman TM, White SDM, Charlot S, Tremonti C, et al. 2003. *MNRAS* 341:33–53
Kaviraj S, Schawinski K, Devriendt JEG, Ferreras I, Khochfar S, et al. 2007. *Ap. J. Suppl.* 173:619–42
Keller SC, Wood PR. 2006. *Ap. J.* 642:834–41
Kelson DD, Holden BP. 2010. *Ap. J. Lett.* 713:L28–32
Kelson DD, Illingworth GD, Franx M, van Dokkum PG. 2001. *Ap. J. Lett.* 552:L17–21
Kelson DD, Illingworth GD, Franx M, van Dokkum PG. 2006. *Ap. J.* 653:159–83
Kennicutt RC, Evans NJ. 2012. *Annu. Rev. Astron. Astrophys.* 50:531–608
Kennicutt RC Jr. 1998. *Annu. Rev. Astron. Astrophys.* 36:189–232
Kennicutt RC Jr, Calzetti D, Walter F, Helou G, Hollenback DJ, et al. 2007. *Ap. J.* 671:333–48
Kobulnicky HA, Fryer CL. 2007. *Ap. J.* 670:747–65
Koleva M, Prugniel P, Bouchard A, Wu Y. 2009. *Astron. Astrophys.* 501:1269–79
Koleva M, Prugniel P, Ocvirk P, Le Borgne D, Soubiran C. 2008. *MNRAS* 385:1998–2010
Kong X, Charlot S, Brinchmann J, Fall SM. 2004. *MNRAS* 349:769–78
Korn AJ, Maraston C, Thomas D. 2005. *Astron. Astrophys.* 438:685–704
Kriek M, Labbé I, Conroy C, Whitaker KE, van Dokkum PG, et al. 2010. *Ap. J. Lett.* 722:L64–69
Kriek M, van Dokkum PG, Whitaker KE, Labbé I, Franx M, Brammer GB. 2011. *Ap. J.* 743:168
Kriek M, van Dokkum PG, Franx M, Illingworth GD, Marchesini D, et al. 2008. *Ap. J.* 677:219–37

Kroupa P. 2001. *MNRAS* 322:231–46
Kučinskas A, Hauschildt PH, Ludwig HG, Brott I, Vansevičius V, et al. 2005. *Astron. Astrophys.* 442:281–308
Kuntschner H. 2000. *MNRAS* 315:184–208
Kurucz RL. 2011. *Can. J. Phys.* 89:417–28
Labbé I, Oesch PA, Bouwens RJ, Illingworth GD, Magee D, et al. 2012. *Ap. J. Lett.* Submitted (arXiv:1209.3037)
Lançon A, Mouhcine M. 2002. *Astron. Astrophys.* 393:167–81
Lançon A, Mouhcine M, Fioc M, Silva D. 1999. *Astron. Astrophys.* 344:L21–24
Lançon A, Wood PR. 2000. *Astron. Astrophys. Suppl. Ser.* 146:217–49
Lanz T, Hubeny I. 2003. *Ap. J. Suppl.* 146:417–41
Le Borgne JF, Bruzual G, Pelló R, Lançon A, Rocca-Volmerange B, et al. 2003. *Astron. Astrophys.* 402:433–42
Lebzelter T, Seifahrt A, Uttenthaler S, Ramsay S, Hartman H, et al. 2012. *Astron. Astrophys.* 539:A109
Lee H-C, Worthey G, Dotter A, Chaboyer B, Jevremović D, et al. 2009a. *Ap. J.* 694:902–23
Lee H-C, Worthey G, Trager SC, Faber SM. 2007. *Ap. J.* 664:215–25
Lee H-C, Yoon SJ, Lee YW. 2000. *Astron. J.* 120:998–1005
Lee SK, Ferguson HC, Somerville RS, Wiklind T, Giavalisco M. 2010. *Ap. J.* 725:1644–51
Lee SK, Idzi R, Ferguson HC, Somerville RS, Wiklind T, Giavalisco M. 2009b. *Ap. J. Suppl.* 184:100–32
Lee YS, Beer TC, Sivarani T, Allende Prieto C, Koesterke L, et al. 2008. *Astron. J.* 136:2022–49
Leitherer C, Schaerer D, Doldader JD, González Delgado RM, Robert C, et al. 1999. *Ap. J. Suppl.* 123:3–40
Leitner SN. 2012. *Ap. J.* 745:149
Lejeune T, Cuisinier F, Buser R. 1997. *Astron. Astrophys. Suppl.* 125:229–46
Lejeune T, Cuisinier F, Buser R. 1998. *Astron. Astrophys. Suppl.* 130:65–75
Leonardi AJ, Rose JA. 1996. *Astron. J.* 111:182
Levesque EM, Leitherer C, Ekstrom S, Meynet G, Schaerer D. 2012. *Ap. J.* 751:67
Longhetti M, Saracco P. 2009. *MNRAS* 394:774–94
Lotz JM, Ferguson HC, Bohlin RC. 2000. *Ap. J.* 532:830–44
MacArthur LA, Courteau S, Bell E, Holtzman JA. 2004. *Ap. J. Suppl.* 152:175–99
MacArthur LA, González JJ, Courteau S. 2009. *MNRAS* 395:28–63
MacArthur LA, McDonald M, Courteau S, Jesús González J. 2010. *Ap. J.* 718:768–73
Madden SC, Galliano F, Jones AP, Sauvage M. 2006. *Astron. Astrophys.* 446:877–96
Maeder A, Meynet G. 2000. *Annu. Rev. Astron. Astrophys.* 38:143–90
Maeder A, Meynet G. 2012. *Rev. Mod. Phys.* 84:25–63
Maraston C. 1998. *MNRAS* 300:872–92
Maraston C. 2005. *MNRAS* 362:799–825
Maraston C, Daddi E, Renzini A, Cimatti A, Dickinson M, et al. 2006. *Ap. J.* 652:85–96
Maraston C, Pforr J, Renzini A, Daddi E, Dickinson M, et al. 2010. *MNRAS* 407:830–45
Maraston C, Thomas D. 2000. *Ap. J.* 541:126–33
Marchesini D, van Dokkum PG, Förster Schreiber NM, Franx M, Labbé I, Wuyts S. 2009. *Ap. J.* 701:1765–96
Marigo P. 2001. *Astron. Astrophys.* 370:194–217
Marigo P, Girardi L. 2007. *Astron. Astrophys.* 469:239–63
Marigo P, Girardi L, Bressan A, Groenewegen MAT, Silva L, Granato GL. 2008. *Astron. Astrophys.* 482:883–905
Martins LP, Coelho P. 2007. *MNRAS* 381:1329–46
Martins LP, González Delgado RM, Leitherer C, Cerviño M, Hauschildt P. 2005. *MNRAS* 358:49–65
Mathis JS, Rumpl W, Nordsieck KH. 1977. *Ap. J.* 217:425–33
Melbourne J, Williams BF, Dalcanton JJ, Rosenfield P, Girardi L, et al. 2012. *Ap. J.* 748:47
Meurer GR, Heckman TM, Calzetti D. 1999. *Ap. J.* 521:64–80
Meynet G, Maeder A. 2000. *Astron. Astrophys.* 361:101–20
Miller GE, Scalo JM. 1979. *Ap. J. Suppl.* 41:513–47
Miner J, Rose JA, Cecil G. 2011. *Ap. J. Lett.* 727:L15
Moles M, Benítez N, Aguerri JAL, Alfaro EJ, Broadhurst T, et al. 2008. *Astron. J.* 136:1325–39
Mollá M, García-Vargas ML, Bressan A. 2009. *MNRAS* 398:451–70
Monachesi A, Trager SC, Lauer TR, Freedman W, Dressler A, et al. 2011. *Ap. J.* 727:55

Moustakas J, Coil A, Aird J, Blanton MR, Cool RJ, et al. 2013. *Ap. J.* 767:50
Munari U, Sordo R, Castelli F, Zwitter T. 2005. *Astron. Astrophys.* 442:1127–34
Muzzin A, Marchesini D, van Dokkum PG, Labbé I, Kriek M, Franx M. 2009. *Ap. J.* 701:1839–64
Muzzin A, van Dokkum P, Kriek M, Labbé I, Cury I, et al. 2010. *Ap. J.* 725:742–49
Noeske KG, Weiner BJ, Faber SM, Papovich C, Koo DC, et al. 2007. *Ap. J. Lett.* 660:L43
Noll S, Burgarella D, Giovannoli E, Buat V, Marcillac D, Muñoz-Mateos JC. 2009a. *Astron. Astrophys.* 507:1793–813
Noll S, Pierini D, Cimatti A, Daddi E, Kurk JD, et al. 2009b. *Astron. Astrophys.* 499:69–85
Nordstroem B, Andersen J, Andersen MI. 1997. *Astron. Astrophys.* 322:460–76
O'Connell RW. 1976. *Ap. J.* 206:370–90
O'Connell RW. 1980. *Ap. J.* 236:430–40
O'Connell RW. 1999. *Annu. Rev. Astron. Astrophys.* 37:603–48
Ocvirk P, Pichon C, Lançon A, Thiébaut E. 2006. *MNRAS* 365:46–73
Osterbrock DE. 1989. *Astrophysics of Gaseous Nebulae and Active Galactic Nuclei*. Mill Valley, CA: Univ. Sci. Books
Pacifici C, Charlot S, Blaizot J, Brinchmann J. 2012. *MNRAS* 421:2002–24
Panuzzo P, Bressan A, Granato GL, Silva L, Danese L. 2003. *Astron. Astrophys.* 409:99–114
Panuzzo P, Granato GL, Buat V, Inoue AK, Silva L, et al. 2007. *MNRAS* 375:640–48
Papovich C, Dickinson M, Ferguson HC. 2001. *Ap. J.* 559:620–53
Papovich C, Finkelstein SL, Ferguson HC, Lotz JM, Giavalisco M. 2011. *MNRAS* 412:1123–36
Papovich C, Rudnick G, Le Floc'h E, van Dokkum PG, Rieke GH, et al. 2007. *Ap. J.* 668:45–61
Paxton B, Bildsten L, Dotter A, Herwig F, Lesaffre P, Timmes F. 2011. *Ap. J. Suppl.* 192:3
Pei YC. 1992. *Ap. J.* 395:130–39
Peletier RF. 1989. *Elliptical galaxies—structure and stellar content*. PhD thesis. Univ. Groningen, Neth.
Percival SM, Salaris M. 2011. *MNRAS* 412:2445–53
Percival SM, Salaris M, Cassisi S, Pietrinferni A. 2009. *Ap. J.* 690:427–39
Pérez-González PG, Cava A, Barro G, Villar V, Cardiel N, et al. 2013. *Ap. J.* 762:46
Perrin G, Coudé du Foresto V, Ridgway ST, Mariotti JM, Traub WA, et al. 1998. *Astron. Astrophys.* 331:619–26
Peterson RC. 1976. *Ap. J. Lett.* 210:L123–26
Pforr J, Maraston C, Tonini C. 2012. *MNRAS* 422:3285–326
Pickles AJ. 1998. *Publ. Astron. Soc. Pac.* 110:863–78
Pietrinferni A, Cassisi S, Salaris M, Castelli F. 2004. *Ap. J.* 612:168–90
Piovan L, Tantalo R, Chiosi C. 2003. *Astron. Astrophys.* 408:559–79
Piovan L, Tantalo R, Chiosi C. 2006. *MNRAS* 366:923–44
Ponder JM, Burstein D, O'Connell RW, Rose JA, Frogel JA, et al. 1998. *Astron. J.* 116:2297–314
Pope A, Scott D, Dickinson M, Chary R-R, Morrison G, et al. 2006. *MNRAS* 370:1185–207
Popescu CC, Misiriotis A, Kylafis ND, Tuffs RJ, Fischera J. 2000. *Astron. Astrophys.* 362:138–50
Popescu CC, Tuffs RJ, Dopita MA, Fischera J, Kylafis ND, Madore BF. 2011. *Astron. Astrophys.* 527:A109
Prugniel P, Soubiran C. 2001. *Astron. Astrophys.* 369:1048–57
Rabin D. 1982. *Ap. J.* 261:85–101
Ramírez I, Meléndez J. 2005. *Ap. J.* 626:465–85
Rauch T. 2003. *Astron. Astrophys.* 403:709–14
Rayner JT, Cushing MC, Vacca WD. 2009. *Ap. J. Suppl.* 185:289–432
Reddy NA, Pettini M, Steidel CC, Shapley AE, Erb DK, Law DR. 2012. *Ap. J.* 754:25
Reddy NA, Erb DK, Pettini M, Steidel CC, Shapley AE. 2010. *Ap. J.* 712:1070–91
Reddy NA, Steidel CC. 2009. *Ap. J.* 692:778–803
Renzini A. 2006. *Annu. Rev. Astron. Astrophys.* 44:141–92
Renzini A, Buzzoni A. 1986. In *Spectral Evolution of Galaxies*, Vol. 122, ed. C Chiosi, A Renzini, pp. 195–231. Dordrecht: Reidel
Renzini A, Ciotti L. 1993. *Ap. J. Lett.* 416:L49
Renzini A, Greggio L, Ritossa C, Ferrario L. 1992. *Ap. J.* 400:280–303
Rose JA. 1984. *Astron. J.* 89:1238–51
Rose JA. 1985. *Astron. J.* 90:1927–56

Rujopakarn W, Rieke GH, Weiner BJ, Rex M, Walth GL, Kartaltepe JS. 2012. *Ap. J.* 755:168
Saglia RP, Maraston C, Thomas D, Bender R, Colless M. 2002. *Ap. J. Lett.* 579:L13–16
Salim S, Fang JJ, Rich RM, Faber SM, Thilker DA. 2012. *Ap. J.* 755:105
Salim S, Rich RM. 2010. *Ap. J. Lett.* 714:L290–94
Salim S, Rich RM, Charlot S, Brinchmann J, Johnson BD, et al. 2007. *Ap. J. Suppl.* 173:267–92
Salpeter EE. 1955. *Ap. J.* 121:161
Sana H, Evans CJ. 2011. In *Active OB Stars: Structure, Evolution, Mass Loss, and Critical Limits, IAU Symp. 272*, ed. C Neiner, G Wade, G Meynet, G Peters, pp. 474–85. Cambridge, UK: Cambridge Univ. Press
Sánchez SF, Kennicutt RC, Gil de Paz A, van de Ven G, Vílchez JM, et al. 2012. *Astron. Astrophys.* 538:A8
Sánchez-Blázquez P, Ocvirk P, Gibson BK, Pérez I, Peletier RF. 2011. *MNRAS* 415:709–31
Sánchez-Blázquez P, Peletier RF, Jiménez-Vicente J, Cardiel N, Cenarro AJ, et al. 2006. *MNRAS* 371:703–18
Santini P, Fontana A, Grazian A, Salimbeni S, Fiore F, et al. 2009. *Astron. Astrophys.* 504:751–67
Sargent BA, Srinivasan S, Meixner M. 2011. *Ap. J.* 728:93
Sawicki M, Yee HKC. 1998. *Astron. J.* 115:1329–39
Scalo J, Vazquez-Semadeni E, Chappell D, Passot T. 1998. *Ap. J.* 504:835
Scalo JM. 1986. *Fundam. Cosm. Phys.* 11:1–278
Schaerer D. 2003. *Astron. Astrophys.* 397:527–38
Schaerer D, de Barros S. 2010. *Astron. Astrophys.* 515:A73
Schaller G, Schaerer D, Meynet G, Maeder A. 1992. *Astron. Astrophys. Suppl.* 96:269–331
Schiavon RP. 2007. *Ap. J. Suppl.* 171:146–205
Schiavon RP. 2010. *Publ. Korean Astron. Soc.* 25:83–90
Schiavon RP, Barbuy B, Bruzual AG. 2000. *Ap. J.* 532:453–60
Schiavon RP, Barbuy B, Rossi SCF, Milone A. 1997. *Ap. J.* 479:902
Schiavon RP, Barbuy B, Singh PD. 1997. *Ap. J.* 484:499
Schiavon RP, Dalessandro E, Sohn ST, Rood RT, O'Connell RW, et al. 2012. *Astron. J.* 143:121
Schiavon RP, Rose JA, Courteau S, MacArthur LA. 2004. *Ap. J. Lett.* 608:L33–36
Schmidt M. 1959. *Ap. J.* 129:243
Schoenberner D. 1983. *Ap. J.* 272:708–14
Schwarzschild M, Harm R. 1968. *Astron. J. Suppl.* 73:35
Searle L, Sargent WLW, Bagnuolo WG. 1973. *Ap. J.* 179:427–38
Serra P, Trager SC. 2007. *MNRAS* 374:769–74
Serven J, Worthey G, Briley MM. 2005. *Ap. J.* 627:754–66
Serven J, Worthey G, Toloba E, Sánchez-Blázquez P. 2011. *Astron. J.* 141:184
Shapley AE, Steidel CC, Adelberger KL, Dickinson M, Giavalisco M, Pettini M. 2001. *Ap. J.* 562:95–123
Shapley AE, Steidel CC, Erb DK, Reddy NA, Adelberger KL, et al. 2005. *Ap. J.* 626:698–722
Shapley AE, Steidel CC, Pettini M, Adelberger KL, Erb DK. 2006. *Ap. J.* 651:688–703
Silva L, Granato GL, Bressan A, Danese L. 1998. *Ap. J.* 509:103–17
Smith LJ, Norris RPF, Crowther PA. 2002. *MNRAS* 337:1309–28
Smith RJ, Lucey JR, Carter D. 2012. *MNRAS* 421:2982–97
Smith RJ, Lucey JR, Hudson MJ. 2009. *MNRAS* 400:1690–705
Smith RJ, Lucey JR, Hudson MJ, Bridges TJ. 2009. *MNRAS* 398:119–32
Sonnenfeld A, Treu T, Gavazzi R, Marshall PJ, Auger MW, et al. 2012. *Ap. J.* 752:163
Spiniello C, Trager SC, Koopmans LVE, Chen YP. 2012. *Ap. J. Lett.* 753:L32
Spinrad H. 1962. *Ap. J.* 135:715
Spinrad H, Taylor BJ. 1971. *Ap. J. Suppl.* 22:445
Srinivasan S, Sargent BA, Meixner M. 2011. *Astron. Astrophys.* 532:A54
Stark DP, Ellis RS, Bunker A, Bundy K, Targett T, et al. 2009. *Ap. J.* 697:1493
Stothers RB. 1991. *Ap. J.* 383:820–36
Taylor EN, Hopkins AM, Baldry IK, Brown MJI, Driver SP, et al. 2011. *MNRAS* 418:1587–620
Thomas D, Maraston C, Bender R. 2003a. *MNRAS* 343:279–83
Thomas D, Maraston C, Bender R. 2003b. *MNRAS* 339:897–911
Thomas D, Maraston C, Bender R, Mendes de Oliveira C. 2005. *Ap. J.* 621:673–94
Thomas D, Maraston C, Korn A. 2004. *MNRAS* 351:L19–23

Thomas J, Saglia RP, Bender R, Thomas D, Gebhardt K, et al. 2011. *MNRAS* 415:545–62
Tinsley BM. 1968. *Ap. J.* 151:547
Tinsley BM. 1979. *Ap. J.* 229:1046–56
Tinsley BM. 1980. *Fundam. Cosm. Phys.* 5:287–388
Tinsley BM, Gunn JE. 1976. *Ap. J.* 203:52–62
Tojeiro R, Heavens AF, Jimenez R, Panter B. 2007. *MNRAS* 381:1252–66
Tojeiro R, Percival WJ, Heavens AF, Jimenez R. 2011. *MNRAS* 413:434–60
Tojeiro R, Wilkins S, Heavens AF, Panter B, Jimenez R. 2009. *Ap. J. Suppl.* 185:1–19
Trager SC, Faber SM, Dressler A. 2008. *MNRAS* 386:715–47
Trager SC, Faber SM, Worthey G, González JJ. 2000a. *Astron. J.* 120:165–88
Trager SC, Faber SM, Worthey G, González JJ. 2000b. *Astron. J.* 119:1645–76
Trager SC, Somerville RS. 2009. *MNRAS* 395:608–24
Trager SC, Worthey G, Faber SM, Burstein D, Gonzalez JJ. 1998. *Ap. J. Suppl.* 116:1
Trager SC, Worthey G, Faber SM, Dressler A. 2005. *MNRAS* 362:2–8
Treu T, Auger MW, Koopmans LVE, Gavazzi R, Marshall PJ, Bolton AS. 2010. *Ap. J.* 709:1195–202
Tripicco MJ, Bell RA. 1995. *Astron. J.* 110:3035
Valdes F, Gupta R, Rose JA, Singh HP, Bell DJ. 2004. *Ap. J. Suppl.* 152:251–59
van Dokkum PG. 2008. *Ap. J.* 674:29–50
van Dokkum PG, Conroy C. 2010. *Nature* 468:940–42
van Dokkum PG, Conroy C. 2012. *Ap. J.* 760:70
VandenBerg DA, Bell RA. 1985. *Ap. J. Suppl.* 58:561–621
VandenBerg DA, Bell RA. 2001. *New Astron. Rev.* 45:577–82
VandenBerg DA, Bergbusch PA, Dowler PD. 2006. *Ap. J. Suppl.* 162:375–87
VandenBerg DA, Stetson PB. 2004. *Publ. Astron. Soc. Pac.* 116:997–1011
Vassiliadis E, Wood PR. 1994. *Ap. J. Suppl.* 92:125–44
Vazdekis A. 1999. *Ap. J.* 513:224–41
Vazdekis A, Casuso E, Peletier RF, Beckman JE. 1996. *Ap. J. Suppl.* 106:307
Vazdekis A, Peletier RF, Beckman JE, Casuso E. 1997. *Ap. J. Suppl.* 111:203
Vazdekis A, Sánchez-Blázquez P, Falcón-Barroso J, Cenarro AJ, Beasley MA, et al. 2010. *MNRAS* 404:1639–71
Vázquez GA, Leitherer C, Schaerer D, Meynet G, Maeder A. 2007. *Ap. J.* 663:995–1020
Venn KA, Irwin M, Shetrone MD, Tout CA, Hill V, Tolstoy E. 2004. *Astron. J.* 128:1177–95
Ventura P, Marigo P. 2010. *MNRAS* 408:2476–86
Voit GM. 1992. *MNRAS* 258:841–48
Walcher CJ, Coelho P, Gallazzi A, Charlot S. 2009. *MNRAS* 398:L44–48
Walcher J, Groves B, Budavári T, Dale D. 2011. *Ap. Space Sci.* 331:1–52
Wallerstein G. 1962. *Ap. J. Suppl.* 6:407
Weingartner JC, Draine BT. 2001. *Ap. J.* 548:296–309
Weisz DR, Dalcanton JJ, Williams BF, Gilbert KM, Skillman ED, et al. 2011. *Ap. J.* 739:5
Westera P, Lejeune T, Buser R, Cuisinier F, Bruzual G. 2002. *Astron. Astrophys.* 381:524–38
Whitaker KE, Labbé I, van Dokkum PG, Brammer G, Kriek M, et al. 2011. *Ap. J.* 735:86
Whitaker KE, van Dokkum PG, Brammer G, Kriek M, Franx M, et al. 2010. *Ap. J.* 719:1715–32
Whitford AE. 1977. *Ap. J.* 211:527–38
Wijesinghe DB, Hopkins AM, Sharp R, Gunawardhana M, Brough S, et al. 2011. *MNRAS* 410:2291–301
Wild V, Charlot S, Brinchmann J, Heckman T, Vince O, et al. 2011. *MNRAS* 417:1760–86
Wilkins SM, Trentham N, Hopkins AM. 2008. *MNRAS* 385:687–94
Williams RJ, Quadri RF, Franx M, van Dokkum P, Labbé I. 2009. *Ap. J.* 691:1879–95
Willson LA. 2000. *Annu. Rev. Astron. Astrophys.* 38:573–611
Witt AN, Gordon KD. 2000. *Ap. J.* 528:799–816
Wolf C, Meisenheimer K, Kleinheinrich M, Borch A, Dye S, et al. 2004. *Astron. Astrophys.* 421:913–36
Worthey G. 1994. *Ap. J. Suppl.* 95:107–49
Worthey G, Dorman B, Jones LA. 1996. *Astron. J.* 112:948
Worthey G, Faber SM, Gonzalez JJ. 1992. *Ap. J.* 398:69–73
Worthey G, Faber SM, Gonzalez JJ, Burstein D. 1994. *Ap. J. Suppl.* 94:687–722

Worthey G, Ingermann BA, Serven J. 2011. *Ap. J.* 729:148
Wuyts S, Franx M, Cox TJ, Hernquist L, Hopkins PF, et al. 2009. *Ap. J.* 696:348–69
Wuyts S, Labbé I, Franx M, Rudnick G, van Dokkum PG, et al. 2007. *Ap. J.* 655:51–65
Wuyts S, Förster Schreiber NM, Genzel R, Guo Y, Barro G, et al. 2012. *Ap. J.* 753:114
Wuyts S, Förster Schreiber NM, Lutz D, Nordon R, Berta S, et al. 2011. *Ap. J.* 738:106
Yi S, Demarque P, Kim YC, Lee YW, Ree CH, et al. 2001. *Ap. J. Suppl.* 136:417–37
Yi S, Demarque P, Oemler A Jr. 1997. *Ap. J.* 486:201
Yi S, Lee YW, Woo JH, Park JH, Demarque P, Oemler A Jr. 1999. *Ap. J.* 513:128–41
Yi SK. 2003. *Ap. J.* 582:202–14
Yi SK. 2008. In *Hot Subdwarf Stars and Related Objects*, ed. U Heber, CS Jeffery, R Napiwotzki, *ASP Conf. Ser.* 392:3–14. San Francisco: ASP
Yi SK, Kim YC, Demarque P. 2003. *Ap. J. Suppl.* 144:259–61
Yi SK, Yoon S-J, Kaviraj S, Deharveng J-M, Rich RM, et al. 2005. *Ap. J. Lett.* 619:L111–14
Zhang F, Han Z, Li L, Hurley JR. 2005. *MNRAS* 357:1088–103
Zibetti S, Charlot S, Rix HW. 2009. *MNRAS* 400:1181–98
Zibetti S, Gallazzi A, Charlot S, Pierini D, Pasquali A. 2012. *MNRAS* 428:1479–97
Zubko V, Dwek E, Arendt RG. 2004. *Ap. J. Suppl.* 152:211–49

Annual Review of Astronomy and Astrophysics

Volume 51, 2013

Contents